

THE PENNSYLVANIA STATE UNIVERSITY  
SCHREYER HONORS COLLEGE

DEPARTMENT OF MECHANICAL ENGINEERING

Development of an Empirical Correlation for the Manganese Sulfate Bath Neutron Absorption in  
Manganese Fraction Using the Monte Carlo N-Particle Code

SCOUT BUCKS  
SPRING 2024

A thesis  
submitted in partial fulfillment  
of the requirements  
for baccalaureate degrees  
in Mechanical Engineering and Nuclear Engineering  
with honors in Mechanical Engineering

Reviewed and approved\* by the following:

Marek Flaska  
Associate Professor of Nuclear Engineering  
Thesis Supervisor

Margaret Byron  
Assistant Professor of Mechanical Engineering  
Honors Adviser

Guha Manogharan  
Associate Professor of Mechanical Engineering  
Faculty Reader

\* Electronic approvals are on file.

## ABSTRACT

The manganese (Mn) sulfate ( $\text{SO}_4$ ) bath is the primary tool for making high-precision measurements of isotopic neutron source emission rates. When a neutron source is submerged in aqueous  $\text{MnSO}_4$  solution, neutrons from the source are absorbed in Mn, thereby producing  $\gamma$ -radiation. These photons are then measured to accurately calculate the neutron source strength. A key parameter for these measurement systems is the fraction of neutrons leaving the source that are absorbed in Mn as opposed to other Mn bath components or leaking from the Mn bath. This manganese absorption fraction is usually calculated with Monte Carlo methods.<sup>1</sup>

To support the creation of a Mn bath facility at The Pennsylvania State University, simulations of a generalized manganese bath were performed using the Monte Carlo N-Particle (MCNP) code. The goal was to generate empirical correlations for calculating the manganese absorption fraction for different spherical bath radii, solution densities, and neutron source types. The expected leakage from Mn baths was also explored. Extensive work went into transforming physical phenomena into their simulated equivalents, and the resulting MCNP framework was validated against three simulations published in the literature.

In total, 336 simulations were performed using one million neutrons for each run to provide acceptable statistical variances. Am-Be, Cf, and Pu-Be sources were studied for bath radii between 10 and 75 cm and for solution densities between 1.05 and  $1.40 \frac{\text{g}}{\text{cm}^3}$ . An empirical correlation in terms of radius and density was created for each source type. These correlations matched the simulation data to within 2% for baths with a bath radius of 20 cm or larger. These correlations and the MCNP tools developed for this project will aid in an actual design of a new manganese bath facility.

## TABLE OF CONTENTS

LIST OF FIGURES .....	iv
LIST OF TABLES .....	vi
ACKNOWLEDGEMENTS.....	vii
Chapter 1 Introduction .....	1
Chapter 2 Literature Review.....	3
2.1 Nuclear Physics Review .....	3
2.2 Mn Bath Characterization Parameters.....	8
2.3 Monte Carlo N-Particle (MCNP) Code.....	9
2.4 Overview of Current Mn Baths.....	12
2.5 Past Work.....	14
Chapter 3 Methodology.....	22
3.1 Mn Bath Parameters Considered and Their Implementation.....	22
3.1.1 Source Type .....	22
3.1.2 Mn Bath Radius.....	26
3.1.3 Solution Density .....	27
3.1.4 Temperature .....	29
3.1.5 Minor Parameters .....	32
3.2 Validation of MCNP Capabilities .....	39
3.2.1 NPL.....	41
3.2.2 Golestan University .....	43
3.2.3 ENEA-INMRI .....	44
3.2.4 Validation Conclusions.....	45
3.3 Simulation Model Setup .....	46
3.3.1 Geometry.....	46
3.3.2 Source .....	50
3.3.3 Tallies .....	52
3.3.4 Materials .....	54
3.4 Running and Processing Simulations .....	55
Chapter 4 Results and Discussion.....	58
4.1 Manganese Absorption Fraction Analysis.....	61
4.2 Leakage Analysis .....	66
4.3 Limitations and Future Work.....	67
4.4 Conclusions.....	68
Appendix A Simulation Data .....	71

Appendix B MCNP Codes .....	80
Appendix C Python Codes .....	92
Appendix D MATLAB Codes.....	100
BIBLIOGRAPHY.....	109

## LIST OF FIGURES

Figure 1. Relevant MnSO <sub>4</sub> solution isotope microscopic cross sections from ENDF/B-VII.0. <sup>7</sup> .....	6
Figure 2. Mn bath reaction and decay scheme. ....	7
Figure 3. Comparison of H to Mn ratio and solution density correlations adapted with permission from four sources. <sup>9,20-22</sup> .....	15
Figure 4. Relative percent error between H to Mn ratios for two published empirical correlations. <sup>20,21</sup> .....	16
Figure 5. Fraction of neutrons absorbed in Mn as a function of solution density adapted with permission from Amendola et al. <sup>9</sup> .....	18
Figure 6. Fraction of neutrons absorbed in Mn as a function of spherical Mn bath radius reprinted with permission from Khabaz. <sup>12</sup> .....	19
Figure 7. Fraction of neutrons absorbed in Mn as a function of cylindrical Mn bath radius reprinted with permission from Khabaz. <sup>13</sup> .....	20
Figure 8. Neutron spectra probability histograms for Am-Be, Cf, and Pu-Be sources from three references. <sup>15,23,25</sup> .....	25
Figure 9. Thermal model of the Mn bath for thermal resistance analysis.....	30
Figure 10. Visualization of 50 simulated neutrons using the surface area emission and cosine distribution models for a source with 1.5 cm radius and 3 cm height.....	35
Figure 11. Visualization of 50 simulated neutrons using the solid angle emission and isotropic distribution models for a source with 1.5 cm radius and 3 cm height.....	35
Figure 12. Diagram of the Mn bath model geometry showing dimensions and material, cell, and surface numbers.....	47
Figure 13. Mn absorption fraction simulation results. ....	58
Figure 14. Mn bath leakage fraction simulation results with 1% leakage level indicated in red.....	58
Figure 15. Mn absorption fraction simulation variance and relative error.....	60
Figure 16. Mn bath leakage fraction simulation variance and relative error.....	60
Figure 17. Comparison of the Mn absorption fraction between Am-Be and Pu-Be.....	62

Figure 18. Power fits with respect to density for constant radii for Am-Be Mn absorption fraction data. ....	63
Figure 19. Exponential fits with respect to radius for power fit coefficients for Am-Be Mn absorption fraction data. ....	64
Figure 20. Relative error between the Mn absorption fraction empirical correlations and simulation data. ....	66
Figure 21. 1% leakage boundary curves. ....	67

## LIST OF TABLES

Table 1. $\gamma$ -rays produced from $^{56}\text{Mn}$ decay with absolute intensity per decay and $1\sigma$ uncertainties. <sup>8</sup> .....	7
Table 2. Neutron reaction probabilities adapted from Amendola et al. for a Mn bath density of $1.1564\text{ g/cm}^3$ . <sup>9</sup> .....	18
Table 3. Average neutron energy for each spectrum calculated by MCNP. ....	25
Table 4. 316L stainless steel isotope composition with density of $7.93\text{ g/cm}^3$ . <sup>25</sup> .....	37
Table 5. Neutron source capsule dimensions. ....	37
Table 6. Neutron source material densities and compositions. ....	39
Table 7. Validation against NPL results.....	41
Table 8. Validation against Golestan Am-Be results. ....	43
Table 9. Validation against Golestan Cf results. ....	44
Table 10. Validation against ENEA-INMRI results. ....	45
Table 11. MCNP input file cell definitions. ....	49
Table 12. MCNP input file source definition summary.....	50
Table 13. Sample F1 and F2 tallies at different surfaces for an Am-Be source in a 40 cm radius Mn bath with $1.3\text{ g/cm}^3$ solution density.....	53
Table 14. Simulation material definition summary. ....	54

## ACKNOWLEDGEMENTS

I would first like to thank almighty God for his grace, my life, and the ability to write this thesis. “For from him and through him and for him are all things. To him be the glory forever! Amen.” (Romans 11:36).

Second, without my family, I would not be here. You all are a constant source of love and support that I cherish most dearly in this life. I would especially like to acknowledge my grandfather, Rodney Bucks. You are the person I look up to the most, and I credit my academic success to you. By teaching me to learn, you have taught me more than any degree. “Learn all you can, all your life, and you’ll never be out of a job.”

Next, I will always be grateful to my supervisor and mentor Dr. Marek Flaska. When you offered me this research project, it changed my academic life. Thank you also for your support in completing this project and your professional advice about graduate school.

Thank you to Dr. Guha Manogharan for bridging the gap between my suspiciously nuclear-engineering-oriented thesis and my honors in mechanical engineering. Without you, this thesis could not have been completed.

Additionally, I am indebted to my past and present honors advisors, Dr. Jacqueline O’Connor and Dr. Margaret Byron. Thank you both for your instruction in writing and formatting this document, advice on scheduling and honors college requirements, and sharp eyes for deadlines.

Finally, thank you to all my professors and peers at Penn State who helped to make my undergraduate career a successful and edifying experience.

## Chapter 1

### Introduction

As society seeks to reduce carbon emissions through green energy production, it seems that nuclear energy must play a key role if this future production is to be both safe and reliable.<sup>2</sup> But, to keep up with ever-increasing demand, nuclear energy must also grow. New nuclear reactor technology will be crucial to meeting sustainability goals, but such growth does not happen in a vacuum. The implementation of new reactors will require an improvement in the available fundamental nuclear data.<sup>3</sup> Similarly, more reactors will require advances in health physics, nuclear security, and waste management. In other words, the entire nuclear industry and supporting infrastructure must continually advance to help society meet its energy goals.

Undergirding all of this infrastructure are neutrons themselves. A well characterized source of neutrons is required for most experimental nuclear research. Some of the most common neutron sources are isotopic neutron sources.<sup>1</sup> These are generally hand-sized capsules that produce a continuous neutron output from fundamental nuclear reactions. Neutron sources can be partially characterized by their strength (rate of total neutron emission) and their spectrum (distribution of emitted neutron energies). For nuclear research, more accurately characterized neutron sources will produce more accurate results. In other aspects of the nuclear industry, well-characterized sources are needed to calibrate radiation detection equipment, which is used abundantly in dose monitoring and security applications.

Around the world, the primary method for measuring neutron source strength is the manganese sulfate bath (shortened to Mn bath).<sup>1,4</sup> A neutron source is immersed in an aqueous

solution of  $\text{MnSO}_4$  which effectively converts neutrons to  $\gamma$ -rays. Technology for counting  $\gamma$ -rays is much more accurate than direct neutron counting, so the neutron strength calculated from the  $\gamma$ -ray measurements provides a higher accuracy. In the U.S., the National Institute of Standards and Technology (NIST) maintains a Mn bath (the only Mn bath facility in the U.S.) for performing legally standardized calibrations for customers including isotopic source manufacturers, detection equipment producers, power plants, fuel suppliers, the Department of Defense, and National Laboratories.<sup>4</sup> The Mn bath facility also supports various other nuclear labs at the NIST. Mn baths are ultimately responsible for the emission rate calibration of the vast majority of well-characterized (traceable) neutron sources in the U.S. and around the globe.

Mn bath technology must continue to grow and improve to support the growth of the nuclear industry. Comparisons of the same neutron source at different National Laboratories' Mn baths have shown that room for improvement exists in terms of determining correction factors to convert from  $\gamma$ -ray measurements to neutron strength.<sup>1</sup> Also, experiments done with Mn baths may help resolve questions regarding modeling and nuclear data.<sup>5</sup> However, it is difficult to justify changing the setup of an integral National Laboratories facility for experimental purposes. To this end, plans are being laid to build a Mn bath facility at the Pennsylvania State University. A Mn bath at the university would be used for research both on and with the Mn bath, in-house measurements of university neutron sources, and education in the nuclear engineering department. This thesis seeks to support this project by developing simulation models and empirical relationships that can be used for future Mn bath design.

## Chapter 2

### Literature Review

#### 2.1 Nuclear Physics Review

As has been previously described, a Mn bath is a neutron detection system that works by converting neutrons into  $\gamma$ -rays. To better understand this process and the need for such conversion, it is helpful to have a basic understanding of some nuclear physics concepts. The topics presented in the following discussion are taken from a nuclear engineering textbook by Lamarsh and Baratta.<sup>6</sup>

A neutron is a subatomic particle with similar mass to a proton, but no electric charge. This lack of charge is partially what makes them difficult to detect, as they do not interact with electromagnetic fields. Another complicating factor is their poor ability to directly ionize matter. Ionization refers to the removal of an electron from an atom. With most other forms of radiation ( $\alpha$ ,  $\beta$ , and  $\gamma$  for example), this newly removed electron, which has a unit charge, can be detected electromagnetically to measure the preceding radiation levels. Thus, a device like a Mn bath is useful for converting neutrons to a more manageable radiation type –  $\gamma$ -rays in this case.

This neutron-to- $\gamma$ -ray conversion is a process that starts with a neutron reaction (absorption). The rate of reaction  $i$  between a group of the same atoms and a population of neutrons is given mathematically by Equation (1).

$$R_i = \sigma_i N \phi \quad (1)$$

In Equation (1), the parameter,  $N$ , is the number density (atoms per volume) of the absorbing material. The quantity,  $\phi$ , is known as the neutron flux, usually measured in neutrons per square-centimeter per second. Heuristically, it describes the number of neutrons passing

through a unit area in a unit time. The final factor,  $\sigma_i$ , is known as the microscopic cross section of the reaction. This may be considered a probability correction factor that balances the two sides of the rate equation and has a unit of area. One commonly used unit is the barn, where  $1 \text{ b} = 10^{-24} \text{ cm}^2$ . The microscopic cross section for any reaction with any atom is a function of neutron energy. Entire databases are devoted to recording cross section data. The product of  $N$  and  $\sigma_i$  is defined as the macroscopic cross section  $\Sigma_i$ . An arbitrary neutron reaction with isotope X is often abbreviated as X(n,j)Y. Here, j represents the lighter reaction product, and the heavier product (Y) and reaction type are implied by balancing the subatomic particles involved.

Cross sections are usually higher for neutrons of lower kinetic energies. Primarily for low-Z materials, neutrons lose energy through repetitive collisions with matter in a process called moderation. These collisions can be described as neutron reactions called scattering ( $i = s$  in Equation (1)). The most prevalent type of scattering (elastic) is analogous to billiard balls. If the mass of the involved particles represents the weight of the billiards, momentum considerations return the fact that 1-H is the most efficient moderator. This is because the 1-H nucleus is only a proton, which has nearly the same mass as a neutron.

The most important class of neutron reactions for this discussion is absorption ( $i = a$  in Equation (1)). In an absorption reaction, a neutron is assimilated into the nucleus of an atom. When an atom absorbs a neutron, the nucleus usually becomes energetically unstable, and a plethora of events may follow to regain stability, including the ejection of a photon or particle from the nucleus. Another possibility is fission, though this is not pertinent to the Mn bath.

Following the absorption of a neutron and the ejection of the minor product, the resulting major product might still be energetically unstable. When this phenomenon occurs, the product is said to be activated and is radioactive. Radioactivity is essentially a means for a nucleus to regain

stability by ejecting particles or photons known as radiation. A population of radioactive atoms can be described using Equation (2).

$$N(t) = N_0 e^{-\lambda t} \quad (2)$$

Here,  $N_0$  is the number density of the radioactive isotope at time  $t = 0$ . The constant  $\lambda$  is called the decay constant and has been precisely measured for most isotopes. The product of the number density and the decay constant is known as the activity of the isotope  $A(t)$ . This describes the number of decays occurring each second (if  $\lambda$  is measured in Hz) per unit volume. One decay per second (dps) is called a Becquerel (Bq), which can be converted to the historically more common unit of Curie (Ci), where  $1 \text{ Ci} = 3.7 * 10^{10} \text{ Bq}$ .

These fundamental topics may be applied to the Mn bath. When a neutron source is placed in the Mn bath, it creates a neutron flux throughout the Mn bath. Various isotopes exist within the Mn bath and its structure for neutrons to react with. These include Mn, S, O, and H in the Mn bath solution and any additional elements present in the Mn bath shell, source holder, and source material itself. Through scattering reactions, the neutrons are moderated, and absorption becomes more likely. The fact that  $^1\text{H}$  is such an efficient moderator makes water a prime candidate for the solvent. The microscopic absorption cross sections of all relevant isotopes in the Mn bath solution are shown in Figure 1. When analyzing available nuclear data to create Figure 1, relevancy was determined based on the cross section magnitude and natural abundance of each isotope. Thus, less abundant isotopes of H, O, and S are not pictured as well as cross sections that did not exceed 0.001 b over the pictured energy range. The average energy of well-moderated neutrons – so-called thermal neutrons at 0.0253 eV in a room temperature moderator – is also noted. All neutrons in the Mn bath will tend to move towards this energy.

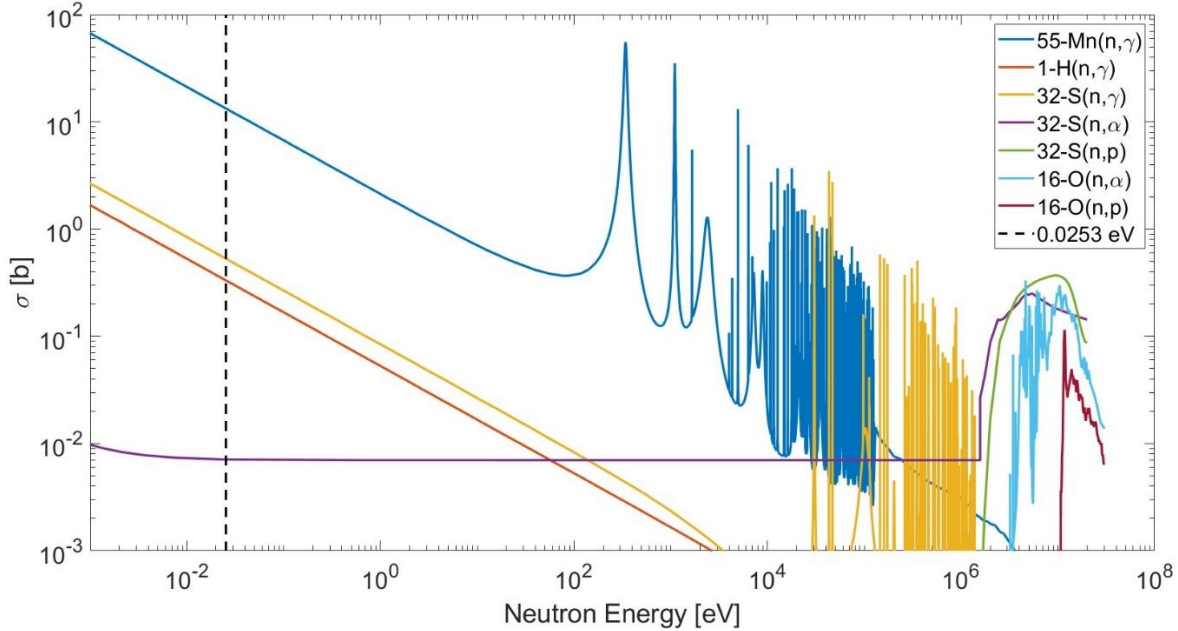


**Figure 1. Relevant  $\text{MnSO}_4$  solution isotope microscopic cross sections from ENDF/B-VII.0.<sup>7</sup>**

Simply from the cross section magnitudes, it may be surmised that a large fraction of the neutrons will be absorbed in the Mn of the solution, which is intentional. There will be some parasitic absorption of neutrons by the other elements, especially 1-H. Although its cross section is lower than of Mn, its number density in the Mn bath is significantly higher (see Equation (1)). For the neutrons that are absorbed by Mn, the only natural isotope of Mn is 55-Mn, so a 55-Mn(n,γ) absorption reaction will occur to produce 56-Mn. This activated 56-Mn decays into 56-Fe by emission of beta minus radiation with a decay constant of  $\lambda = 7.4660 \times 10^{-5} \text{ Hz}$ .<sup>8</sup> This corresponds to a half-life of 2 hours, 34 minutes, and 44 seconds. The resultant 56-Fe is unstable itself and emits a  $\gamma$ -ray to decrease its energy. It is these  $\gamma$ -rays – those emitted by the 56-Fe – that are finally detected. However,  $\gamma$ -rays of several different energies can be produced, which are summarized in Table 1. Nominally, all these photons are detected by the Mn bath detector, but the 846.78 keV is the most important. It is known as a characteristic  $\gamma$ -ray of 56-Mn decay, and it

is what one refers to when speaking of a Mn bath converting neutrons to  $\gamma$ -rays. This process is summarized in Figure 2.

**Table 1.  $\gamma$ -rays produced from  $^{56}\text{Mn}$  decay with absolute intensity per decay and  $1\sigma$  uncertainties.<sup>8</sup>**

Energy [keV]	Energy $\sigma$ [keV]	Intensity [%]	Intensity $\sigma$ [%]
846.7638	0.0019	98.85	0.03
1037.8333	0.0024	0.040	0.005
1238.2746	0.0022	0.040	0.004
1810.726	0.004	26.9	0.4
2113.092	0.006	14.2	0.3
2523.06	0.05	1.018	0.020
2598.438	0.004	0.0198	0.0020
2657.56	0.01	0.645	0.007
2959.92	0.01	0.306	0.005
3369.81	0.04	0.168	0.010

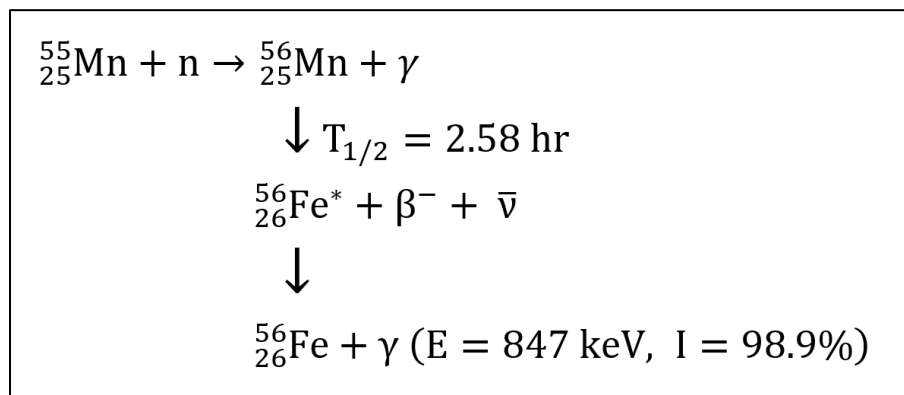


**Figure 2. Mn bath reaction and decay scheme.**

## 2.2 Mn Bath Characterization Parameters

The  $\gamma$ -rays produced by the Mn bath are detected by a variety of means that will be discussed later. However, knowing the number of  $\gamma$ -rays intercepted by the detector is not enough to know the strength of the neutron source. Some conversion must be performed. Throughout the literature, various authors write this conversion differently, but it can be summarized most simply by Equation (3).<sup>9</sup>

$$S = \frac{C}{\varepsilon_d \varepsilon_{Mn}} \quad (3)$$

In Equation (3),  $S$  is the strength of the neutron source in neutrons produced per second, and  $C$  is the number of  $\gamma$ -rays counted by the detector per second. The two remaining terms are correction factors. First,  $\varepsilon_d$  is the absolute detector efficiency. This term describes the fraction of  $\gamma$ -rays counted on the detector per 56-Mn activation. It accounts for the fact that only a small number of the  $\gamma$ -rays produced by 56-Mn decay will be detected. More information on the absolute efficiency of radiation detection equipment can be found in Knoll.<sup>10</sup>

In practice, detector efficiency is commonly found by preparing a solution of 56-Mn with known activity. Knowledge of the  $\gamma$  activity is gained via well-established detection methods, namely  $4\pi\beta$ - $\gamma$  coincidence liquid scintillation counting.<sup>9,11</sup> These methods are too involved to perform for every usage of the Mn bath, but they provide very precise measurements. The known solution is then introduced into the Mn bath detection system and allowed to decay. During the decay, a series of measurements are taken with the Mn bath detector. For a measurement starting at time  $t$  after introduction of the solution and lasting for some other time  $T$ , the detector will record  $\hat{C}$  net counts. Such measurements can be used to find the detector efficiency with the formulation given by Amendola et al. in Equation (4).<sup>9</sup>

$$\varepsilon_d = \frac{\lambda e^{\lambda t}}{A_0} * \frac{\hat{C} - BT}{1 - e^{-\lambda T}} \quad (4)$$

Equation (4) may be derived using Equation (2) and integration. In Equation (4),  $A_0$  is the initial  $^{56}\text{Mn}$  activity at  $t = 0$ , and  $B$  is the background radiation level in counts per time. This background level can be found by taking a measurement without activated solution. The detector efficiency is highly dependent on the geometry of the detection system and the type of detector used, but it only needs to be determined once for a particular bath-detector combination.

The other correction factor,  $\varepsilon_{Mn}$ , describes the ratio of neutrons absorbed in  $^{55}\text{Mn}$  to neutrons emitted by the source. This is highly dependent on the Mn bath geometry, solution density, temperature, and source type. In the past, analytical approximations for  $\varepsilon_{Mn}$  have been developed and can be found in several papers.<sup>9,11,12</sup> These approaches rely on splitting  $\varepsilon_{Mn}$  into four parameters and approximating each separately. However, most facilities now rely on simulations to calculate a single value of  $\varepsilon_{Mn}$ . Simulations can handle more accurate cross section data, account for a larger variety of Mn bath designs, and are independent of the assumptions used in the analytical approach. The most popular code used by National Laboratories is the Monte Carlo N-Particle program (MCNP).<sup>5,9,11-14</sup>

### 2.3 Monte Carlo N-Particle (MCNP) Code

MCNP is a Monte Carlo radiation transport code developed and maintained by Los Alamos National Laboratory.<sup>15,16</sup> It is a versatile code that can be used to determine the behavior of neutrons, photons, and electrons in a user defined space. Monte Carlo methods solve radiation transport problems by simulating the statistical probabilities of possible interactions. Taking the case of a Mn bath, a user can create the relevant Mn bath geometry and populate the spaces with

materials of specified compositions and densities. Next, a neutron source can be defined to produce neutrons into this space having certain distributions of energy and direction. The code then tracks the life of each neutron, one after another. Probability distributions are used to choose the next event experienced by the neutron until its termination. This termination can be escape from the defined geometry or absorption, among other things. By simulating a large number of neutrons, a realistic description of the Mn bath can be achieved. With MCNP, so-called “tallies” can be set up to count the number of neutrons absorbed in Mn, among many other quantities. If performed correctly, this allows for the determination of  $\varepsilon_{Mn}$ .

Three important tallies used in Mn bath simulations in the literature are the F1, F2, and F4 tallies. The F1 and F2 tallies have both been used to calculate the leakage of neutrons out of the Mn bath in several papers; however, the descriptions in the MCNP user manual seem to suggest that the F1 tally would be better suited to this job.<sup>5,9,12,16</sup> The F1 tally counts the total number of particles that pass through a surface in any direction. The F2 tally estimates the net current on a surface by taking the limit as the thickness of a corresponding volume goes to zero. The MCNP documentation calls F1 the current and F2 the surface flux, even though the F2 tally aligns with the reactor physics definition of current. F2 seems to have the benefit of directional dependence, but its incorporation actually results in particles that graze the surface contributing more to the flux than particles that pass through normal to the surface. Meanwhile, directional dependence can be applied to the F1 tally through angular binning. The practical differences between the F1 and F2 tallies will be explored further in Section 3.3.3. On the other hand, agreement exists on the use of the F4 tally. This is used to calculate reaction rates in MCNP. It sums the path length of each neutron in a certain space and averages by the volume. This essentially gives the neutron flux

specified in Equation (1), and cross sections and target atom number densities can be applied by MCNP to calculate reaction rates.

Because of the probabilistic nature of Monte Carlo methods, MCNP always reports an uncertainty with every tally.<sup>16</sup> This is given as a relative error ( $E_R$ ) defined as the sample standard deviation of the tally (variance to  $1\sigma$ ) divided by the average tally value. The MCNP manual suggests that relative errors more than 0.50 (50%) are not meaningful at all. Only once the relative error is reduced below 0.10 is it designated as “generally reliable.” Between these relative errors, results are still questionable.

One of the benefits of MCNP is that it uses continuous cross section data while some radiation transport solution methods require averaging these cross sections. This results in more accurate solutions overall. Accordingly, the choice of cross section database (also called a library) used by MCNP has been seen to affect the simulation results. Among most research, the preferred library is the Evaluated Nuclear Data File (ENDF) of the U.S. and Canada. However, in the comparison of eight National Laboratories, two labs used older versions of the library (ENDF/B-V.0) which caused a noticeable difference in their measurements of the same neutron source compared to other participants.<sup>11</sup> When their results were recalculated using ENDF/B-VI.0, an approximate 2% increase in measured source strength occurred, which smoothed out the discrepancies. Khabaz also remarks on the importance of ENDF version.<sup>12</sup> Both papers agree that the issue lies with the  $^{16}\text{O}(n,\alpha)$  reaction data. ENDF/B-V.0 and ENDF/B-VII.0 show agreement, while ENDF/B-VI.0 and ENDF/B-VI.8 return larger values.

The National Laboratories comparison results were published in the same year that ENDF/B-VII.0 was released.<sup>7,11</sup> The consensus then seemed to be that ENDF/B-VII.0 was the most accurate in terms of the  $^{16}\text{O}$  cross section.<sup>5</sup> Vasiliev et al. support this claim by comparing

ENDF data to the independently determined JENDL (Japan) data for  $^{16}\text{O}(n,\alpha)$ .<sup>17</sup> ENDF/B-VII.0 most closely matched JENDL compared to ENDF/B-VI.8. In 2018, ENDF/B-VIII.0 was released.<sup>7</sup> However, this is too new to be included in MCNP distributions, so it is not relevant to this work.<sup>16</sup>

Despite this issue, MCNP remains the top method for determining  $\varepsilon_{Mn}$  at National Laboratories, especially in the West.<sup>11</sup> Of the eight labs mentioned above, five used MCNP. Two of the outliers were Russian and Chinese labs. The last was the U.S. NIST, which cited the 16-O cross section data as the reason for avoiding the use of MCNP. Additionally, one author suggests that experiments performed on Mn baths might provide one avenue for exploring the discrepancies between cross section data for  $\text{MnSO}_4$  constituent elements.<sup>5</sup>

## 2.4 Overview of Current Mn Baths

Mn baths exist at National Laboratories and universities around the globe. A survey of their similarities and differences may inform research into the design of such devices. First, there is the Mn bath structure itself. The majority of labs use stainless steel spheres.<sup>11,18</sup> However, polyethylene is another suitable material, and cylinders are also used. The benefit to using a sphere is that it is easier to understand in one dimension, which was especially important historically. One material to be avoided is aluminum, which corrodes under interaction with the  $\text{MnSO}_4$  solution. Mn baths, like the one at the NIST, must be coated in a secondary material if aluminum is used structurally.<sup>19</sup>

Mn bath sizes range from 50 cm to 130 cm in diameter.<sup>9,11-14,18</sup> Mn bath size is known to affect the manageable range of source strengths, so a few labs maintain two Mn baths of different sizes.<sup>14</sup> Solution density also varies across the literature from 1.05 to 1.40 g/cm<sup>3</sup>. Most Mn baths

operate above  $1.20 \text{ g/cm}^3$  though.<sup>11</sup> As far as the  $\gamma$ -ray detection system is considered, NaI systems are the norm – although the NIST has the option to use a high purity Ge detector (HPGe).<sup>4,11,18</sup> More information on NaI and HPGe detectors can be found in Knoll.<sup>10</sup>

Perhaps the greatest variability between Mn baths lies in their operation. When a source is introduced into the Mn bath (at time  $t = 0 \text{ s}$ ), the activity of the Mn increases according to Equation (5):

$$A(t) = S\varepsilon_{Mn}(1 - e^{-\lambda t}) \quad (5)$$

For normal measurements, all facilities wait between 24 and 48 hours for the 56-Mn activity to approach its asymptotic value.<sup>11</sup> From here, several Mn baths circulate the solution past a detector that is spatially separated from the main Mn bath volume. Others replace the source with the detector or take a solution sample to a detector. The first method has the advantage of being able to measure the steady state activity of the Mn bath, eliminating extra time dependence in the measurement. Time dependence is introduced when the source is removed from the Mn bath and the Mn activity begins to decay as seen in Equation (2). However, less piping reduces the possibility of solution leakage, and a pump can add unwanted heat to the solution that changes the density. A detector cannot generally be placed in the Mn bath near the source for two reasons. First, neutrons would then have the potential to activate the detector. Second, the prompt  $\gamma$ -rays produced from the conversion of 55-Mn to 56-Mn and other Mn bath reactions would further complicate the conversion ratio between detector counts and Mn activity.

Special attention should also be given to the Mn bath at the NIST as an outlier in terms of measurement procedure.<sup>4,19</sup> All the other Mn baths – and much of the previous discussion – have assumed that an absolute measurement of the neutron source is desired. This requires knowing the  $\varepsilon_d$  and  $\varepsilon_{Mn}$  factors. However, the NIST performs comparative calibrations. For every

measurement, a corresponding measurement is made of NBS-1 (the National Bureau of Standards was the precursor to the NIST), a U.S. legal standard neutron source whose strength is known and set. The strength of the new source is measured via the ratio of the induced detector counts from the new source and NBS-1. This frees the NIST from needing to accurately know the Mn bath properties as long as they are kept constant between measurements. The obvious disadvantage is that every measurement is tied to a metrological artifact rather than first principles.

## 2.5 Past Work

In order to perform MCNP simulations of Mn baths, information on the solution density and source type is required. In terms of density, MCNP must know either the mass density or number density of each material in the simulation.<sup>16</sup> Additionally, the relative fraction of each isotope in the material must be known. In the lab, it is relatively simple to determine the density of a solution sample.<sup>9,20,21</sup> However, this overall density is not enough to define the concentration of the solution from first chemical principles. Thus, in many reports, solutions are also characterized by their ratio of H to Mn atoms, for this can be easily used to determine the isotope fractions for input to MCNP. This ratio can be experimentally determined, but it is much more tedious than measuring density.  $\text{MnSO}_4$  concentration is another commonly quoted parameter. This is the easiest to control when mixing solution. Bittencourt et al. show that knowledge of two of these parameters mathematically defines the third via Equation (6).<sup>20</sup>

$$\rho = \left( 1 + \frac{1}{2} \frac{N_H}{N_{Mn}} \frac{\bar{A}_{H_2O}}{\bar{A}_{MnSO_4}} \right) C_V \quad (6)$$

In Equation (6),  $\rho$  is the solution mass density, and  $C_V$  is the solution concentration (mass of solute per volume of solution). The  $\bar{A}$  parameters represent atomic weights, and  $N$  again stands

for number density. If the number density ratio is treated as a single parameter, this equation has three variables. Thus, having an empirical relationship between solution density and H to Mn ratio or  $C_V$  would be extremely useful for performing more than a single simulation. Such a relationship would allow for a complete MCNP input definition given a single solution density input parameter.

Work has been done to develop such a relationship. Deckwer gives seven discrete pairs of density and concentration measurements at 20 °C.<sup>22</sup> A formula for adjusting density for temperature is also given. Bittencourt et al. give an empirical relationship between the H to Mn ratio and  $MnSO_4$  concentration at 20 °C.<sup>20</sup> Additionally, Amendola et al. record several density-concentration pairs in the course of their work at low densities.<sup>9</sup> Finally, De Volpi et al. give a polynomial fit for a collection of density and concentration values at 30 °C.<sup>21</sup> These four independent determinations are plotted on the same graph in Figure 3 for density and H to Mn ratio. The data from De Volpi et al. has been corrected to 20 °C using the formula reported by Deckwer. In Figure 4, the relative percent error between the correlations given by Bittencourt et al. and De Volpi et al. is graphed as a function of solution density.

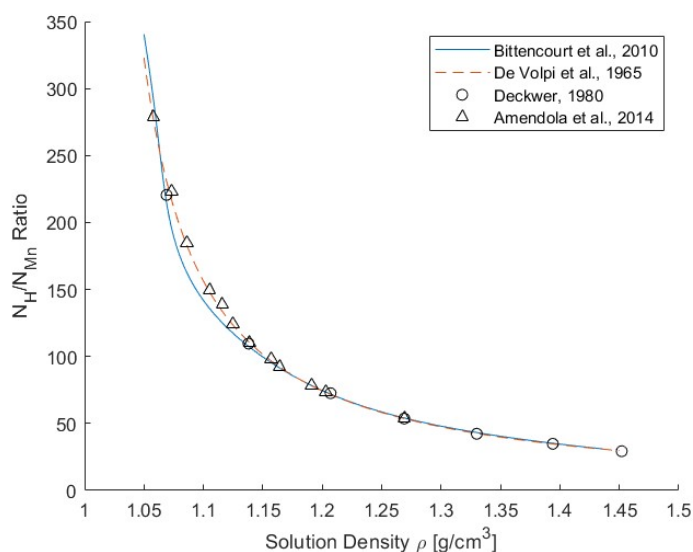


**Figure 3. Comparison of H to Mn ratio and solution density correlations adapted with permission from four sources.<sup>9,20-22</sup>**

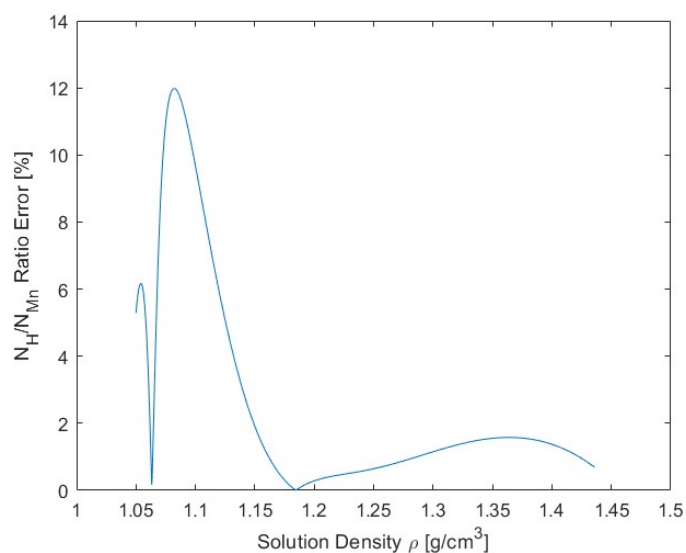


**Figure 4. Relative percent error between H to Mn ratios for two published empirical correlations.**<sup>20,21</sup>

For solution densities above 1.2 g/cm<sup>3</sup>, the disagreement between the two empirical correlations is less than 2%. However, smaller densities differ by almost as much as 12% at 1.08 g/cm<sup>3</sup>. For these low densities, the correlation by De Volpi et al. more accurately represents the discrete data. Thus, this correlation is the strongest candidate for determining simulation inputs.

Source type refers to the manner in which a source makes neutrons. The method of neutron production affects the birth energy distribution of the neutrons, known as the neutron spectrum. The energy of the neutrons affects the cross sections within the Mn bath, changing  $\epsilon_{Mn}$ . One popular source is 252-Cf, which produces neutrons through spontaneous fission. This is a type of radioactive decay where the atom simply fissions, producing two lighter elements and a few neutrons. The neutron spectrum of 252-Cf is described by the Watt fission spectrum (WFS), which is built into MCNP.<sup>15</sup> Two other common sources are Pu-Be and Am-Be. Here an isotope of Pu or 241-Am decays by  $\alpha$  radiation, which goes on to cause a 9-Be ( $\alpha$ , n) reaction. To use these spectra in MCNP, a histogram giving the probability of a neutron being born within a certain

energy range is needed. Data for producing these histograms can be found in the International Atomic Energy Agency's (IAEA) neutron spectra compendium.<sup>23</sup> The method for processing this data will be explored in Section 3.1.1.

The majority of published Mn bath simulations are meant to supplement research at a particular facility, rather than promote the creation of new Mn baths. For example, Roberts and Parfitt performed a simulation of the remodeled Mn bath facility at the National Physical Laboratory in the U.K.<sup>14</sup> Interestingly, a Chinese software called MCAM was used to convert a computer-aided-drafting file of the facility to the MCNP format. This allowed for a far more intricate geometrical input to MCNP than is normally obtained. Additionally, the so-called "room return" was evaluated in MCNP. This describes the number of neutrons which leave the Mn bath and subsequently return after scattering off the surroundings. In fact, 5.5% of the neutrons that leaked from the Mn bath eventually returned.

The work of Ogheard et al. was performed to determine the  $\varepsilon_{Mn}$  factor for the Mn bath at the Henri Becquerel National Laboratory in France.<sup>5</sup> Similarly, the simulation domain was also extended to evaluate room return. Uniquely, a method for determining the validity of the  $\varepsilon_{Mn}$  determination is proposed by varying Mn bath parameters to predictably change  $\varepsilon_{Mn}$  then comparing the resulting measurements.

A few papers have started to generalize the Mn bath simulation process. Amendola et al. are mainly focused on characterizing the Mn bath at the Italian National Institute of Ionizing Radiation Metrology, but they performed simulations over a range of densities.<sup>9</sup> The Mn bath in question is a 100 cm diameter stainless steel sphere with 5 mm thick walls. An Am-Be source is held within a polytetrafluoroethylene (PTFE) cylinder in the center of the Mn bath. The probability of neutron capture in Mn as a function of density for this Mn bath is shown in Figure 5. When the

nominal operating density of the Mn bath was set in the MCNP simulation, the results shown in Table 2 were obtained. From a separate experiment,  $\epsilon_d$  was found to be  $(7.21 \pm 0.05) * 10^{-5}$ . The trend in Figure 5 clearly shows that greater solution density increases the Mn absorption fraction. This is because a denser solution contains more Mn compared to H, so the  $^{55}\text{Mn}(n,\gamma)$  reaction rate will be relatively higher.

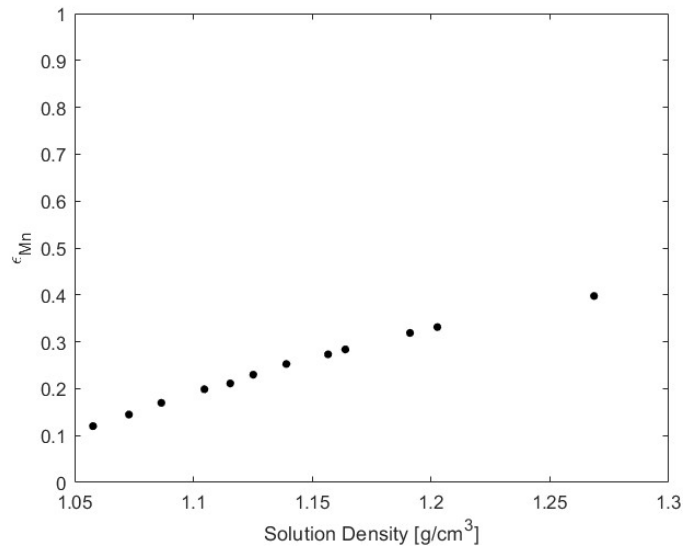


**Figure 5. Fraction of neutrons absorbed in Mn as a function of solution density adapted with permission from Amendola et al.<sup>9</sup>**

**Table 2. Neutron reaction probabilities adapted from Amendola et al. for a Mn bath density of 1.1564 g/cm<sup>3</sup>.<sup>9</sup>**

<b>Reaction</b>	<b>Probability</b>	<b>Relative Error</b>
H(n,Total)	0.65666	0.0015
O(n,Total)	0.01688	0.1422
S(n,Total)	0.01266	0.0711
Mn(n, $\gamma$ )	0.27185	0.0037
Leakage	0.02073	0.4824
Holder and Source Absorption	0.02814	0.1862

In two papers, Khabaz performed MCNP simulations of spherical and cylindrical Mn baths at varying radii.<sup>12,13</sup> Two source types were studied, namely <sup>252</sup>Cf and Am-Be with minor variations in solution density for the cylindrical case. For both Mn bath types, empirical correlations describing the fraction of neutrons that leak from the Mn bath are provided as functions of bath radius. These correlations are simple exponential functions. Khabaz notes that the shape of the Mn bath is inconsequential as long as it is large enough to prevent the majority of neutrons from leaking. This was monitored quantitatively by proposing a cap of 1% on neutron leakage. These papers also demonstrate the importance of source type, as Am-Be sources required a larger Mn bath diameter (by about 40 cm) than <sup>252</sup>Cf to meet the leakage requirement. This is due to the higher-energy spectra of Am-Be sources. The more energetic neutrons require a larger volume of water to be moderated for absorption. The  $\epsilon_{Mn}$  factors computed by Khabaz for the spherical Mn bath are shown in Figure 6 as a function of Mn bath radius. The larger values for <sup>252</sup>Cf are again due to the spectra differences.

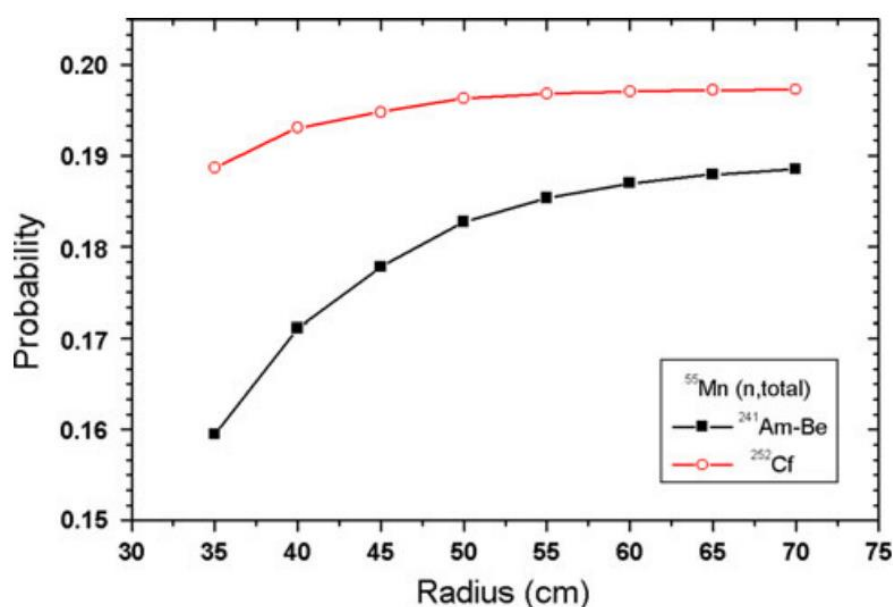


**Figure 6. Fraction of neutrons absorbed in Mn as a function of spherical Mn bath radius** reprinted with permission from Khabaz.<sup>12</sup>

The same results obtained for the cylindrical Mn baths (with height equal to diameter) are shown in Figure 7 below. Here, CI, CII, and CIII denote solutions of increasing  $\text{MnSO}_4$  concentration. Raising the solution concentration increases the Mn number density. This makes neutron interactions with  $\text{MnSO}_4$  more likely, increasing  $\epsilon_{Mn}$ .

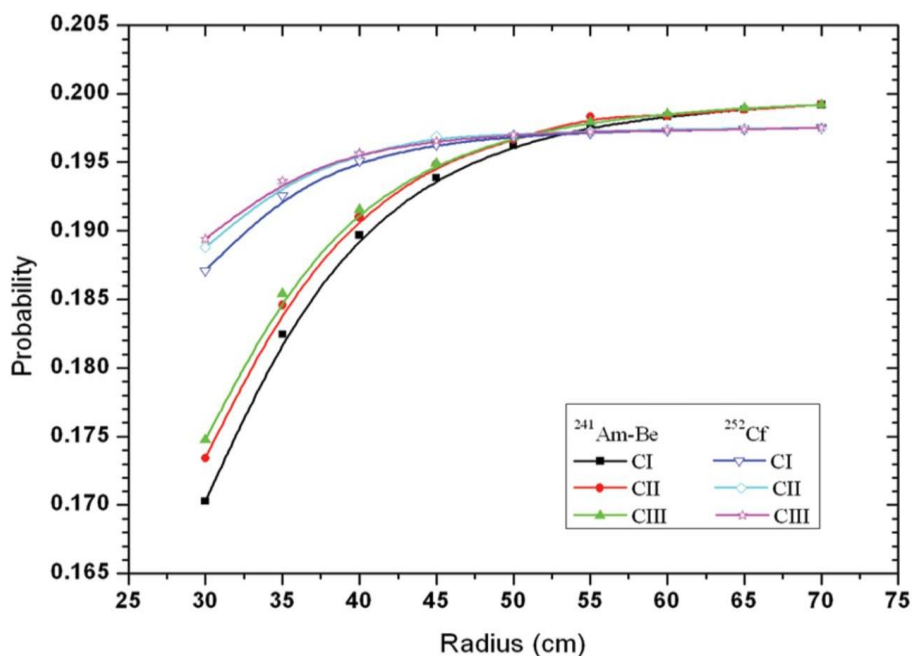


**Figure 7. Fraction of neutrons absorbed in Mn as a function of cylindrical Mn bath radius reprinted with permission from Khabaz.<sup>13</sup>**

Figure 6 and Figure 7 demonstrate that the Mn absorption fraction increases asymptotically for larger radii. For larger Mn baths, neutrons undergo more moderation and are less likely to escape. To balance this, the fraction of neutrons that are absorbed must increase, so  $\epsilon_{Mn}$  increases. As the probability of leakage tends towards zero for increasingly large Mn baths, absorption is nearly guaranteed, so the  $\epsilon_{Mn}$  stabilizes for a certain concentration.

The current literature surrounding Mn bath technology shows that it is a well-established method for measuring the strength of neutron sources. A variety of Mn baths are in use at National Laboratories around the world. Despite the differences in procedure, they all operate by counting

the  $\gamma$ -rays produced from the decay of  $^{56}\text{Mn}$  originating from the absorption of neutrons by  $^{55}\text{Mn}$  in the Mn bath. A key to successful use of the Mn bath is knowledge of the fraction of source neutrons absorbed in Mn,  $\epsilon_{Mn}$ . This parameter is commonly found via MCNP simulations, which allows for the creation of very specific Mn bath models. Despite the near-universal use of Monte Carlo methods in the determination of  $\epsilon_{Mn}$ , very little work has been done to unify these discrete simulations under one empirical correlation. The lack of a more general correlation may be due to the static nature of the Mn baths in use. Each laboratory has a certain Mn bath, so there is no need to perform a range of simulations for unchanging parameters.

However, for a lab attempting to build an optimized Mn bath, a general correlation would be very helpful. Such a relation could severely reduce the number of simulations required for Mn bath design. Additionally, it could remove much of the learning curve associated with MCNP, opening Mn bath design to a more diverse range of researchers and engineers. Accordingly, the objective of this thesis is to combine the effects of several Mn bath parameters – namely radius, source type, and solution density – into a single empirical correlation for  $\epsilon_{Mn}$ . This is to support the eventual goal of bringing a Mn bath to The Pennsylvania State University. A byproduct of this thesis will be a collection of validated and robust MCNP simulations and programming infrastructure that can be used by future researchers for additional work on the Mn bath.

## Chapter 3

### Methodology

#### 3.1 Mn Bath Parameters Considered and Their Implementation

Many Mn bath characteristics contribute to the final value of the Mn absorption fraction. The following subsections describe the parameters considered and how each was implemented in MCNP. The goal is to describe the assumptions and interpretations used to translate a physical situation into a simulation. From the literature, four primary parameters were identified for inclusion in the desired empirical correlation as source type (source spectrum), Mn bath radius, solution density, and solution temperature. However, an argument will be made for neglecting the effects of temperature. Additionally, minor parameters like source spatial distribution, cross section library, and source material affect  $\varepsilon_{Mn}$  but were not included in the final correlation.

##### 3.1.1 Source Type

The primary effect of using a different isotopic neutron source type is that the average energy of the neutron spectrum will change.<sup>12,13</sup> More energetic neutrons will require a larger volume of water to be moderated for absorption. Thus, sources with faster spectra tend to have lower values of  $\varepsilon_{Mn}$  and more leakage for the same Mn bath. It was decided to test the effect of three different sources on  $\varepsilon_{Mn}$ , namely Am-Be, Cf, and Pu-Be. The Am-Be and Pu-Be sources generate neutrons via the  $^9\text{Be}(\alpha, n)$  reaction while the  $^{252}\text{Cf}$  source undergoes spontaneous fission. It is quite difficult to measure the spectrum of a neutron source due to the need to moderate neutrons before capture and detection.<sup>10</sup> This usually destroys – or at least heavily discretizes –

the neutron energy information. Additionally, the isotopic purity of Cf and Pu in these source types affects the spectra.<sup>1,24</sup> It is very difficult to control the purity of 252-Cf and 239-Pu in comparison to other isotopes of Cf and Pu during source fabrication. Similar difficulties arise in measuring the purity in a way that does not affect the neutron spectrum, and the purity changes noticeably over time due to decay into other radioactive products. In the literature, the 241-Am-Be spectrum is often taken from the International Organization for Standardization (ISO) 8529-1 standard.<sup>9,12,25</sup> This reference also contains a 252-Cf spectrum, but MCNP already has a built-in distribution for the WFS.<sup>15</sup> The Pu-Be source as applied to the Mn bath is not often encountered in available literature, and no ISO reference exists for this source type.

However, the ISO spectra are not freely available, and it was desired to have one reference for all three spectra for this project. Accordingly, a compendium of neutron spectra published by the IAEA has been used as the spectra reference for this work.<sup>23</sup> The compendium gives spectra data for a large variety of source types in the form of neutron flux per unit change in lethargy ( $\phi(u)$ ). Neutron lethargy is a way to measure neutron energy where a change in lethargy is given by Equation (7).<sup>1</sup>

$$\Delta u = \ln\left(\frac{E_{high}}{E_{low}}\right) \quad (7)$$

The values of  $E_{high}$  and  $E_{low}$  are the energy bin bounds for which the flux ( $\phi$ ) has been calculated. However, MCNP most readily accepts spectra inputs in the form of a histogram where each bin corresponds to an energy range and the height gives the probability ( $P$ ) that a neutron will be born in that energy range.<sup>15</sup> To convert from the IAEA presentation to an MCNP histogram, the discretized approximation of Equation (8) was used.

$$P(E_{low} < E < E_{high}) = \frac{1}{\eta} \int_{u_{high}}^{u_{low}} \phi(u) du \approx \frac{\phi(u) \Delta u}{\eta} = \frac{\phi(u)}{\eta} * \ln\left(\frac{E_{high}}{E_{low}}\right) \quad (8)$$

The normalization term  $\eta$  was chosen such that the sum of all bin probabilities was unity. For each source type,  $\eta$  was found to be  $\frac{1}{10} \ln(10)$ . This may suggest that the lethargy bins were originally calculated using a base-10 logarithm which would make  $\eta = \frac{1}{10}$ .

The probability histograms for 241-Am-Be, 252-Cf, and 239-Pu-Be spectra taken from the IAEA have been plotted in Figure 8. The WFS used by MCNP for 252-Cf has also been plotted with the same number of energy bins as the IAEA 252-Cf spectrum. This has been generated from the WFS continuous probability distribution function shown in Equation (9) for energy in MeV.<sup>15</sup>

$$\chi(E) = 0.6395 * e^{\left(-\frac{E}{1.18}\right)} * \sinh(\sqrt{1.03419E}) \quad (9)$$

The number of neutrons born into the incremental energy region  $dE$  is given by  $\chi(E)dE$ . Thus, numerical integration from the low to high energy bounds of each bin was used to convert Equation (9) into discrete probabilities. Additionally, Roberts gives a histogram generated from the ISO standard in an example MCNP input file.<sup>25</sup> This has also been included in Figure 8 for comparison.

Figure 8 shows that there is close agreement between the IAEA Cf spectrum and the analytical WFS. Indeed, when MCNP is given a histogram, it reports the average energy of the distribution. These average energies are reported in Table 3, and the IAEA Cf average matches the WFS average within 7%. The agreement between these two spectra – both in shape and average energy – affirms the method of processing the IAEA data shown in Equation (8). However, the shape of the IAEA and ISO Am-Be spectra are clearly different, although the average energies agree within 4%. One possible source of this discrepancy is that the underlying measurements behind each spectrum may be different. This would highlight the need to improve available nuclear data and the difficulty of measuring neutron spectra.

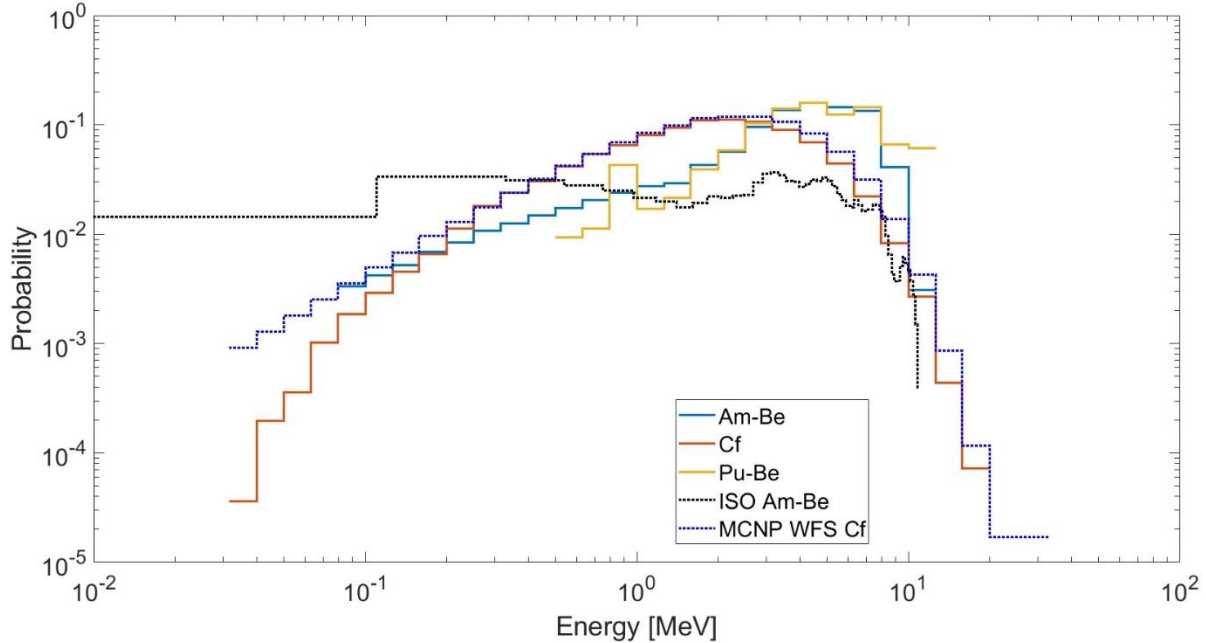


**Figure 8. Neutron spectra probability histograms for Am-Be, Cf, and Pu-Be sources from three references.**<sup>15,23,25</sup>

**Table 3. Average neutron energy for each spectrum calculated by MCNP.**

Spectrum	Average Energy [MeV]
IAEA 241-Am-Be	3.9993
IAEA 252-Cf	2.2759
IAEA 239-Pu-Be	4.8396
ISO 241-Am-Be	4.1581
WFS 252-Cf	2.1300

Because of the generalized nature of the research goal, the IAEA spectra have been deemed acceptable for the present work. The facts that many spectra (for sources beyond Am-Be, Cf, and Pu-Be as well) are readily available and that a method for processing this data into MCNP has been established outweigh the benefit of the more acknowledged ISO spectra. Except in some

validation work, the IAEA spectra was used for Am-Be and Pu-Be sources, and the WFS was used for Cf in this thesis.

### 3.1.2 Mn Bath Radius

The size of a Mn bath affects the Mn absorption fraction by changing the amount of available moderation before a neutron reaches the shell and escapes.<sup>1</sup> For a very large Mn bath, practically all of the neutrons that escape the source holder will be moderated and absorbed in the Mn bath solution. Thus,  $\varepsilon_{Mn}$  would be determined mainly by the solution concentration and to a lesser extent by the holder shape and material. However, as the Mn bath shrinks, the probability that a neutron leaks increases, so the overall solution absorption goes down. It should be noted that there is a disadvantage to having an overly large Mn bath. When the solution is mixed, the specific activity (activity per unit volume) will be small, which makes detection of the  $\gamma$ -rays less probable. Thus, longer counting times will be required to achieve the same statistical uncertainty.

Because the vast majority of Mn baths are spherical, this work considered a spherical Mn bath. Accordingly, the size of the Mn bath was controlled by the radius. This was taken as the radius of the sphere making up the inner shell of the Mn bath. The range of radii to be studied was set at 10 cm to 75 cm. This encompasses all of the Mn baths encountered in the literature.

In MCNP, the simplest means for defining the 3D simulation geometry is through the union and intersection of basic mathematical surfaces.<sup>15</sup> Cylinders, planes, and spheres can be defined by their geometrical parameters and positions, and volumes (cells) are defined by the intersection and union of the spaces bounded by these surfaces. To simplify the simulation, the Mn bath was modeled as a complete sphere filled with solution – ignoring the port for inserting the source.

Without specific knowledge of the Mn bath design, this was the best way to generalize the final simulations. Additionally, several other authors use this same simplification.<sup>9,12</sup> More information on the final Mn bath geometry can be found in Section 3.3.1.

### 3.1.3 Solution Density

The density of the Mn bath solution affects  $\varepsilon_{Mn}$  because the density determines the concentration of the solution components, and reaction rate is directly proportional to atomic number density (see Equation (1)). An MCNP simulation requires the overall solution density (number or mass) and the fractional composition of the solution (atomic or mass) for defining the solution material, and it needs the solution element number densities for computing reaction rate F4 tallies.<sup>15</sup>

As has been discussed in Section 2.5, a single parameter can mathematically define the solution if Equation (6) and an empirical correlation between density and concentration are used. The mass density ( $\rho$ ) of the solution was used as the controlling parameter in this work due to its prominence in MCNP input files. An explanation of the calculations of the other parameters needed for MCNP follows.

First, the empirical correlation proposed by De Volpi et al. is repeated in Equation (10) below.<sup>21</sup>

$$C_M = -1.4088 + 1.4227(\rho^*) + 0.56713(\rho^*)^2 - 0.77726(\rho^*)^3 + 0.20073(\rho^*)^4 \quad (10)$$

Here,  $C_M$  denotes the solution concentration in terms of solute mass per mass of solution ( $\frac{g}{g}$ ), and

$\rho^*$  is the solution mass density ( $\frac{g}{cm^3}$ ) measured at 30 °C. De Volpi et al. also give an expression

for  $C_V$  (mass of solute per solution volume) which is required for Equation (6). However,  $C_M$  is

not dependent on temperature while  $C_V$  changes with the thermal expansion of water. Thus, the  $C_M$  equation serves as the starting point for solution parameter calculations.

It was desired to carry out simulations assuming room temperature conditions, so Equation (11) from Deckwer was used to convert a desired density ( $\rho$ ) at 20 °C to the  $T^* = 30$  °C equivalent.<sup>22</sup>

$$\rho^* = \rho - \left(5.3 * 10^{-4} \frac{\text{g}}{\text{cm}^3 \text{ } ^\circ\text{C}}\right) (T^* - 20 \text{ } ^\circ\text{C}) \quad (11)$$

Combining Equations (10) and (11) allows for the calculation of  $C_M$  from  $\rho$ . Next,  $C_V$  can be calculated from  $C_M$  using Equation (12).

$$C_V = \rho C_M \quad (12)$$

Next, basic stoichiometry allows for the calculation of the number densities of the solution components in Equation (12).

$$\begin{bmatrix} N_H \\ N_{Mn} \\ N_O \\ N_S \end{bmatrix} = \begin{bmatrix} \frac{2N_A(\rho - C_V)}{\bar{A}_{H_2O}} \\ \frac{N_A C_V}{\bar{A}_{MnSO_4}} \\ \frac{N_H}{2} + 4N_{Mn} \\ N_{Mn} \end{bmatrix} \quad (13)$$

The  $\bar{A}$  parameters are atomic weights, and  $N_A$  is Avogadro's number. As a check on Equation (13), dividing  $N_H$  by  $N_{Mn}$  and rearranging returns Equation (6). Finally, the atomic fractions of each element in the solution can be found by dividing the element's number density by the sum of the four number densities. With this and Equations (10) through (13), a full MCNP input – at least in terms of the  $\text{MnSO}_4$  solution – can be derived from a chosen solution density. A MATLAB script (`Mn_Bath_MCNP_Parameters.m`) has been developed for calculating MCNP input parameters from a given density or density range using a function to implement the correlation by De Volpi et al. (`MNSO4_NumDen_DV2.m`). These can be

found in Appendix D. Based upon common operating densities and the range of data used to develop Equation (10), a range of 1.05 to 1.40  $\frac{\text{g}}{\text{cm}^3}$  was studied for the final empirical correlation.

### 3.1.4 Temperature

The temperature of the Mn bath solution theoretically has a dual effect on Mn bath performance. First, thermal expansion of the solution decreases solution density, which lowers the reaction rates between neutrons and the Mn bath solution. From Equation (11), a 10 K increase in temperature corresponds to  $0.0053 \frac{\text{g}}{\text{cm}^3}$  decrease in solution density. Carrying this through yields a drop in number densities of 0.44%.

Additionally, increased water temperature increases the final average energy of moderated neutrons.<sup>6</sup> In a room temperature environment (20 °C = 293 K), the average thermal neutron energy is 0.025 eV, which can be calculated using Equation (14).

$$\bar{E} = k_B T \quad (14)$$

The temperature must be measured in Kelvin, and  $k_B = 8.617 * 10^{-5} \frac{\text{eV}}{\text{K}}$  is Boltzmann's constant.<sup>6</sup>

As seen in Figure 1, thermal neutron energies lie in the region of exponentially decreasing slope for the 55-Mn and 1-H(n, $\gamma$ ) reactions – two of the most important reactions in the Mn bath. This region is known as the “one-over-V” region, as cross section magnitude is proportional to the inverse of velocity.<sup>6</sup> Alternatively, since the neutron energy is kinetic, this region follows the inverse of the square root of energy. Thus, Equation (15) can be derived from Equation (14).

$$\sigma_{1/v} \propto \frac{1}{\sqrt{E}} \propto \frac{1}{\sqrt{T}} \quad (15)$$

Accordingly, a 10 K increase from room temperature will reduce the cross section by 1.7%. Combining the change in Mn cross section with the number density reduction gives a 2.1% decrease in the Mn absorption reaction rate. For comparison, the  $^{16}\text{O}(n,\alpha)$  cross-section discrepancy mentioned in Section 2.3 was caused by a 32% change in cross section data.<sup>17</sup> Mathematically, a change of this magnitude could not be achieved without boiling or freezing the solution. Thus, a significant change in temperature will affect the Mn absorption fraction of the Mn bath, but less so than other parameters.

For a simple Mn bath where the source is replaced by the detector, the temperature is not expected to change beyond the climate control capabilities of the room. However, a circulation loop pump presents a potential heat source. To evaluate the effect of such heating, a simplified thermal model based on the Mn bath presented by Amendola et al. was used.<sup>9</sup> The Mn bath was taken as a filled sphere of 50 cm interior radius ( $r$ ). The wall of the Mn bath was a 5 mm thick ( $t$ ) stainless steel spherical shell. In reality, the pump would add energy to the pipe flow outside of the Mn bath, but the heat ( $q$ ) was modelled as passing through the solution to the environment. The ambient temperature was taken as 20 °C ( $T_{Air}$ ). This model is depicted in Figure 9.

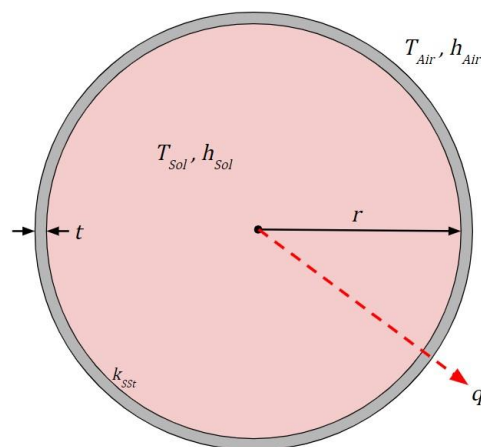


**Figure 9. Thermal model of the Mn bath for thermal resistance analysis.**

In the model, the thermal conductivity of stainless-steel was  $k_{SSt} = 13.4 \frac{W}{m \cdot K}$ .<sup>26</sup> The convective heat transfer coefficients were roundly approximated at  $h_{Air} = 10 \frac{W}{m^2 \cdot K}$  for free gas convection and  $h_{Sol} = 1000 \frac{W}{m^2 \cdot K}$  for forced liquid convection. This formulation left  $q$  and  $T_{Sol}$  (the bulk solution temperature) as variables. Solving for  $T_{Sol}$  gave an approximation of the potential temperature levels seen in a Mn bath.

To approximate the heat added by pumping, a flowrate of  $1000 \frac{L}{hr}$  was used from Amendola et al.<sup>9</sup> The pressure drop ( $\Delta P$ ) across the 1 m tall Mn bath for a  $1.2 \frac{g}{cm^3}$  dense solution was found using Equation (16).<sup>26</sup>

$$\Delta P = \rho g * 2r \quad (16)$$

With the gravitational acceleration of  $9.8 \frac{m}{s^2}$ , the pressure drop was 11.8 kPa. This was multiplied by the flow rate to approximate the pump power as 3.27 W. To account for additional pressure drops in the piping and the pump efficiency, a very conservative value of 100 W may be assumed. Since the heat energy added to the water must be less than the pump power, 100 W also serves as a very conservative estimate of the heat,  $q$ , moving through the Mn bath.

Using a thermal resistance model of the Mn bath shell and convection regions, the total thermal resistance is given by Equation (17).<sup>26</sup>

$$R_{total} = \frac{1}{4\pi h_{Sol} r^2} + \frac{t}{4\pi k_{SSt} r(r+t)} + \frac{1}{4\pi h_{Air} (r+t)^2} \quad (17)$$

This resulted in a system thermal resistance of  $0.032 \frac{K}{W}$ . The resistance was multiplied by  $q$  and the product was added to  $T_{Air}$  to find  $T_{Sol} = 23 \text{ }^\circ\text{C}$ .

The predicted temperature increase was not significant enough to be considered in the final empirical correlation. The predicted  $3 \text{ }^\circ\text{C}$  rise is barely out of usual room temperature conditions.

Additionally, the use of a hydraulic circuit which necessitates a pump is optional to the design of a Mn bath. If this is pursued, a heat exchanger could be added to maintain a more consistent system temperature. Finally, none of the simulations reviewed in the literature considered temperature as a factor. Accounting for temperature changes in the final MCNP was not necessary or helpful, so all simulations were performed at room temperature.

### 3.1.5 Minor Parameters

When designing an MCNP simulation of a Mn bath, there are several other, less important parameters that need to be considered. These include the neutron source spatial distribution, the cross section library, and the source capsule sizes and materials. The effects of these parameters were not included in the final empirical correlation; rather, a consistent choice was applied across all simulations.

The source distribution describes where the simulated neutrons are first placed into the MCNP model and their initial trajectories (speed is dictated via their kinetic energy). In MCNP, source distributions are defined in much the same way that material volumes are created.<sup>15</sup> Mathematical surfaces are defined, and neutrons are emitted from those surfaces with chosen angular distributions. The simplest source distribution is an isotropic point source. However, this is not particularly accurate in the case of the Mn bath. If the point source is placed at the center of the source material, neutrons will have a chance to be absorbed in the source before entering the Mn bath solution. The final Mn absorption tally would thus more closely denote the fraction of neutrons produced in the source that are captured in Mn. However, in real applications, one is interested in measuring the neutrons that are actually emitted from the source, and  $\varepsilon_{Mn}$  is the

fraction of neutrons emitted from the source that are absorbed in Mn. Thus, a spatial distribution that produces neutrons in MCNP outside of the source capsule is necessary.

In the literature, the most commonly cited method of distributing neutrons outside of the source is by using a non-physical spherical surface slightly larger than the source capsule.<sup>12,25</sup> This is used due to the ease of defining a sphere in MCNP. This may not be ideal, as source capsules are predominately cylindrical, so gaps will exist between the neutron birth locations and the capsule surface. Thus, a cylindrical source distribution was used for the MCNP source definition (SDEF) card.

This cylindrical SDEF was obtained by making three source emission surfaces: the cylinder wall, the top disk, and the bottom disk. Neutrons were born evenly across each surface. To do this, MCNP needs to know what fraction of the total simulated neutrons should originate from each of the three surfaces. For a physical source, anisotropy measurements could be used to choose these fractions. However, such data is highly dependent on the source type and construction. Accordingly, two idealized models were considered for dividing the neutrons between the surfaces. First, the source was assumed to be symmetrical about the horizontal midplane, so the emission fractions of the top and bottom surfaces are the same ( $f_t = f_b = f_{tb}$ ). Because the emission fractions must sum to unity, Equation (18) can be used to find the side wall emission fraction ( $f_s$ ).

$$f_s = 1 - f_t - f_b = 1 - 2f_{tb} \quad (18)$$

From here, the first model uses the ratio of the circular emission surface area to the total surface area to compute  $f_{tb}$ . For a cylinder of radius  $r$  and height  $h$ , this ratio is given by Equation (19).

$$f_{tb} = \frac{\pi r^2}{2\pi r h + 2\pi r^2} = \frac{r}{2(h+r)} \quad (19)$$

The second model computes  $f_{tb}$  as the solid angle subtended by the top surface about the center of the source cylinder as a fraction of  $4\pi$  sr as in Equation (20).<sup>10</sup>

$$f_{tb} = \frac{2\pi}{4\pi} \left( 1 - \frac{\frac{h}{2}}{\sqrt{r^2 + \left(\frac{h}{2}\right)^2}} \right) = \frac{1}{2} \left( 1 - \frac{h}{\sqrt{4r^2 + h^2}} \right) \quad (20)$$

Mathematically, there is little difference between the surface area and solid angle models. The difference between  $f_{tb}$  calculated each way does not exceed 0.05 in absolute value. Thus, the absolute difference between the  $f_s$  values does not exceed 0.1.

To complete the SDEF, the user needs to specify the initial direction of travel for the simulated neutrons. Initial trajectories are specified by the cosine of the angle between the emission surface normal vector and the neutron velocity. The MCNP default is a cosine distribution, where the probability that a neutron will be born with direction cosine  $\mu$  is  $2\mu$ .<sup>15</sup> Another possible model is to emit neutrons isotropically, so that each  $\mu$  is equally likely. For both cases,  $\mu$  is sampled from 0 to 1 to ensure that all neutrons are emitted heading away from the source. Figure 10 and Figure 11 show the differences between the four models for the first 50 simulated neutrons. This data can be obtained from an MCNP run using table 110.<sup>15</sup> In the figures,  $f^*$  represents the emission fraction calculated from the first 50 particles, and the dashed red line shows the ideal direction cosine distribution. The practical effects of the emission fraction and initial trajectory models on manganese absorption fraction will be considered in Section 3.2.

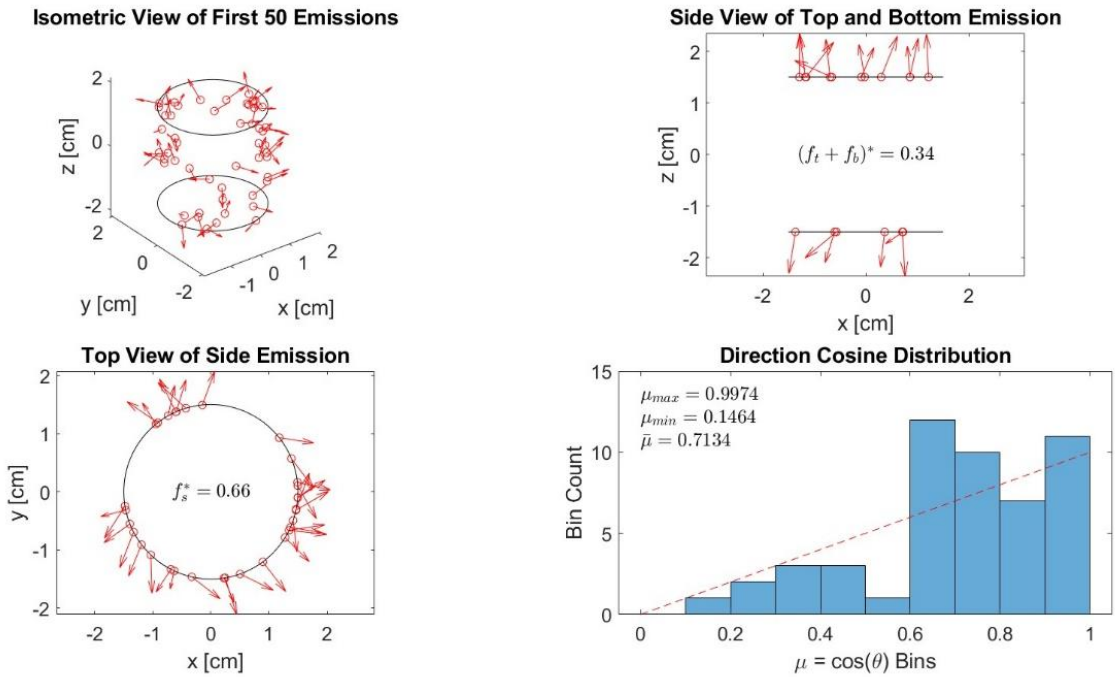


Figure 10. Visualization of 50 simulated neutrons using the surface area emission and cosine distribution models for a source with 1.5 cm radius and 3 cm height.

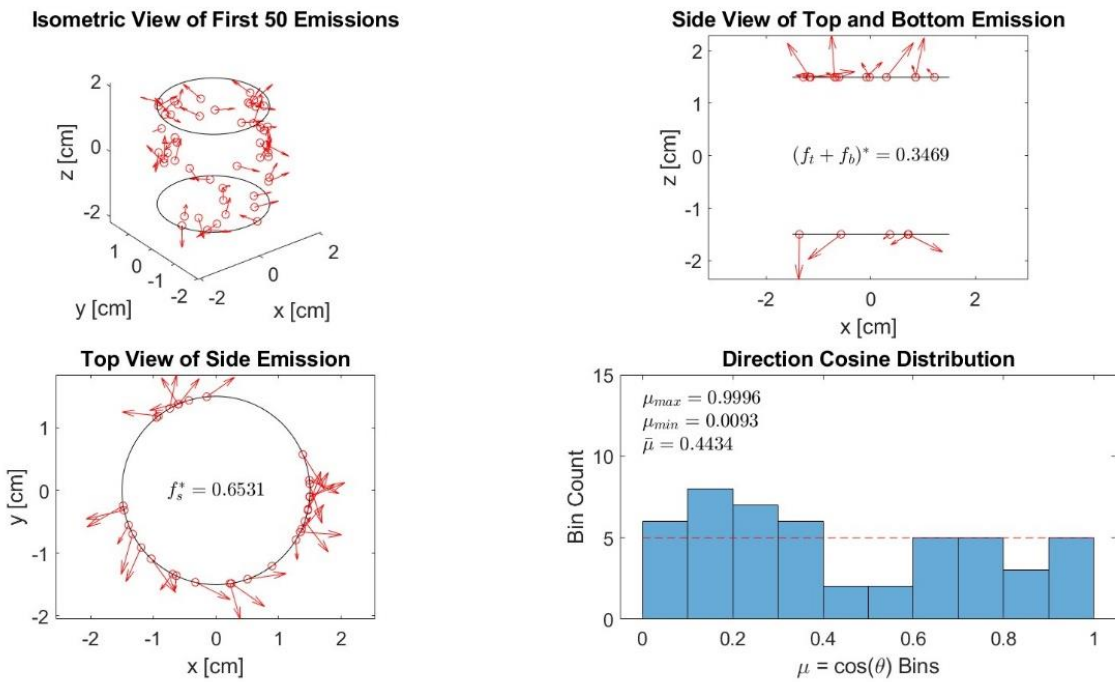


Figure 11. Visualization of 50 simulated neutrons using the solid angle emission and isotropic distribution models for a source with 1.5 cm radius and 3 cm height.

The choice of cross section library is another parameter affecting the simulations. Based on the discussion presented in Section 2.3, ENDF/B-VII.0 was used for the final simulations. This is the default library chosen by MCNP 6.2 (the program version obtained by the author), as it is the most recent library included within the release. For the simulations, the most naturally abundant isotope was specified for each element, unless a specific isotope was desired ( $^{241}\text{Am}$  for example). The only exception to this was C. ENDF/B-VII.0 data is not available for  $^{12}\text{C}$ , so natural C was used.<sup>16</sup> This tells MCNP to treat the simulated C atoms as a mixture of the naturally occurring isotopes of carbon using their natural abundances. MCNP has  $^{12}\text{C}$  cross section data from ENDF/B-V.0, but the decision was made to use natural carbon for the sake of maintaining a consistent and up-to-date library. Water also requires special treatment in MCNP. When neutron moderation is important, as is the case with a Mn bath, the light water option should be specified which modifies the  $^1\text{H}$  cross section at low energies<sup>15,16</sup>. This is needed because bonding to O changes the scattering characteristics of  $^1\text{H}$  compared to pure H. For the simulations, the light water cross section from ENDF/B-VII.0 was used for the  $^1\text{H}$  in the  $\text{MnSO}_4$  aqueous solution.

Finally, the material and dimensions of the neutron sources need to be set for each source type. As with the  $\text{MnSO}_4$  solution, MCNP needs an overall material density and isotope component fractions to define a material. A simple summary of such information for commercially available or common sources could not be found, so the requisite information was pieced together from a variety of sources. The sources were sized to produce around  $4 * 10^6 \frac{\text{n}}{\text{s}}$  (equivalent to 1 mCi of  $^{252}\text{Cf}$ ), as this is the upper bound of the measurement range target for the planned Mn bath facility.

First, the encapsulation material for each source was 316L stainless steel.<sup>11,27</sup> The composition of this material was taken from the example MCNP simulation published by Roberts et al. and is shown in Table 4.

**Table 4. 316L stainless steel isotope composition with density of 7.93 g/cm<sup>3</sup>.<sup>25</sup>**

Isotope	56-Fe	52-Cr	58-Ni	55-Mn	28-Si	C	31-P	32-S	98-Mo
Mass Fraction	0.65395	0.17	0.12	0.02	0.01	0.0003	0.00045	0.0003	0.025

The dimensions of the stainless steel capsules are reported in Table 5. QSA Global, a supplier of neutron sources, lists the neutron yield of their 241-Am-Be sources as  $2.2 * 10^6 \frac{n}{s * Ci}$ .<sup>27</sup> Basic nuclear data and the definition of activity can be used to calculate the yield from a certain mass of 252-Cf to be  $2.3 * 10^6 \frac{n}{s * \mu g}$ .<sup>8</sup> Thus, the target maximum emission rate should be produced by about 2 Ci of 241-Am or 2  $\mu g$  of 252-Cf. Matching this to the list of neutron sources studied by Roberts et al. in their analysis of neutron source characterization techniques suggests that the X3 and X1 capsule types are best suited for the Am and Cf sources respectively.<sup>1</sup> For the Pu-Be source, the specific  $\alpha$ -decay activity of 241-Am is two orders of magnitude higher than 239-Pu.<sup>8</sup> However, Pu is roughly ten times as dense as the AmO<sub>2</sub> used in Am-Be sources.<sup>6,28</sup> This suggests that a 20 Ci Am-Be source is the right size for a  $4 * 10^6 \frac{n}{s}$  Pu-Be source. Accordingly, the X14 capsule was chosen for the Pu-Be source.

**Table 5. Neutron source capsule dimensions.**

Source Type	Capsule	Height [cm] <sup>27</sup>	Radius [cm] <sup>27</sup>	Wall Thickness [cm] <sup>12,25,27</sup>
Am-Be	X3	3.12	1.125	0.30
Cf	X1	1.00	0.390	0.15
Pu-Be	X14	6.02	1.505	0.30

The source material densities and compositions were defined from stoichiometric calculations and inputs from a variety of sources. The final parameters are reported in Table 6. For all sources, the neutron-producing material was assumed to be evenly and homogeneously distributed throughout the interior of the source capsule. This simplification was necessary due to the lack of generalized information on source construction and is justified by the fact that neutrons originate outside of the source for the purposes of the MCNP simulations. For the calculations, molar masses were taken from the IAEA chart of nuclides for the specified or most naturally abundant isotope.<sup>8</sup>

First, Amendola et al. report that their X3 Am-Be capsules contain 0.32 g of AmO<sub>2</sub> and 4.62 g of Be.<sup>9</sup> The atom and mass fractions of each isotope are easily calculated from here. The density of a mixture ( $\rho_m$ ) can be found with Equation (21).

$$\rho_m = \left( \sum_i \frac{w_i}{\rho_i} \right)^{-1} \quad (21)$$

In this case, the source contains two compounds: AmO<sub>2</sub> and Be. These have mass fractions of  $w_{AmO_2} = 0.0648$  and  $w_{Be} = 0.9352$  and mass densities of  $\rho_{AmO_2} = 11.76 \frac{\text{g}}{\text{cm}^3}$  and  $\rho_{Be} = 1.85 \frac{\text{g}}{\text{cm}^3}$ .<sup>6,28</sup>

Second, Cf spontaneous fission sources are normally constructed with Cf<sub>2</sub>O<sub>3</sub>.<sup>29</sup> Calculation of the atom fractions is simple. However, if the cavity of an X1 capsule were filled completely with Cf<sub>2</sub>O<sub>3</sub>, the total mass of Cf would be in the order of grams, rather than the required micrograms. Thus, an effective density was inputted into MCNP assuming 2  $\mu\text{g}$  of 252-Cf with the accompanying 16-O.

Finally, Pu-Be sources use Pu metal, rather than an oxide.<sup>24</sup> Due to manufacturing difficulties, Pu-Be sources contain a variety of Pu isotopes. For simplicity, this was reduced to

solely 239-Pu. This choice is supported by the work of Bagi et al., who measured the isotopic composition of six Pu-Be sources and found that greater than 75% of the Pu was 239-Pu.<sup>30</sup> Their paper also suggests that for a desired neutron emission, around 50 g of Pu must be present. Using  $\rho_{Pu} = 19.6 \frac{\text{g}}{\text{cm}^3}$  and  $\rho_{Be} = 1.85 \frac{\text{g}}{\text{cm}^3}$  allowed for the calculation of the mass of 9-Be needed to fill the remainder of the X14 capsule.<sup>6</sup> With these masses and molar masses, the atom and mass fractions were calculated. Lastly, the Pu-Be mixture density was calculated using Equation (21) using  $w_{Pu} = 0.5491$  and  $w_{Be} = 0.4509$ .

**Table 6. Neutron source material densities and compositions.**

Source	Mass Density $\left[\frac{\text{g}}{\text{cm}^3}\right]$	Isotope	Atom Fraction
Am-Be	1.96	16-O	0.0045
		241-Am	0.0023
		9-Be	0.9932
Cf	$1.73 * 10^{-5}$	16-O	0.6
		252-Cf	0.4
Pu-Be	3.68	239-Pu	0.0439
		9-Be	0.9561

### 3.2 Validation of MCNP Capabilities

Section 3.1 focused on the various physical variables that affect Mn absorption and how these might be modeled. Before performing the final simulations however, it was desired to validate the author's MCNP capabilities against previously published Mn bath simulations. Ultimately, the only way to truly validate the simulation framework is to compare it to experimental data, but this defeats the purpose of designing a Mn bath a priori. Thus, validation

was performed by using the Mn bath descriptions published by three authors as inputs to the MCNP code and comparing the results (neutron absorption in various components and leakage) against the published data. The goal was to match the published results within  $\pm 10\%$  which would demonstrate that the author's MCNP framework is at least commensurate with other published work. For the validations, the models discussed in Section 3.1 were used unless the author gave more specific details on how their models were set up.

The three published papers used in this validation come from two National Laboratories and one university. The first is by Roberts from the U.K.'s National Physical Laboratory (NPL).<sup>25</sup> This paper gives the most detail on the simulation input parameters, going so far as to provide the MCNP code used. This allowed for exact matching of the material and geometry specifications. The example code also includes the ISO 8529 Am-Be neutron energy spectrum which could then be used for further validations. The NPL simulation used MCNP-4B with a variety of cross section libraries. The reported results include leakage, oxygen capture, sulfur capture, source self-absorption, and absorption in the cavity around the source.

The second paper by Khabaz is from Golestan University in Iran.<sup>12</sup> This used MCNPX and was repeated for four different ENDF/B libraries (V, VI.0, VI.8, and VII.0). The geometry and material specifications are slightly less detailed than the NPL paper, especially in the possible existence of a rod above the source holder. The given results are for absorption in all four elements of the Mn bath solution, combined source and holder absorption, and leakage.

The final paper is by Amendola et al. from the ENEA-INMRI lab in Italy using MCNPX.<sup>9</sup> This paper gives the least detail on the simulation inputs. The source spatial distribution, several geometrical parameters, and cross section library are unknown. Results are recorded for absorption in Mn, H, O, S, the source, and the holder cavity, as well as leakage from the Mn bath.

To validate the new simulation, input parameters were iteratively tweaked to better match the results obtained in the published simulations. This provided an in-depth understanding of which parameters had the greatest effect on  $\varepsilon_{Mn}$  and what assumptions were being made by other authors. The MCNP input files that produced the best results are given in Appendix B.

### 3.2.1 NPL

Running the code given in the NPL paper alone was not enough to match the reported results. The original simulation allowed for default cross-sections, which change between MCNP versions. After amending the code to account for this, the results in Table 7 were achieved.<sup>16</sup> It shows the probability per source neutron that a neutron will leak from the Mn bath or be parasitically absorbed in various ways. The new probabilities have been rounded to match the precision of those reported. The relative error calculated by MCNP (one standard deviation divided by the probability) is only reported for the new simulation, as Roberts did not include this information. The percent differences (calculated using higher precision than shown) between the new simulation and the reported results are also given.

**Table 7. Validation against NPL results.**

<b>Neutron Termination</b>	<b>NPL Probability</b>	<b>Simulation Probability</b>	<b>Relative Error [%]</b>	<b>Difference [%]</b>
Leakage	0.0141	0.0141	0.68	-0.26
O Abs.	0.0265	0.0264	0.16	-0.24
S Abs.	0.0069	0.0069	0.08	-0.27
Source Abs.	0.0005	0.0005	1.83	0.66
Cavity Abs.	0.0152	0.0151	0.39	-0.91

Table 7 gives perhaps the best-case scenario for a simulation validation of this kind. Even with exact knowledge of the input parameters, the statistical nature of MCNP leads to some lingering difference, albeit less than one percent.

With this well-established simulation, other input variations could be tested for their effect on the  $\varepsilon_{Mn}$  parameter. For example, it is known that increasing the number of threads (parallel neutron simulations) employed by MCNP reduces the time needed to finish a simulation.<sup>15</sup> However, doing this seemed to increase the statistical uncertainty by causing multiple tallies to fail the figure-of-merit (FOM) check performed by MCNP. The FOM is computed based on the tally value and computer time, and failing the check could indicate an issue with the tally convergence.<sup>15</sup> This was found to be a false warning, as using 1, 2, 4, and 8 threads all returned the exact same probabilities and uncertainties for a certain seed. The warning was likely caused by the desynchronization of the tally and time data caused by running simultaneous simulations.

Additionally, it was found that changing the neutron source spatial distribution from spherical to cylindrical did not change the resulting Mn absorption fraction by more than one standard deviation. Similarly, the way in which the neutron emission was divided between the cylinder source capsule surfaces and the direction relative to the surface normal distribution did not affect the  $\varepsilon_{Mn}$  result. Thus, the simple sphere is not statistically less accurate than the more complex and realistic cylindrical distribution when considering the Mn absorption fraction.

Another perturbation on the NPL simulation showed that a difference of 1.3 standard deviations in the Mn absorption fraction was created by changing the voided cavities to air-filled cavities. Thus, such an assumption was not made in the final simulations. More importantly, the neutron spectrum for the Am-Be source simulated had a large effect on  $\varepsilon_{Mn}$ . Switching from the

given ISO 8529 spectrum to the IAEA spectrum increased the Mn absorption fraction by seven standard deviations.

### 3.2.2 Golestan University

Validations against the Golestan simulations were less successful. The best results for an Am-Be source using ENDF/B-VI.0 are given in Table 8. The simulation which gave these results used a cylindrical source distribution with the ISO 8529 spectrum. The solution composition was taken directly from the reference, and one million neutrons were simulated.

**Table 8. Validation against Golestan Am-Be results.**

<b>Neutron Termination</b>	<b>Golestan Probability</b>	<b>Relative Error [%]</b>	<b>Simulation Probability</b>	<b>Relative Error [%]</b>	<b>Difference [%]</b>
Leakage	0.03460	0.60	0.01914	0.76	-44.69
H Abs.	0.72800	0.06	0.75269	0.05	3.39
O Abs.	0.04092	0.26	0.02421	0.20	-40.84
S Abs.	0.00904	0.05	0.00864	0.04	-4.48
Mn Abs.	0.18300	0.06	0.18890	0.05	3.22
Source & Holder Abs.	0.00805	3.24	0.00671	0.37	-16.68

In all, 14 different combinations of input parameters were tested, and only one returned a better result for the O absorption, and a few gave closer results for Mn absorption. However, many of these were obtained with inputs directly contradictory to those stated by Khabaz. Even this best-case scenario used a cylindrical source distribution, while it seems Khabaz used a sphere. One possible source of error beyond a mistake could be the inclusion of a rod above the source holder. This is pictured in a diagram, but dimensions and materials are never described. Another

error may lie in the neutron spectrum. This is suggested because the same simulation performed with a 252-Cf source and Watt Fission Spectrum returned the results shown in Table 9. As can be seen, these agree much more closely with Khabaz's 252-Cf results. However, there is still a discrepancy in the O absorption, and the source/holder absorption is much worse. The exact reason for the large disagreement with these results remains unclear.

**Table 9. Validation against Golestan Cf results.**

<b>Neutron Termination</b>	<b>Golestan Probability</b>	<b>Relative Error [%]</b>	<b>Simulation Probability</b>	<b>Relative Error [%]</b>	<b>Difference [%]</b>
Leakage	0.00649	1.59	0.00466	1.56	-28.18
H Abs.	0.78200	0.06	0.78839	0.05	0.82
O Abs.	0.00613	0.55	0.00524	0.42	-14.65
S Abs.	0.00801	0.06	0.00801	0.04	0.01
Mn Abs.	0.19600	0.06	0.19784	0.05	0.94
Source & Holder Abs.	0.00125	6.73	0.00243	0.57	94.12

### 3.2.3 ENEA-INMRI

Matching the results from Amendola et al. required the most guess work. It was assumed that the source holder was solid with no cavity, and ENDF/B-VI.8 was assumed when available with VI.6 as an alternative. Once again, one million neutrons were simulated, and the solution composition was taken directly from the paper. The ISO Am-Be spectrum was used with a cylindrical source emission and cosine surface normal distribution to produce Table 10.

**Table 10. Validation against ENEA-INMRI results.**

<b>Neutron Termination</b>	<b>ENEA-INMRI Probability</b>	<b>Relative Error [%]</b>	<b>Simulation Probability</b>	<b>Relative Error [%]</b>	<b>Difference [%]</b>
Leakage	0.02073	1.00	0.01983	1.00	-4.32
H Abs.	0.65666	0.10	0.65627	0.05	-0.06
O Abs.	0.01688	0.24	0.01686	0.23	-0.12
S Abs.	0.01266	0.09	0.01221	0.04	-3.55
Mn Abs.	0.27185	0.10	0.27193	0.05	0.03
Source Abs.	0.00654	0.51	0.00670	0.69	2.44
Holder Abs.	0.02160	0.12	0.02354	0.12	9.00

These results meet the goal of 10% difference. This is encouraging considering that this paper gave the least information about the simulation inputs. This demonstrates that the MCNP simulation framework and parameters are well understood. Furthermore, the largest disagreement occurs in the source holder absorption which also had an unspecified thickness. If a cavity were added to the simulation, the results might improve. One aspect that was noted during work with this validation was that the source distribution change was more noticeable. Changing the particle direction with respect to the surface normal was enough to change the holder absorption difference from nine to 12%. However, changes to  $\epsilon_{Mn}$  were still within one or two standard deviations, agreeing with the NPL conclusions. This suggests that the Mn absorption fraction is less sensitive to certain changes than other metrics.

### 3.2.4 Validation Conclusions

Overall, the results of this validation process showed that the MCNP simulation framework was well understood and ready to be utilized for the larger project. The NPL paper and results

showed that several assumptions will not affect the final  $\varepsilon_{Mn}$  metric. Recreating the work from ENEA-INMRI greatly increased confidence in the MCNP code. Although the results from Golestan University could not be satisfactorily replicated, possible sources of error have been proposed.

It was demonstrated that the choice of source spatial distribution will not ultimately affect the major result of interest (Mn absorption fraction). Additionally, multiple threads can be safely used simultaneously to increase simulation speed. It was also learned that air-filled cavities should not be approximated as voids. However, the cross-section library and source spectrum have the largest impact on  $\varepsilon_{Mn}$  of the inputs evaluated. Unfortunately, the validation work performed here cannot come to bear on the question of which cross-section library and which spectrum will provide the most physically accurate results.

### 3.3 Simulation Model Setup

This section describes the creation of the MCNP input file. This file sets up the simulation with the geometry, source, tallies, and materials. For the purpose of running multiple simulations, a “blank” input file was created with variables in place of numerical values. Using Python, these variables were replaced to create the case-specific input file as described in Section 3.4. A copy of the blank input file is included in Appendix B as Blank\_Bath. The details of this file follow.

#### 3.3.1 Geometry

The most basic MCNP input files contain three sections. The first two describe the cell (volume) and surface geometries respectively. The surfaces are mathematically defined, and the

cells are constructed from the union and intersection of regions bounded by each surface<sup>15</sup>. In order to create these sections, it is helpful to have a diagram of the surfaces required to define each cell. A section view through the middle of the desired Mn bath is shown in Figure 12. In three dimensions, the diagram should be revolved about the vertical dotted line creating a spherical Mn bath with a cylindrical source arrangement.

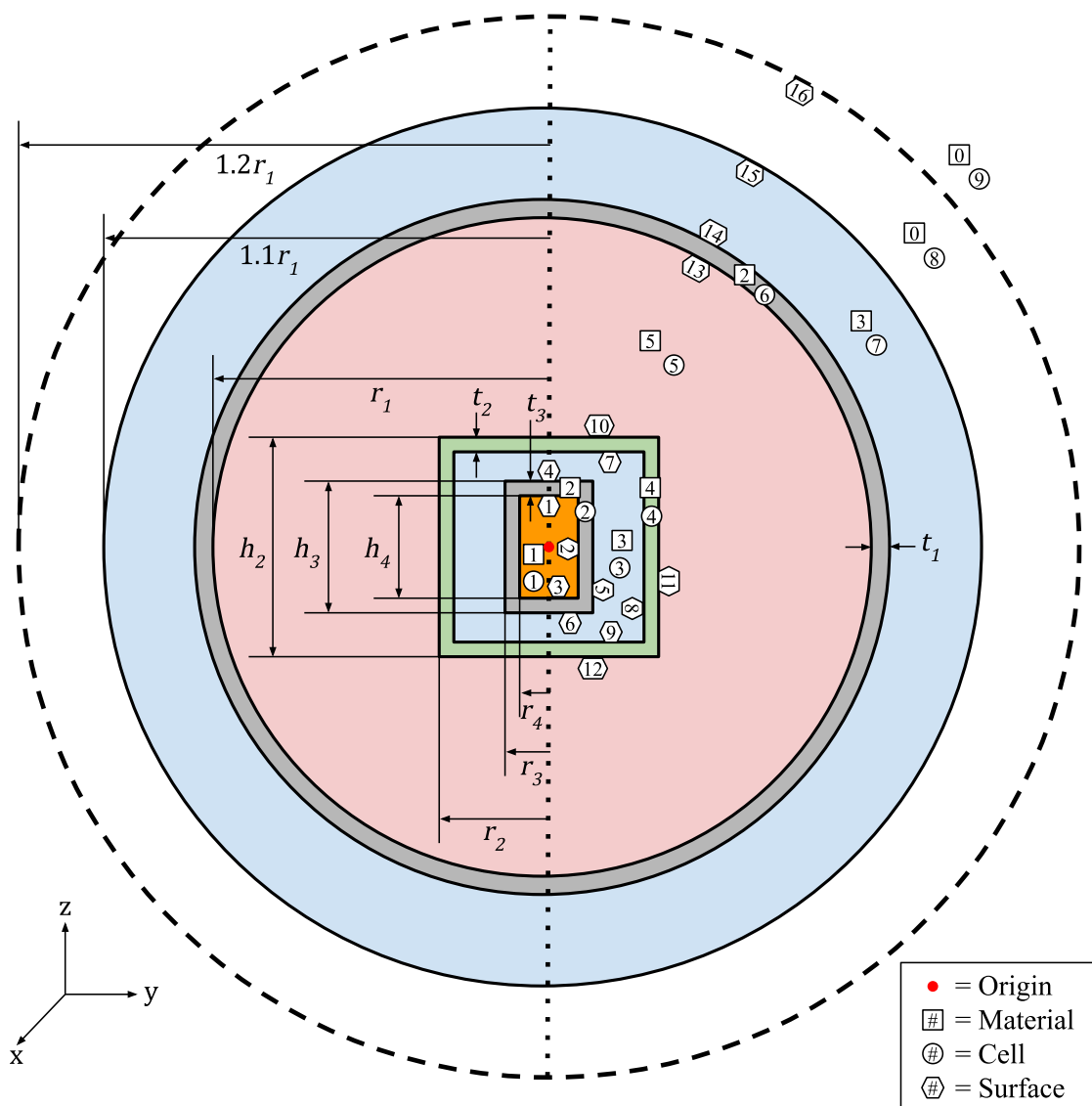


**Figure 12. Diagram of the Mn bath model geometry showing dimensions and material, cell, and surface numbers.**

Starting from the interior, the Mn bath model begins with the source material enclosed by its stainless steel containment. The dimensions of these cells vary with the source type. They sit within an air-filled cavity within the source holder. The air was modeled as 79.1% 14-N and 20.9% 16-O by atom fraction. The holder material is polytetrafluoroethylene (PTFE) with a density of  $2.2 \frac{\text{g}}{\text{cm}^3}$  and number fractions of one-third C and two-thirds 19-F similar to the Golestan University and ENEA-INMRI simulations.<sup>9,12</sup> The dimensions of the holder were chosen arbitrarily to fit within the minimum simulated Mn bath inner radius (10 cm) and to encase the Pu-Be (largest) source capsule. The holder is surrounded by the  $\text{MnSO}_4$  solution enclosed in a stainless steel sphere. Outside of the sphere, there is an air-filled region and then a void. Outside of the void region (the dotted circle in Figure 12) the simulation ends and neutrons are terminated.

Defining a cell requires five pieces of information: the cell number, material number, material density, boundary surfaces, and neutron importance.<sup>15</sup> The cell numbers are chosen by the user and are shown in Figure 12. The material for each cell is specified by noting the material number which is defined in the third section of the MCNP input file, and its density is a simple numerical input. The default density unit is  $\frac{\text{atoms}}{\text{b} \cdot \text{cm}}$ , but this can be changed to  $\frac{\text{g}}{\text{cm}^3}$  by negating the density input. Material number zero means a void and does not require a density input. The cell bounding surfaces can be specified using the intersection and union of certain regions bounded by each surface. For example, the steel source container is within surfaces 4, 5, and 6 but outside surfaces 1, 2, and 3. The cell is defined as:

$$-4 -5 6 (1:2:-3)$$

Here, spaces between surface numbers indicate an intersection, and a colon denotes a union. The negation of a surface indicates the opposite region bounded by the surface. For a sphere and cylinder, positive is the exterior while negative is the interior. For a horizontal plane, positive is

above the plane while negative is below. Parentheses group their contents. Finally, the neutron importance is often used in advanced models to enhance the simulation statistics, but for these simple simulations, only importances of one and zero are necessary. Unity importance tells MCNP to track neutrons in the cell as usual, but neutrons are terminated upon entering a cell with zero importance. Thus, only cell 9 has zero importance. A summary of the cell definition information is given in Table 11. The source and solution densities are left as variables in the blank input file.

**Table 11. MCNP input file cell definitions.**

Description	Cell #	Material	Density $\left[\frac{\text{g}}{\text{cm}^3}\right]$	Boundary	Importance
Source Material	1	1	-SRCDEN	-1 -2 3	1
Steel Container	2	2	-7.93	-4 -5 6 (1:2:-3)	1
Holder Air Cavity	3	3	-0.0012	-7 -8 9 (4:5:-6)	1
PTFE Holder	4	4	-2.2	-10 -11 12 (7:8:-9)	1
MnSO <sub>4</sub> Solution	5	5	-SOLDEN	-13 (10:11:-12)	1
Steel Bath Shell	6	2	-7.93	-14 13	1
Air Around Bath	7	3	-0.0012	-15 14	1
Void Around Air	8	0		-16 15	1
Termination	9	0		16	0

The MCNP surfaces for this simulation consist of spheres, cylinders along the z-axis, and planes perpendicular to the z-axis. Spheres and cylinders are defined by their radii, and such planes are defined by their z-position. For the blank Mn bath file, these dimensions were left as variables using the nomenclature seen in Figure 12.

### 3.3.2 Source

The third and final section of the MCNP input file defines the source, tallies, and materials. The source is defined by specifying eight parameters, though more advanced simulations can include more. These parameters are summarized in Table 12. As has been discussed in Section 3.1.5, the source is defined over three surfaces of a closed cylinder (two circles and the cylinder wall) using the surface area emission fraction calculation and cosine initial trajectory distribution.

**Table 12. MCNP input file source definition summary.**

Parameter	Value	Description
PAR	1	The source will emit neutrons.
AXS	0 0 1	The axis of the cylindrical emission surface will be aligned with the z-axis.
ERG	d1	The energy spectrum will follow distribution 1.
SUR	d2	The emission surface will follow distribution 2.
POS	FSUR d3	The emission surface position will follow distribution 3 based on the value of SUR.
RAD	FSUR d4	The neutron birth position radius on the surface will follow distribution 4 based on the value of SUR.
NRM	FSUR d8	The direction of the normal vector of the emission surface will follow distribution 8 based on the value of SUR.
EXT	d9	The neutron birth axial position along the cylinder emission surface will follow distribution 9.

The energy distribution d1 is defined in accordance with the spectra discussed in Section 3.1.1, and the data for these spectra in the form used in MCNP is included in Appendix B. In the blank input file, this is left as the variable SPEC. Distribution d2 chooses between surfaces 5, 4, and 6 (side, top, and bottom of the source capsule) with probabilities set by  $f_s$  and  $f_{tb}$ . The POS

parameter essentially defines an origin for each emission surface. Thus, based on the choice of emission surface number, POS will be given the values of  $(0, 0, 0)$ ,  $(0, 0, \frac{h_3}{2})$ , and  $(0, 0, -\frac{h_3}{2})$  for the side, top, and bottom surfaces respectively (this is distribution d3). The RAD parameter functions similarly, and it defines the radius from the origin at which neutrons will be born. The value of SUR will designate an additional distribution (d5, d6, or d7). For the source capsule sides, d5 is fixed at  $r_3$ , since the cylindrical surface has only one radius. For the top and bottom, neutrons are born evenly between the origin and  $r_3$ . This is accomplished by making d6 and d7 distributions such that the probability of a neutron being born at radius  $r$  is given by  $cr$  where  $c$  is a weighting constant to make the total probability unity. In the input file, distributions are specified by source input (SI) and source probability (SP) entries. As an example, the distribution for d6 is:

SI6 0 r3

SP6 -21 1

The SI card defines the bounds, -21 specifies a power law probability in  $r$ , and 1 gives the exponent on  $r$ . The NRM parameter specifies the surface normal vector direction from which the neutron initial trajectory vector will be calculated. By default, the normal vector of a surface points in the direction of the surface's positive bounded region. From here, the default neutron direction is a cosine distribution between 0 and  $90^\circ$  from the normal vector. Accordingly, the normal vector for the bottom surface (6) must be flipped. Thus, d8 uses the value of SUR to choose 1, 1, or -1 for the side, top, and bottom NRM values respectively. Finally, EXT must be used for the side surface to define the neutron birth location probability along the axial direction of the cylinder. The d9 distribution is set up similarly to the RAD parameter, except that it does not switch based upon

SUR. The SI entry bounds the neutrons between  $-\frac{h_3}{2}$  and  $\frac{h_3}{2}$  with an even sampling over  $z$  using

SP -21 0. Overall, one million neutrons were simulated for each run.

### 3.3.3 Tallies

After the source definition, the tallies are defined. In all, the simulation records 19 tallies: four F1, four F2, and 11 F4. The F1 and F2 tallies are set up to evaluate the leakage from the Mn bath. Because of the uncertainty in the use of F1 or F2 in the literature, these tallies have been duplicated on the inside of the Mn bath shell, the outside of the Mn bath shell, the air-void interface, and the exterior of the void (surfaces 13 through 16). The F1 current tallies count the number of neutrons that pass through a surface. To distinguish between neutrons leaking out of the Mn bath from neutrons scattering back into the Mn bath, two bins were defined for each tally based on the cosine of the angle between the neutron direction and the surface normal. An example F1 tally is:

```
F11:N 13
```

```
C11 0 1
```

The first line defines tally number 1 of type 1 (F11) for neutrons (N) through surface 13. The second line specifies cosine bins for tally 1 of type 1 (C11) as  $-1 < \mu < 0$  (backscatter) and  $0 < \mu < 1$  (leakage). The lower bound of the first bin is -1 by default. The net leakage is calculated as the number of neutrons that pass out of the surface minus the number of neutrons that pass in through the surface (bin two minus bin one).

To evaluate which tally and surface are best used to measure the Mn bath leakage, the results from a sample simulation are shown in Table 13. Within the void cell, there are no atoms

to scatter or absorb neutrons, so any neutron that crosses surface 15 with an outward direction must also cross surface 16. This condition is not met by the F2 tally, since it gives particles moving parallel to the surface a greater weight in the tally.<sup>15</sup> Thus, the current F1 tally is the more accurate way to evaluate Mn bath leakage. An F1 tally on surface 15 will be used as the measure of leakage for the final simulations.

**Table 13. Sample F1 and F2 tallies at different surfaces for an Am-Be source in a 40 cm radius Mn bath with 1.3 g/cm<sup>3</sup> solution density.**

Surface (#)	Current F1		Flux F2	
	Probability	Variance ( $\sigma$ )	Probability	Variance ( $\sigma$ )
Inner Shell (13)	0.0460566	0.0002418	0.0936696	0.0007119
Outer Shell (14)	0.0445262	0.0001960	0.0653079	0.0003723
Air-Void (15)	0.0445238	0.0001959	0.0556171	0.0002503
Void Exterior (16)	0.0445238	0.0001959	0.0524572	0.0002308

The F4 absorption tallies were set up to measure the neutron absorption in each cell of the Mn bath excluding the void. Four extra tallies were set up to measure the absorption in the Mn bath solution (cell 5) by each individual element. An F4 tally takes the form:

F114:N 5

FM114 (N\_S 9 -2)

The first line designates the 11<sup>th</sup> tally of type 4 for neutrons in cell 5. In essence, this gives the neutron flux ( $\phi$ ) in cell 5. The next line is a tally multiplier. The three arguments inside the parentheses are a multiplying constant, the interacting material number, and the reaction type respectively. The example tally calculates the absorption in S in the solution. The total absorption cross section ( $\sigma_a$ ) is denoted by reaction number -2, and 9 is an extra material number for only the S in the solution. The scalar multiplier was left as a variable and replaced for each case with the

number density of S ( $N_S$ ) in the solution calculated from the density and in units of  $\frac{\text{atoms}}{\text{b*cm}}$ . If the tally and multipliers are put together, the sulfur absorption reaction rate described by Equation (1) results. This is given on a per-volume basis, so multiplying by the cell volume – which MCNP calculates – returns the total S absorption rate. All of the F4 tallies were set up in a similar manner. For cells where the bulk material matches the tally material, a scalar multiplier of -1 can be used to tell MCNP to use the cell’s number density in the calculation.

### 3.3.4 Materials

Finally, the materials used in the simulation are summarized in Table 12. The reference column specifies a section of this work where the material’s definition and rationale can be found. In an MCNP input file, an isotope is specified by “ZZAAA.mX”. ZZ is the atomic number (number of protons), AAA is the number of nucleons (protons plus neutrons with AAA = 000 being natural), and mX specifies the cross section library to use.<sup>16</sup> In the simulations, mX was omitted to use the default ENDF/B-VII data. Materials 6 through 9 are not pictured in the simulation diagram in Figure 12. These were only used to calculate isotope-specific absorption tallies for each solution component. In the blank MCNP input file, the source material was left as the variable SRCMAT, and the files used to replace these variables are given in Appendix B.

**Table 14. Simulation material definition summary.**

<b>Material (#)</b>	<b>Reference</b>
Source (1)	3.1.5
316L Stainless Steel (2)	3.1.5
Air (3)	3.3
PTFE (4)	3.3

MnSO <sub>4</sub> Solution (5)	3.1.3
Mn (6)	3.3
H (7)	3.3
O (8)	3.3
S (9)	3.3

### 3.4 Running and Processing Simulations

MCNP version 6.2 was used for all simulations. Running the MCNP simulations and extracting the tally data was accomplished using Python. Two Python files were used which will be called the “runner” and the “looper”. The runner file allows a user to run a single MCNP simulation. It handles defining and replacing the variables in the blank input file, creating a new directory to hold the MCNP run files and results, collecting and processing the tallies and variances, and printing the tally results into text files. The looper file repeatedly executes the runner file, changing the Mn bath radius and solution density between runs. It also compiles the individual results from each run into a larger text file. To vary the source type, a runner and looper file were set up for each source.

An example of a runner file set up for Am-Be can be found in Appendix B as AmBe\_Runner.py. To define the variables, the user must input the geometry dimensions seen in Figure 12, the source and solution mass densities, the source type, and the method for calculating the source surface emission fractions. From the specified source type, the code draws on text files seen in Appendix B containing the material and spectrum definitions to replace the SRCMAT and SPEC variables. The runner code then performs the calculations for the emission fractions and

solution number densities. The blank input file is copied, the variables are written over with the desired values, and MCNP is executed in the current directory.

The runner script then collects the tally information from the default MCNP output file. To find the desired outputs and extract the data, a function was adapted from the work of a previous graduate student, Nicholas Greci. The original function uses a keyword to locate information in the MCNP output file and copies the line a certain number of rows below the keyword. This was expanded to include two extra function input arguments to more precisely specify which information to copy after the keyword. The original function and the adaptation are included in Appendix C. With the tallies collected, the runner code also performs simple calculations, like multiplying by the cell volume, subtracting the current bins to find net leakage, and adjusting the variance accordingly. Subsequently, all of the tally data is stored in a “long” results text file, while the Mn absorption tally and the leakage are stored in a “short” results text file.

There are a few types of calculations performed by the runner file to compute the final tally results. For the F1 current tallies, the inward direction bin current is subtracted from the outward direction bin to obtain the net leakage. Since MCNP reports the relative error on each tally, the variance is obtained by multiplying the error by the tally value. The inward and outward variances are then summed in quadrature, and the square root of the sum is the leakage variance reported in the results file. For the F2 flux and F4 absorption tallies, MCNP reports probabilities per area and volume respectively. Thus, the tallies are multiplied by the appropriate geometry factor before being recorded in the results file. The tally variance in this case is simply obtained by multiplying the corrected tally by the reported relative error. Lastly, the runner file adds the absorption tally in each element of the Mn bath solution for comparison to the solution absorption tally. The variance on this sum is computed as the square root of the sum of the component variances in

quadrature. In a similar way, the absorption in every component of the Mn bath is summed for comparison to the leakage results. In this calculation, the solution tally is used rather than the individual component tallies.

A sample looper file is also included in Appendix C for an Am-Be source. This file requires the user to specify the source type as well as the range and step size of radii and densities to consider. From here, the looper file creates a new directory for every case and rewrites a runner file with the case-specific radius and density. The looper file executes the runner file and copies the short and long results produced by the MCNP run. These results are compiled into larger text files for each source.

## Chapter 4

### Results and Discussion

Overall, 336 simulations were performed. Each source was considered with radii from 10 to 75 cm in steps of 5 cm and solution densities from 1.05 to 1.40 g/cm<sup>3</sup> in steps of 0.05 g/cm<sup>3</sup>. Distributing the simulations over eight threads allowed all the simulations to be completed in 4 hours and 32 minutes with one million neutrons in each simulation. The Mn absorption fraction and leakage as a function of Mn bath radius and density are shown in Figure 13 and Figure 14 respectively. The radius axes on the leakage plots have been reversed to best show the leakage curves. The raw data (short results files) behind these figures is included in Appendix A.

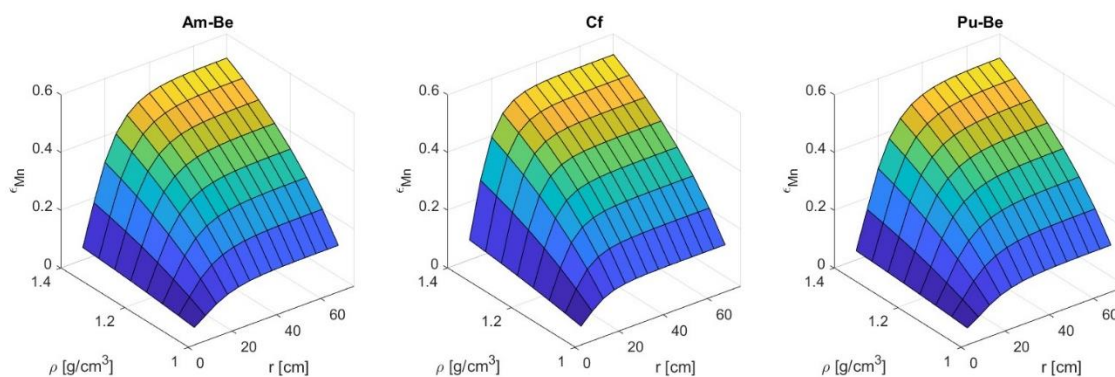


Figure 13. Mn absorption fraction simulation results.

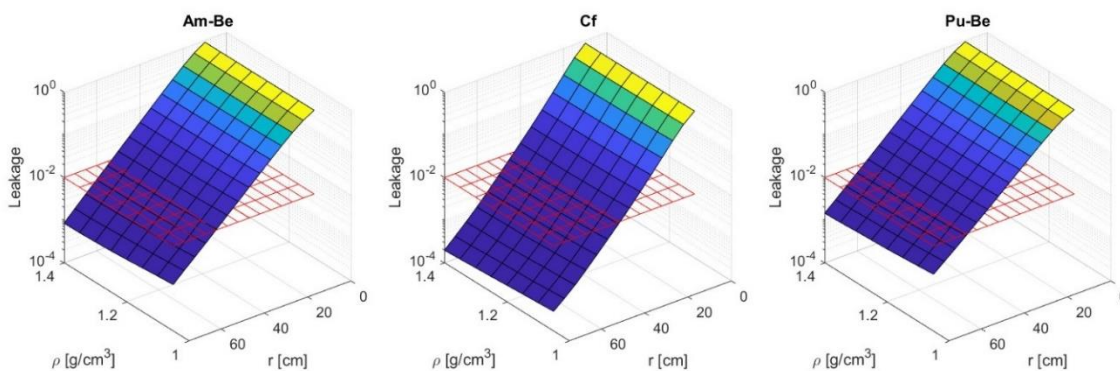


Figure 14. Mn bath leakage fraction simulation results with 1% leakage level indicated in red.

The shapes of the plots agree with what was expected from the literature. Increasing Mn bath radius causes a sharp initial increase in  $\varepsilon_{Mn}$  which eventually levels off as was demonstrated by Khabaz and seen in Figure 6.<sup>12</sup> The solution density has a less severe effect on the Mn absorption fraction with a slightly less-than-linear response much like that seen in the work of Amendola adapted for Figure 5.<sup>9</sup> For leakage, the radius clearly has a much greater effect than solution density. The response to an increase in radius is an exponential decrease in leakage, which matches the style of correlation used by Khabaz.<sup>12,13</sup> By comparison, the solution density has only a small effect on leakage, yet an increase in density still reduces leakage. This suggests that the increase in Mn, S, and O in the solution causes enough extra absorption to counteract the effects of reduced moderation from less H in the solution.

The inherent MCNP tally variances have not been shown in Figure 13 and Figure 14 because they are visually insignificant compared to the scale of the data. The variance ( $\sigma$ ) on the absorption fraction and equivalent relative error ( $E_R$ ) for each source type are shown in Figure 15. Similar plots show the leakage variance and relative error in Figure 16. The variances indicate that the simulation results are reliable from a statistical perspective. In all cases, the relative error is less than the 10% threshold suggested by the MCNP documentation.<sup>16</sup> This is especially true for the Mn absorption fraction, where the maximum relative errors is only 0.360% (Pu-Be,  $r = 10$  cm,  $\rho = 1.4 \frac{\text{g}}{\text{cm}^3}$ ). The leakage shows more uncertainty, with a maximum relative error of 6.65% (Cf,  $r = 75$  cm,  $\rho = 1.4 \frac{\text{g}}{\text{cm}^3}$ ). The maximum  $E_R$  values occur where the respective tallies are minimized. For  $\varepsilon_{Mn}$ , this is for high energy neutrons in a small Mn bath. For leakage, this condition is lower energy neutrons in a very large Mn bath. Solution density has a much lower effect on the relative error. For the Mn absorption and leakage, decreasing the density to  $1.05 \frac{\text{g}}{\text{cm}^3}$

while keeping the same radius only lowers the maximum relative errors by 0.010% and 1.24% respectively.

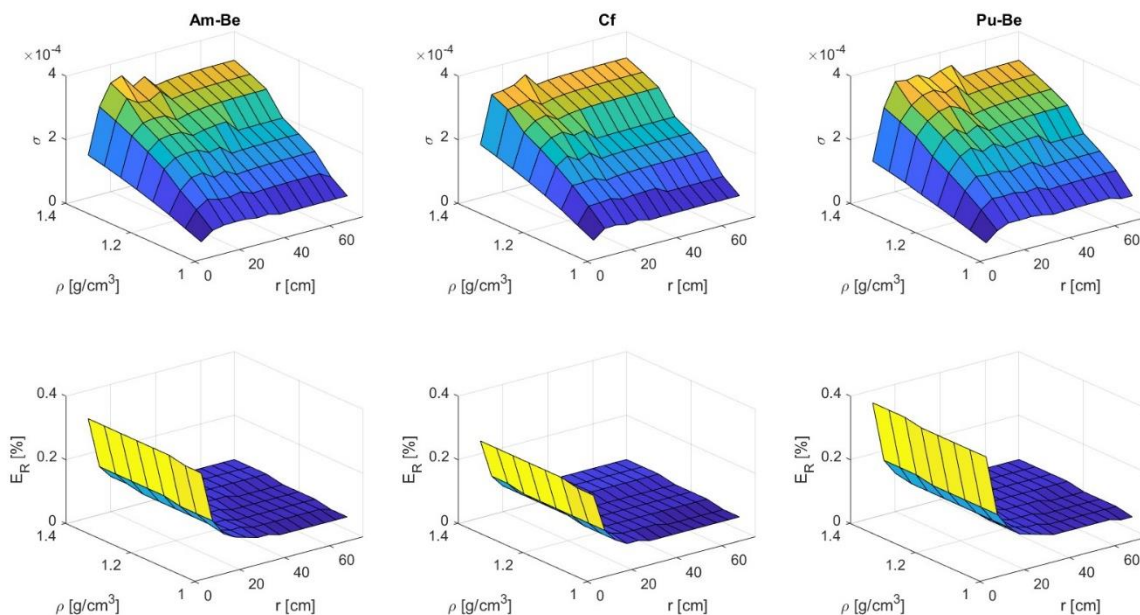


Figure 15. Mn absorption fraction simulation variance and relative error.

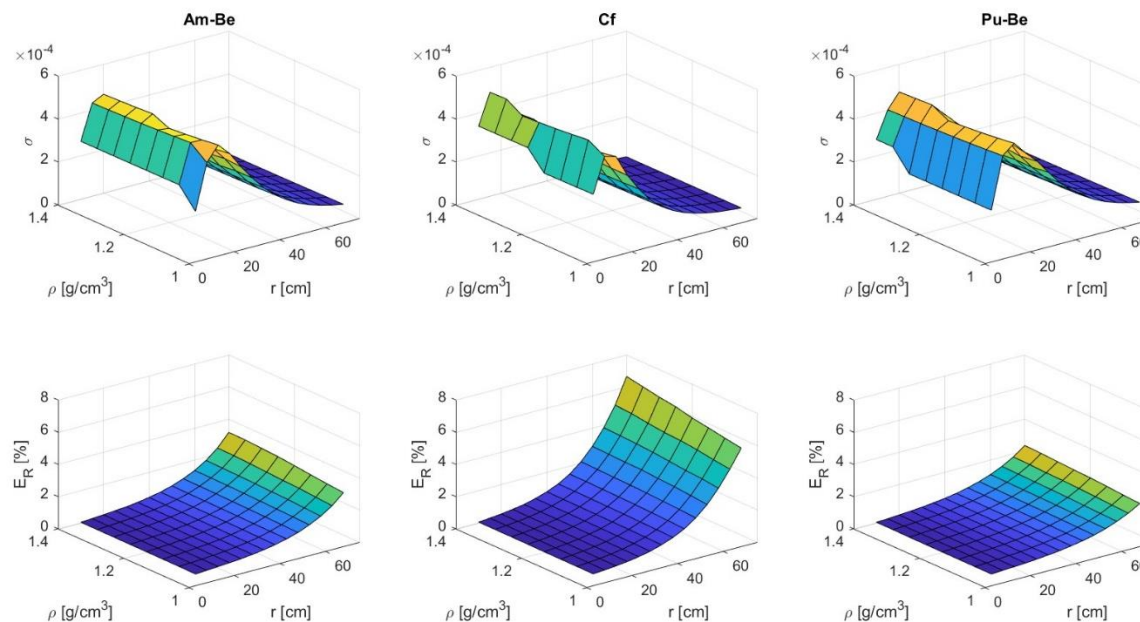
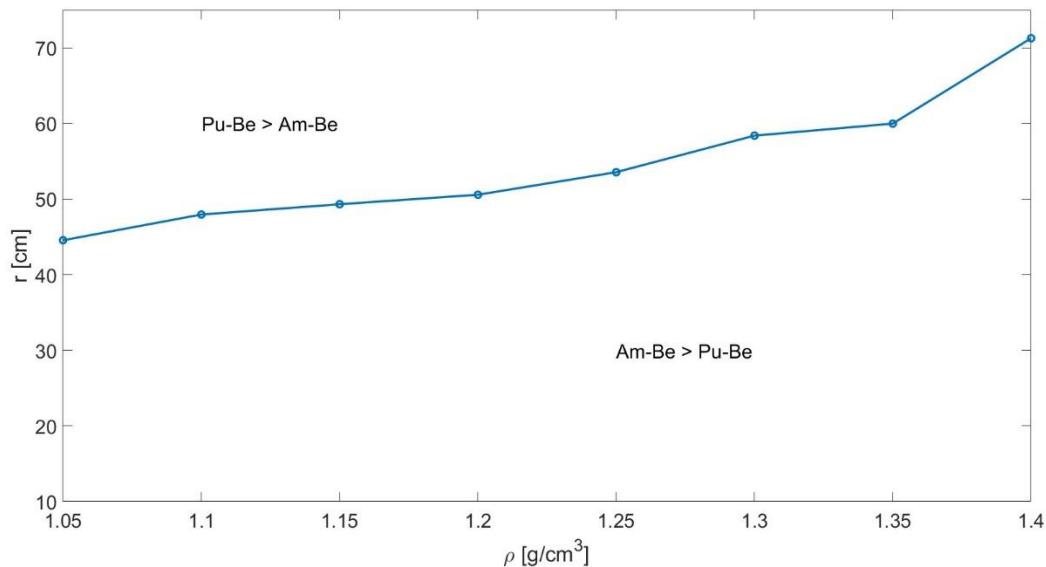


Figure 16. Mn bath leakage fraction simulation variance and relative error.

#### 4.1 Manganese Absorption Fraction Analysis

Comparing the Mn absorption fraction for the three sources,  $\varepsilon_{Mn}$  is greatest for Cf over the simulation domain. This difference ranges from 0.0979 ( $r = 20$  cm,  $\rho = 1.40 \frac{\text{g}}{\text{cm}^3}$ ) to 0.0016 ( $r = 75$  cm,  $\rho = 1.05 \frac{\text{g}}{\text{cm}^3}$ ) as calculated by the Cf source Mn absorption fraction less the average of the Am-Be and Pu-Be  $\varepsilon_{Mn}$  values. Even the lowest difference remains statistically significant, as it is 36 times the Cf  $\varepsilon_{Mn}$  variance at the same radius and density. This is likely due to the average energy of Cf neutrons being about half of that of the other sources as seen in Table 3. Neutrons born at lower energies are more quickly moderated, and thus more readily absorbed.

Between the Am-Be and Pu-Be sources, the gap between average neutron energies is only about 0.8 MeV. This allows the Am-Be source to have larger  $\varepsilon_{Mn}$  values in one region of the domain which is demonstrated in Figure 17. The dividing line was generated using MATLAB's "spline" interpolation method to find the radius where the two  $\varepsilon_{Mn}$  plots intersect for each density. The Am-Be  $\varepsilon_{Mn}$  leads by as much as 0.0234 ( $r = 15$  cm,  $\rho = 1.40 \frac{\text{g}}{\text{cm}^3}$ ), while the Pu-Be  $\varepsilon_{Mn}$  leads by a smaller margin of 0.0016 ( $r = 75$  cm,  $\rho = 1.20 \frac{\text{g}}{\text{cm}^3}$ ) in the other region. However, the smaller difference is still statistically significant at ten times the variance of the Mn absorption fraction averaged between the two sources.



**Figure 17. Comparison of the Mn absorption fraction between Am-Be and Pu-Be.**

The reason for the division seen in Figure 17 is unclear. One possible explanation for this difference is that for small Mn baths, the lower average neutron energy for Am-Be neutrons causes the absorption fraction to be higher. Then, as the Mn bath size increases, the higher Pu-Be energy helps to distribute neutrons throughout the solution, avoiding parasitic absorption in the holder and source. However, this theory is opposed by the fact that the Pu-Be source is 1.3 times as wide and twice as tall as the Am-Be source, so parasitic absorption in the Pu-Be source should be more likely.

Despite the differences between the Mn absorption fractions for the three sources, at the maximum density and radius,  $\varepsilon_{Mn}$  is nearly the same. The maximum Mn absorption fraction is 0.5154 for Am-Be, 0.5273 for Cf, and 0.5155 for Pu-Be. This means that, for usual Mn bath operating conditions, useful neutron absorption will not exceed around 53%.

To create the desired correlations for  $\varepsilon_{Mn}$ , each source was treated separately. This was done primarily because source type cannot be mathematically represented as a single variable like

density or radius. The average neutron energy might be a candidate, but this ignores differences in source material and capsule dimensions. Additionally, if a single variable could describe the source type, there would only be three data sets to fit a correlation which is not ideal. Accordingly, three correlations have been fitted to the data in the form  $\varepsilon_{Mn} = f(r, \rho)$ . These correlations were created using the same procedure, so only development of the Am-Be correlation will be explained.

First, for each simulation data point  $(r, \rho, \varepsilon_{Mn})$  with the same radius value, a power, least-squares fit was applied as a function of density. A power fit was chosen from the available models as the one that best fit the data. This was achieved using MATLAB and follows the form of Equation (22) for constants  $a$ ,  $b$ , and  $c$ . The resulting fits can be seen in Figure 18.

$$\varepsilon_{Mn} = a\rho^b + c \quad (22)$$

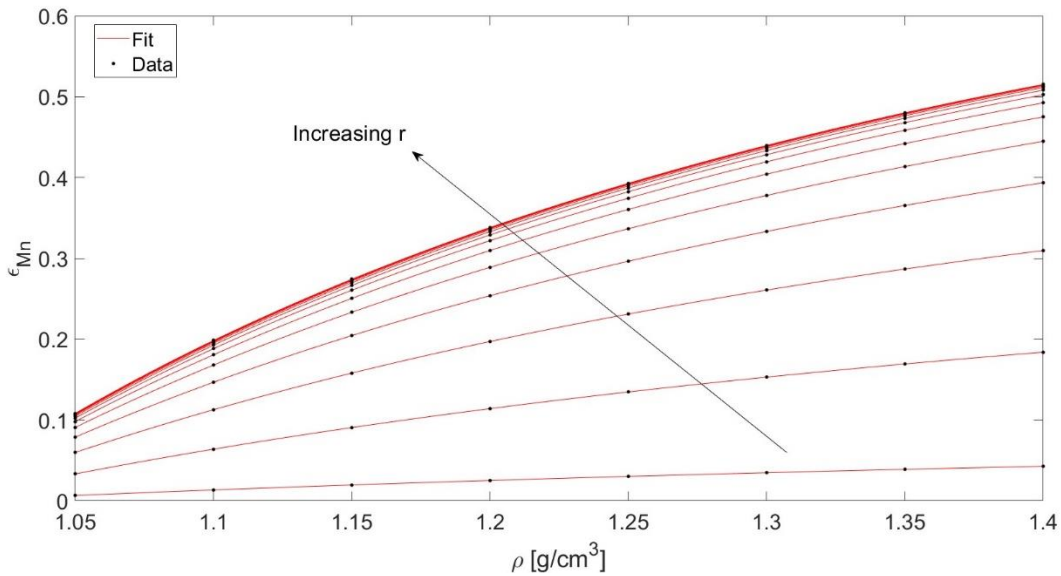


**Figure 18. Power fits with respect to density for constant radii for Am-Be Mn absorption fraction data.**

From here, the 14 sets of  $a$ ,  $b$ , and  $c$  constants were each fit with an exponential function in terms of the radius as shown in Equation (23) and Figure 19. Again, this was a least-squares fit

performed in MATLAB using the model that best described the data. Here,  $a_i$ ,  $b_i$ , and  $c_i$  are all constants for  $i = 1, 2, 3$ . MATLAB does not include the  $i = 3$  term in its default exponential fit capabilities, so these were manually determined by subtracting  $a$ ,  $b$ , or  $c$  at  $r = 75$  cm from each data point. This allowed MATLAB to perform the exponential fit, and the vertical shifts became the  $i = 3$  constants.

$$\begin{bmatrix} a \\ b \\ c \end{bmatrix} = \begin{bmatrix} a_1 e^{a_2 r} + a_3 \\ b_1 e^{b_2 r} + b_3 \\ c_1 e^{c_2 r} + c_3 \end{bmatrix} \quad (23)$$

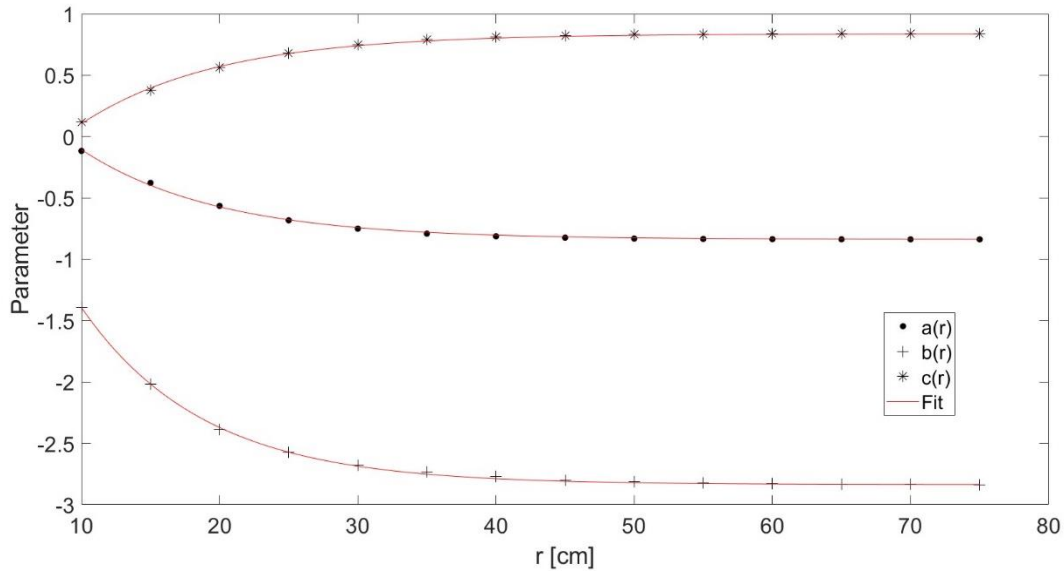


**Figure 19. Exponential fits with respect to radius for power fit coefficients for Am-Be Mn absorption fraction data.**

In this way, the final correlation for the Mn absorption fraction has the form seen in Equation (24). To succinctly represent the nine constants needed to construct the full correlation, a matrix  $M$  was defined as seen in Equation (25).

$$\varepsilon_{Mn} = (a_1 e^{a_2 r} + a_3) * \rho^{(b_1 e^{b_2 r} + b_3)} + (c_1 e^{c_2 r} + c_3) \quad (24)$$

$$M = \begin{bmatrix} a_1 & a_2 & a_3 \\ b_1 & b_2 & b_3 \\ c_1 & c_2 & c_3 \end{bmatrix} \quad (25)$$

The final calculated fit parameter matrices for each source are:

$$M_{AmBe} = \begin{bmatrix} 2.015 & -0.101 & -0.838 \\ 4.475 & -0.113 & -2.836 \\ -2.008 & -0.101 & 0.838 \end{bmatrix}$$

$$M_{Cf} = \begin{bmatrix} 2.786 & -0.142 & -0.867 \\ 6.668 & -0.153 & -2.778 \\ -2.759 & -0.141 & -0.867 \end{bmatrix}$$

$$M_{PuBe} = \begin{bmatrix} 1.939 & -0.095 & -0.826 \\ 4.723 & -0.109 & -2.909 \\ -1.932 & -0.094 & 0.826 \end{bmatrix}$$

In Appendix D, the code used to find the fit coefficients and a function for calculating  $\varepsilon_{Mn}$  an  $M$  matrix are included as `Data_Processing.m` and `FitMatrixEval.m` respectively.

To investigate the validity of these correlations, the relative error between the fit – evaluated at the original radius and density points – and the simulation data was calculated. Plots of these errors are seen in Figure 20 with the radius axis flipped for a better image. For Mn baths with radii greater than or equal to 20 cm, the correlations match the data well with a maximum relative error magnitude of 1.76% (Pu-Be,  $r = 20$  cm,  $\rho = 1.4 \frac{\text{g}}{\text{cm}^3}$ ). This error is about 14.7 times the corresponding simulation variance, so it cannot be ignored. However, it rapidly diminishes to as low as 0.0007% as the radius increases. On the other hand, Mn baths smaller than 20 cm in radius are not well represented by the empirical fits, as the relative error oscillates with a large magnitude. In the worst case, the Pu-Be fit shows a -27.7% error ( $r = 10$  cm,  $\rho = 1.05 \frac{\text{g}}{\text{cm}^3}$ ). This is not a serious detriment to the usefulness of the correlation because such small Mn baths would be impractical to build due to their high leakages. The Mn baths at 10 and 15 cm radii lost between 48 and 94% of their neutrons.

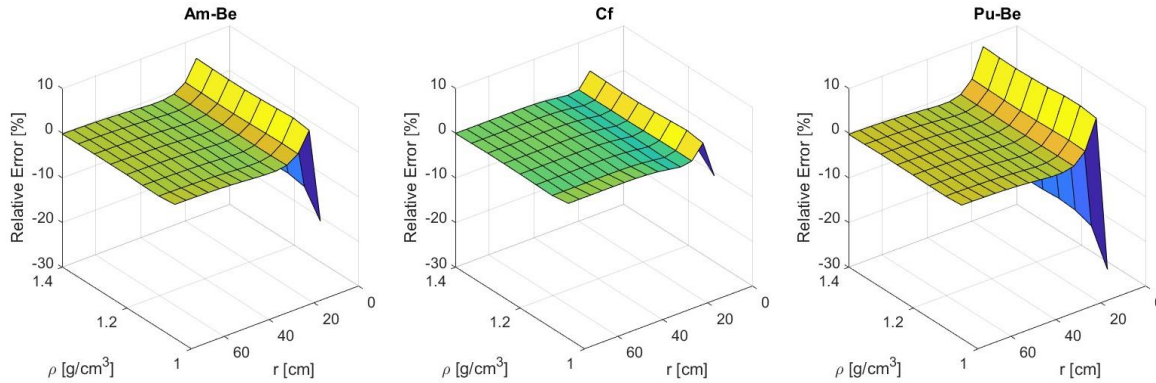


**Figure 20. Relative error between the Mn absorption fraction empirical correlations and simulation data.**

## 4.2 Leakage Analysis

While the leakage characteristics of Mn baths were not the primary concern of this study, the information may aid in design. It is usually desirable to minimize Mn bath leakage to increase  $\varepsilon_{Mn}$  and decrease the radiation field outside of the Mn bath. In the simulation results, the maximum observed leakage fraction was 0.9399 (Pu-Be,  $r = 10$  cm,  $\rho = 1.05 \frac{\text{g}}{\text{cm}^3}$ ), and the minimum was 0.0002 (Cf,  $r = 75$  cm,  $\rho = 1.40 \frac{\text{g}}{\text{cm}^3}$ ). Comparing the leakage plots from the three sources, the Pu-Be always has the largest leakage fraction, followed by Am-Be and then Cf. This is not surprising, as it follows the average neutron energy for each source. In Figure 14, 1% leakage planes were inserted to mark the customary limit identified in the literature.<sup>12,13</sup> To quantify this threshold, intersections between the leakage curve and the 1% plane were interpolated using MATLAB's "spline" method. In this way, Figure 21 was produced. In the figure, regions above each curve show the radius-density domain for which the leakage fraction was found to be below 1%. These curves confirm the earlier observation that leakage is much more dependent on radius than density.

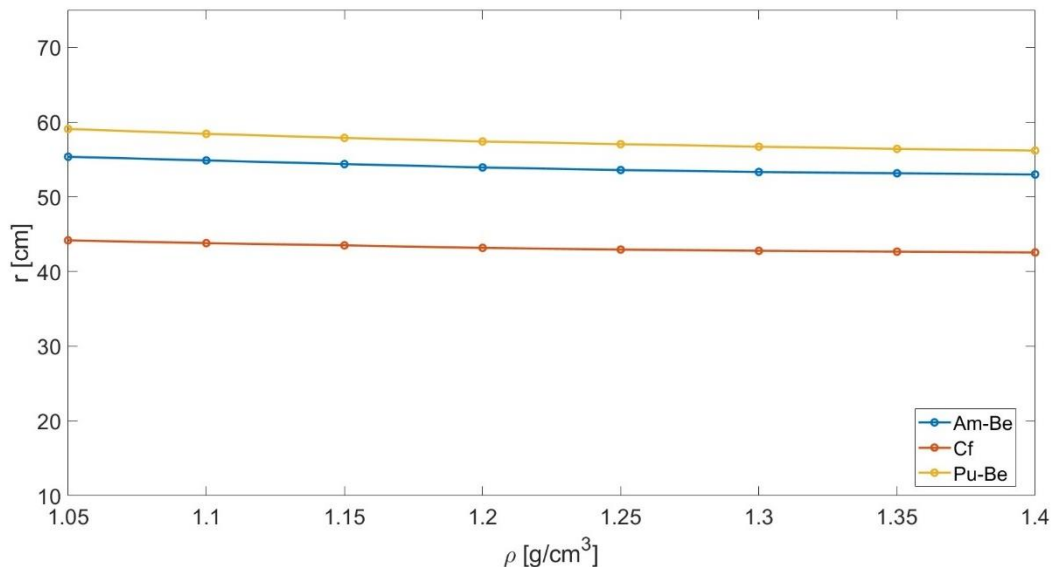


**Figure 21. 1% leakage boundary curves.**

### 4.3 Limitations and Future Work

The primary limitation of this work is the degree of generalization that was required to perform the simulations. Without specific sources and holders to model, assumptions had to be made. Similarly, other Mn bath structures, like a supporting rod for the holder or the opening to the Mn bath were ignored. The simulations could technically be made more accurate by including more specific information, but this was not viable given the nature of the problem. Furthermore, it is unclear how sensitive the simulation results would be to such changes. The validation work suggests that changes to the source spectra would have a large impact on the results, while the addition of a rod above the source holder would not make a statistically significant difference. However, this remains an open area for investigation.

Second, the final empirical correlations for the Mn absorption fraction show a large error for Mn baths smaller than 20 cm in radius. Theoretically, this could be improved by performing

more simulations with smaller radius and density steps or by using a more complicated fitting model. However, such refinements may not yield a justifiable improvement, especially for the more realistic, larger Mn baths where the relative error is already below 2%. Considering the generalizations made to perform the simulations, 2% relative error in the empirical fit may already be insignificant compared to a change in the source spectra for example.

Finally, these simulations have the flaw of being disconnected from physical measurements. Much work went into ensuring that the input data and simulation methods were commensurate with work being performed at National Laboratories and other universities. However, until the data and proposed correlations have been compared to physical measurements, their ultimate accuracy remains in question.

#### 4.4 Conclusions

This document has presented work performed to support the creation of a Mn bath facility at The Pennsylvania State University. Such a facility could be used for experiments, in-house calibrations, and teaching. To design a new Mn bath, it would be helpful to have a way to easily estimate the fraction of neutrons emitted by the source which are usefully absorbed in the Mn of the Mn bath solution. Accordingly, empirical correlations have been developed to calculate  $\epsilon_{Mn}$  for three neutron source types – 241-Am-Be, 252-Cf, and 239-Pu-Be – given the Mn bath radius and solution density. It was found that solution temperature is not expected to change enough to warrant an investigation into the effect of temperature. To determine the correlations, a generalized MCNP model was created, and simulations were performed for radii from 10 to 75 cm

and densities from 1.05 to 1.40  $\frac{\text{g}}{\text{cm}^3}$ . The Mn absorption and leakage tallies from these simulations were then analyzed.

To validate the MCNP model and capabilities, inputs from three published papers were used to perform MCNP simulations with the goal of matching the results. These validations were generally successful and increased confidence in the MCNP model. From this validation work, it was determined that modeling the neutron birth spatial distribution as an isotropic sphere versus a cylinder tight to the source capsule did not make a statistical difference. However, replacing assumed voids with air caused a noticeable change in  $\varepsilon_{Mn}$ . The first result may help reduce coding time for a new MCNP simulation (although a method for implementing the cylindrical distribution is now readily available), and the second indicates that air cavities should not be modeled as voids.

The final  $\varepsilon_{Mn}$  correlations are good approximations of the simulation data for Mn baths larger than 20 cm in radius. Below this limit, leakage from the Mn bath will be so high as to make such a Mn bath impractical. Thus, these simulations can be used to design a new Mn bath facility for the university. Beyond these correlations, curves that give the 1% leakage boundary for each source type were shown. This leakage level is recommended by the literature, and the boundary will help narrow the design window for a future Mn bath. Additionally, this work required the creation of a variety of MCNP, MATLAB, and Python files that may be useful in the future. Particularly, the blank Mn bath MCNP model and runner Python files can be used to input geometry and source data into a new MCNP simulation. This may help reduce the MCNP learning curve for future Mn bath designers should more simulations need to be run. Also, a system for determining the Mn bath solution composition from a single parameter (density in this case) has been proposed and implemented in a MATLAB code. This may be useful from a chemical perspective for building the Mn bath or procuring materials.

Limitations on this work include the generic source and holder input information, the fidelity of the correlations, and the lack of physical experimental support. Despite this, the simulations were performed with the best available data in a way that matches or exceeds the methods and assumptions used by National Laboratories and other universities. Furthermore, many tools and capabilities have been developed for future use in the creation of a Mn bath. For these reasons, this research succeeded in its specific goal of developing empirical correlations for  $\varepsilon_{Mn}$  and its broader goal of supporting the creation of a Mn bath facility at the university.

## Appendix A

### Simulation Data

The shortened results (Mn absorption and leakage) for each source are included in this Appendix. The Rad. column gives the Mn bath radius in cm and the Den. column is the solution density in  $\frac{\text{g}}{\text{cm}^3}$ . The Var. columns give the  $1\sigma$  standard deviations corresponding to the adjacent results.

#### *Am-Be*

Rad.	Den.	Mn Abs.	Var.	Leak.	Var.
10.0	1.05	0.0068144	2.04e-05	0.912057	0.0001824
10.0	1.1	0.0133722	4.01e-05	0.908313	0.0002725
10.0	1.15	0.0194809	6.04e-05	0.904956	0.0002715
10.0	1.2	0.0251046	7.78e-05	0.90203	0.0002706
10.0	1.25	0.0302369	9.37e-05	0.899705	0.0002699
10.0	1.3	0.0349167	0.0001082	0.897556	0.0002693
10.0	1.35	0.0390539	0.0001211	0.89588	0.0002688
10.0	1.4	0.0427326	0.0001325	0.894583	0.0002684
15.0	1.05	0.0334679	4.69e-05	0.65902	0.0003954
15.0	1.1	0.063747	8.92e-05	0.649507	0.0004547
15.0	1.15	0.0905042	0.0001267	0.641695	0.0004492
15.0	1.2	0.1140592	0.0001711	0.635196	0.0004446
15.0	1.25	0.1348745	0.0002023	0.629786	0.0004409
15.0	1.3	0.1531919	0.0002298	0.625518	0.0004379
15.0	1.35	0.1693729	0.0002541	0.621745	0.0004352
15.0	1.4	0.1837475	0.0002756	0.618639	0.000433
20.0	1.05	0.0599743	5.4e-05	0.421617	0.0004638
20.0	1.1	0.1125687	0.0001126	0.41224	0.0004535
20.0	1.15	0.1578659	0.0001579	0.40472	0.0004452
20.0	1.2	0.197105	0.0001971	0.398231	0.0004381
20.0	1.25	0.2312607	0.0002313	0.39287	0.0004714
20.0	1.3	0.2609634	0.000261	0.38871	0.0004665
20.0	1.35	0.2867585	0.0003154	0.385637	0.0004628
20.0	1.4	0.3095684	0.0003405	0.382994	0.0004596
25.0	1.05	0.0787729	5.51e-05	0.256148	0.0004098
25.0	1.1	0.1467365	0.0001027	0.24894	0.0003983

25.0	1.15	0.2044333	0.0001635	0.242774	0.0004127
25.0	1.2	0.2537405	0.000203	0.238234	0.000405
25.0	1.25	0.2964184	0.0002371	0.234335	0.0003984
25.0	1.3	0.3332997	0.0002666	0.231252	0.0003931
25.0	1.35	0.3653952	0.0002923	0.228746	0.0003889
25.0	1.4	0.3935585	0.0003542	0.226717	0.0004081
30.0	1.05	0.0906672	5.44e-05	0.151911	0.0003342
30.0	1.1	0.1681243	0.0001009	0.146929	0.0003379
30.0	1.15	0.2334484	0.0001401	0.142716	0.0003282
30.0	1.2	0.2888137	0.0002022	0.13943	0.0003207
30.0	1.25	0.3365631	0.0002356	0.136888	0.0003285
30.0	1.3	0.3777637	0.0002644	0.134722	0.0003233
30.0	1.35	0.4135013	0.0002895	0.133004	0.0003192
30.0	1.4	0.4448308	0.0003114	0.131575	0.0003158
35.0	1.05	0.0978321	4.89e-05	0.0892636	0.0002678
35.0	1.1	0.1809261	0.0001086	0.0858123	0.000266
35.0	1.15	0.2506455	0.0001504	0.0829628	0.0002572
35.0	1.2	0.3095863	0.0001858	0.0808586	0.0002587
35.0	1.25	0.3604092	0.0002162	0.079004	0.0002528
35.0	1.3	0.4040583	0.0002424	0.0775186	0.0002558
35.0	1.35	0.4418817	0.0003093	0.0763619	0.000252
35.0	1.4	0.4751384	0.0003326	0.0754243	0.0002489
40.0	1.05	0.1021002	5.11e-05	0.0520988	0.0002084
40.0	1.1	0.1885013	9.43e-05	0.0498099	0.0002042
40.0	1.15	0.2607608	0.0001304	0.0479999	0.0002016
40.0	1.2	0.3217695	0.0001931	0.0466454	0.0002006
40.0	1.25	0.3742693	0.0002246	0.0455192	0.0001957
40.0	1.3	0.4193302	0.0002516	0.0445238	0.0001959
40.0	1.35	0.4583048	0.000275	0.0437571	0.0001925
40.0	1.4	0.4926123	0.0002956	0.0431661	0.0001942
45.0	1.05	0.1045772	4.18e-05	0.0304131	0.0001612
45.0	1.1	0.1928679	9.64e-05	0.0289956	0.0001566
45.0	1.15	0.2666159	0.0001333	0.0278143	0.0001558
45.0	1.2	0.3288614	0.0001644	0.0268432	0.000153
45.0	1.25	0.3823045	0.0002294	0.0260981	0.0001514
45.0	1.3	0.4281023	0.0002569	0.0254811	0.0001478
45.0	1.35	0.4677559	0.0002807	0.0250418	0.0001477
45.0	1.4	0.5025642	0.0003015	0.0246728	0.0001456
50.0	1.05	0.1060171	4.24e-05	0.0178066	0.0001246
50.0	1.1	0.1954134	9.77e-05	0.0169081	0.0001217
50.0	1.15	0.2700078	0.000135	0.0161777	0.0001181
50.0	1.2	0.3329195	0.0001665	0.0155455	0.0001166
50.0	1.25	0.3868435	0.0002321	0.015091	0.0001147
50.0	1.3	0.4331135	0.0002599	0.0146411	0.0001127
50.0	1.35	0.4731797	0.0002839	0.0143135	0.0001116

50.0	1.4	0.5083426	0.000305	0.0140339	0.0001109
55.0	1.05	0.1068656	4.27e-05	0.0104	9.46e-05
55.0	1.1	0.1969003	9.85e-05	0.0098474	9.26e-05
55.0	1.15	0.2719872	0.000136	0.0093438	9.06e-05
55.0	1.2	0.3352956	0.0001676	0.0088752	8.79e-05
55.0	1.25	0.3895669	0.0001948	0.0085569	8.64e-05
55.0	1.3	0.4360367	0.0002616	0.0083034	8.55e-05
55.0	1.35	0.4763361	0.0002858	0.0080934	8.42e-05
55.0	1.4	0.5116094	0.000307	0.0079741	8.37e-05
60.0	1.05	0.1073573	4.29e-05	0.0060607	7.27e-05
60.0	1.1	0.1977684	9.89e-05	0.005704	7.07e-05
60.0	1.15	0.2731288	0.0001366	0.0053823	6.84e-05
60.0	1.2	0.336619	0.0001683	0.0051509	6.7e-05
60.0	1.25	0.3910258	0.0001955	0.0049712	6.61e-05
60.0	1.3	0.4376501	0.0002626	0.0048069	6.49e-05
60.0	1.35	0.4780442	0.0002868	0.0046672	6.39e-05
60.0	1.4	0.5134201	0.0003081	0.0046042	6.31e-05
65.0	1.05	0.1076392	4.31e-05	0.0035914	5.57e-05
65.0	1.1	0.19826	9.91e-05	0.0033461	5.39e-05
65.0	1.15	0.2737781	0.0001369	0.0031098	5.19e-05
65.0	1.2	0.3373821	0.0001687	0.0030202	5.13e-05
65.0	1.25	0.3919022	0.000196	0.0028685	4.99e-05
65.0	1.3	0.4386008	0.0002632	0.0027589	4.88e-05
65.0	1.35	0.4790435	0.0002874	0.0027029	4.84e-05
65.0	1.4	0.5144672	0.0003087	0.0026592	4.81e-05
70.0	1.05	0.1078026	4.31e-05	0.0021324	4.29e-05
70.0	1.1	0.1985415	9.93e-05	0.0019945	4.17e-05
70.0	1.15	0.274141	0.0001371	0.0018567	4.03e-05
70.0	1.2	0.3378134	0.0001689	0.0017772	3.93e-05
70.0	1.25	0.3923817	0.0001962	0.0016842	3.82e-05
70.0	1.3	0.4391297	0.0002635	0.0015911	3.71e-05
70.0	1.35	0.4796125	0.0002878	0.0015209	3.62e-05
70.0	1.4	0.5150724	0.000309	0.0015102	3.61e-05
75.0	1.05	0.1079034	4.32e-05	0.0012428	3.28e-05
75.0	1.1	0.1987155	7.95e-05	0.0011625	3.17e-05
75.0	1.15	0.2743669	0.0001372	0.0010781	3.05e-05
75.0	1.2	0.3380795	0.000169	0.0009988	2.94e-05
75.0	1.25	0.3926866	0.0001963	0.0009326	2.84e-05
75.0	1.3	0.4394474	0.0002637	0.0008962	2.78e-05
75.0	1.35	0.4799394	0.000288	0.0008595	2.72e-05
75.0	1.4	0.5154203	0.0003093	0.0008537	2.71e-05

*Cf*

Rad.	Den.	Mn Abs.	Var.	Leak.	Var.
10.0	1.05	0.0110622	2.54e-05	0.873761	0.0002621
10.0	1.1	0.0216625	4.98e-05	0.868159	0.0002604
10.0	1.15	0.031482	7.56e-05	0.863411	0.000259
10.0	1.2	0.0404854	9.72e-05	0.859173	0.0002578
10.0	1.25	0.0487549	0.000117	0.855681	0.0003423
10.0	1.3	0.0561906	0.0001349	0.852774	0.0003411
10.0	1.35	0.0629222	0.000151	0.850335	0.0003401
10.0	1.4	0.0690177	0.0001656	0.848392	0.0003394
15.0	1.05	0.0482081	5.3e-05	0.530552	0.0004244
15.0	1.1	0.0915309	0.0001007	0.518978	0.0004671
15.0	1.15	0.1296528	0.0001426	0.509332	0.0004584
15.0	1.2	0.1632057	0.0001795	0.501278	0.0004512
15.0	1.25	0.1927079	0.000212	0.494799	0.0004453
15.0	1.3	0.218593	0.0002405	0.489724	0.0004408
15.0	1.35	0.241235	0.0002895	0.485971	0.000486
15.0	1.4	0.2613869	0.0003137	0.483046	0.000483
20.0	1.05	0.0779203	5.45e-05	0.273189	0.0004098
20.0	1.1	0.1457194	0.000102	0.26347	0.0003952
20.0	1.15	0.2037531	0.0001426	0.256174	0.0004099
20.0	1.2	0.2538398	0.0002031	0.250014	0.0004
20.0	1.25	0.2971562	0.0002377	0.245483	0.0003928
20.0	1.3	0.3347005	0.0002678	0.241814	0.0004111
20.0	1.35	0.3677101	0.0002942	0.238999	0.0004063
20.0	1.4	0.3965734	0.0003173	0.236878	0.0004027
25.0	1.05	0.0943001	4.72e-05	0.134048	0.0003083
25.0	1.1	0.1749573	0.000105	0.12834	0.000308
25.0	1.15	0.2430256	0.0001458	0.124131	0.0003103
25.0	1.2	0.3011841	0.0001807	0.12059	0.0003015
25.0	1.25	0.3511076	0.0002458	0.118013	0.0003068
25.0	1.3	0.3942045	0.0002759	0.116041	0.0003017
25.0	1.35	0.4320119	0.0003024	0.114392	0.0002974
25.0	1.4	0.4648426	0.0003254	0.113502	0.0003065
30.0	1.05	0.102317	5.12e-05	0.0660164	0.0002311
30.0	1.1	0.1890514	9.45e-05	0.0630524	0.000227
30.0	1.15	0.2618577	0.0001309	0.0607641	0.0002248
30.0	1.2	0.3236967	0.0001942	0.0589674	0.0002241
30.0	1.25	0.3766956	0.000226	0.0575503	0.0002187
30.0	1.3	0.4223077	0.0002534	0.0566001	0.0002207
30.0	1.35	0.4622695	0.0002774	0.0558027	0.0002176
30.0	1.4	0.4971524	0.000348	0.0552627	0.0002155
35.0	1.05	0.106172	4.25e-05	0.0331977	0.000166
35.0	1.1	0.1958567	9.79e-05	0.031561	0.0001641

35.0	1.15	0.2708581	0.0001354	0.0303702	0.000161
35.0	1.2	0.3344515	0.0001672	0.0294099	0.0001588
35.0	1.25	0.3888613	0.0002333	0.0286474	0.0001576
35.0	1.3	0.4356878	0.0002614	0.0281558	0.0001577
35.0	1.35	0.4766941	0.000286	0.0277622	0.0001555
35.0	1.4	0.5124308	0.0003075	0.0274131	0.0001563
40.0	1.05	0.1080759	4.32e-05	0.0170335	0.0001209
40.0	1.1	0.1991622	9.96e-05	0.0162193	0.0001184
40.0	1.15	0.2752384	0.0001376	0.0155933	0.0001169
40.0	1.2	0.3396356	0.0001698	0.0151266	0.000115
40.0	1.25	0.3946988	0.0001973	0.0146982	0.0001132
40.0	1.3	0.4421386	0.0002653	0.0144547	0.0001127
40.0	1.35	0.4836285	0.0002902	0.0142105	0.0001123
40.0	1.4	0.5197296	0.0003118	0.0140746	0.0001126
45.0	1.05	0.1090134	4.36e-05	0.0090153	8.83e-05
45.0	1.1	0.2007994	0.0001004	0.0085928	8.68e-05
45.0	1.15	0.2774275	0.0001387	0.0081997	8.45e-05
45.0	1.2	0.3422659	0.0001711	0.0078741	8.35e-05
45.0	1.25	0.3976555	0.0001988	0.0076568	8.19e-05
45.0	1.3	0.4453541	0.0002672	0.0074977	8.17e-05
45.0	1.35	0.4870913	0.0002923	0.0073628	8.1e-05
45.0	1.4	0.5234385	0.0003141	0.0072946	8.02e-05
50.0	1.05	0.1094995	4.38e-05	0.0048504	6.45e-05
50.0	1.1	0.2016615	8.07e-05	0.0045482	6.28e-05
50.0	1.15	0.2785485	0.0001393	0.0043314	6.15e-05
50.0	1.2	0.3435958	0.0001718	0.0041442	6.05e-05
50.0	1.25	0.3991777	0.0001996	0.0040213	5.95e-05
50.0	1.3	0.4470339	0.0002682	0.0039348	5.9e-05
50.0	1.35	0.4888772	0.0002933	0.0038539	5.86e-05
50.0	1.4	0.5253173	0.0003152	0.0038251	5.81e-05
55.0	1.05	0.1097559	4.39e-05	0.0026151	4.76e-05
55.0	1.1	0.2021046	8.08e-05	0.002419	4.57e-05
55.0	1.15	0.2791225	0.0001396	0.0023112	4.48e-05
55.0	1.2	0.3442825	0.0001721	0.0021975	4.37e-05
55.0	1.25	0.3999544	0.0002	0.0021249	4.31e-05
55.0	1.3	0.4478861	0.0002687	0.0020881	4.28e-05
55.0	1.35	0.4897963	0.0002939	0.0020286	4.22e-05
55.0	1.4	0.526322	0.0003158	0.0019829	4.18e-05
60.0	1.05	0.1098939	4.4e-05	0.0014276	3.51e-05
60.0	1.1	0.2023389	8.09e-05	0.0013244	3.4e-05
60.0	1.15	0.2794369	0.0001397	0.0012472	3.31e-05
60.0	1.2	0.3446437	0.0001723	0.0011958	3.24e-05
60.0	1.25	0.4003704	0.0002002	0.0011334	3.16e-05
60.0	1.3	0.4483353	0.000269	0.0011212	3.14e-05
60.0	1.35	0.4902824	0.0002942	0.0010895	3.09e-05

60.0	1.4	0.5268272	0.0003161	0.0010625	3.05e-05
65.0	1.05	0.1099681	4.4e-05	0.0007964	2.62e-05
65.0	1.1	0.2024594	8.1e-05	0.0007477	2.55e-05
65.0	1.15	0.279596	0.0001398	0.0007217	2.51e-05
65.0	1.2	0.3448301	0.0001724	0.0006807	2.44e-05
65.0	1.25	0.4005791	0.0002003	0.000643	2.37e-05
65.0	1.3	0.4485733	0.0002691	0.0006206	2.33e-05
65.0	1.35	0.490531	0.0002943	0.0006105	2.32e-05
65.0	1.4	0.5270894	0.0003163	0.0005929	2.28e-05
70.0	1.05	0.1100048	4.4e-05	0.0004759	2.04e-05
70.0	1.1	0.2025192	8.1e-05	0.0004488	1.98e-05
70.0	1.15	0.2796767	0.0001398	0.0004181	1.91e-05
70.0	1.2	0.3449257	0.0001725	0.0004017	1.88e-05
70.0	1.25	0.4006773	0.0002003	0.0003887	1.84e-05
70.0	1.3	0.4486861	0.0002692	0.0003714	1.8e-05
70.0	1.35	0.490658	0.0002944	0.0003488	1.74e-05
70.0	1.4	0.5272236	0.0003163	0.0003404	1.72e-05
75.0	1.05	0.1100244	4.4e-05	0.0002941	1.59e-05
75.0	1.1	0.2025556	8.1e-05	0.0002784	1.55e-05
75.0	1.15	0.2797243	0.0001399	0.0002628	1.51e-05
75.0	1.2	0.3449842	0.0001725	0.0002489	1.47e-05
75.0	1.25	0.4007376	0.0002004	0.0002329	1.43e-05
75.0	1.3	0.4487508	0.0002693	0.0002214	1.39e-05
75.0	1.35	0.4907231	0.0002944	0.0002088	1.35e-05
75.0	1.4	0.5272938	0.0003164	0.0001986	1.32e-05

***Pu-Be***

Rad.	Den.	Mn Abs.	Var.	Leak.	Var.
10	1.05	0.0049086	1.72E-05	0.939876	0.000188
10	1.1	0.0096832	3.39E-05	0.936219	0.0001872
10	1.15	0.0141712	4.96E-05	0.933023	0.0001866
10	1.2	0.0182926	6.40E-05	0.93027	0.0001861
10	1.25	0.0221491	7.75E-05	0.927835	0.0001856
10	1.3	0.0256214	9.22E-05	0.925607	0.0001851
10	1.35	0.0287879	0.0001036	0.923667	0.0002771
10	1.4	0.0314545	0.0001132	0.922127	0.0002766
15	1.05	0.0289797	4.64E-05	0.713122	0.0004279
15	1.1	0.0553619	8.86E-05	0.702903	0.0004217
15	1.15	0.0785681	0.0001257	0.694978	0.000417
15	1.2	0.0992976	0.0001589	0.687822	0.0004127
15	1.25	0.1175203	0.000188	0.681944	0.0004092
15	1.3	0.1337183	0.0002273	0.676679	0.000406

15	1.35	0.1478832	0.0002514	0.672869	0.0004037
15	1.4	0.1603792	0.0002726	0.6692	0.0004015
20	1.05	0.0557439	6.13E-05	0.471666	0.0004717
20	1.1	0.1046542	0.0001151	0.461175	0.0004612
20	1.15	0.1468608	0.0001615	0.452443	0.0004524
20	1.2	0.1834267	0.0002018	0.44545	0.0004455
20	1.25	0.215124	0.0002366	0.439605	0.0004396
20	1.3	0.2426303	0.0002669	0.434842	0.0004783
20	1.35	0.2666693	0.0002933	0.431116	0.0004742
20	1.4	0.2877419	0.0003453	0.427664	0.0004704
25	1.05	0.0757188	6.06E-05	0.294544	0.0004124
25	1.1	0.1409529	0.0001128	0.286218	0.0004293
25	1.15	0.1964058	0.0001571	0.27948	0.0004192
25	1.2	0.2437699	0.0002194	0.273907	0.0004109
25	1.25	0.2846042	0.0002561	0.269385	0.0004041
25	1.3	0.3197351	0.0002878	0.265521	0.0004248
25	1.35	0.3506155	0.0003156	0.262527	0.00042
25	1.4	0.3772793	0.0003396	0.260027	0.000416
30	1.05	0.0886977	6.21E-05	0.180123	0.0003602
30	1.1	0.1642507	0.000115	0.174103	0.0003482
30	1.15	0.2279541	0.0001596	0.169286	0.0003555
30	1.2	0.2820851	0.0001975	0.165277	0.0003471
30	1.25	0.3285025	0.00023	0.16208	0.0003404
30	1.3	0.3683991	0.0002947	0.159329	0.0003505
30	1.35	0.4032742	0.0003226	0.157042	0.0003455
30	1.4	0.4333738	0.0003467	0.155213	0.0003415
35	1.05	0.0967727	5.81E-05	0.109188	0.0002948
35	1.1	0.1786729	0.0001072	0.10495	0.0002834
35	1.15	0.2474252	0.0001485	0.101584	0.0002844
35	1.2	0.3056042	0.0002139	0.0987056	0.0002764
35	1.25	0.3553883	0.0002488	0.0965946	0.0002801
35	1.3	0.3979519	0.0002786	0.0946561	0.0002745
35	1.35	0.4351907	0.0003046	0.0931277	0.0002701
35	1.4	0.4672726	0.0003271	0.0918908	0.0002757
40	1.05	0.1016522	5.08E-05	0.0660819	0.0002313
40	1.1	0.1873188	0.0001124	0.063328	0.000228
40	1.15	0.2589972	0.0001554	0.0610483	0.0002259
40	1.2	0.3195455	0.0001917	0.0591072	0.0002187
40	1.25	0.3712996	0.0002228	0.0576523	0.0002191
40	1.3	0.4153849	0.0002492	0.0563781	0.0002142
40	1.35	0.454044	0.0003178	0.0551287	0.000215
40	1.4	0.4872557	0.0003411	0.0543631	0.000212
45	1.05	0.1046039	5.23E-05	0.0400638	0.0001843
45	1.1	0.1925358	9.63E-05	0.0381173	0.0001792
45	1.15	0.2660107	0.0001596	0.0365128	0.0001753

45	1.2	0.3279533	0.0001968	0.0352801	0.0001729
45	1.25	0.38083	0.0002285	0.0343354	0.0001717
45	1.3	0.4258435	0.0002555	0.0334957	0.0001675
45	1.35	0.4652418	0.0002791	0.0327239	0.0001669
45	1.4	0.4991397	0.0003494	0.0321699	0.0001641
50	1.05	0.1063809	5.32E-05	0.0243587	0.0001437
50	1.1	0.1956236	9.78E-05	0.0231372	0.0001388
50	1.15	0.2700993	0.000135	0.0222351	0.0001379
50	1.2	0.3328452	0.0001997	0.0213013	0.0001342
50	1.25	0.3863849	0.0002318	0.0206067	0.0001319
50	1.3	0.4319565	0.0002592	0.0199993	0.00013
50	1.35	0.4717844	0.0002831	0.0195493	0.000129
50	1.4	0.5061567	0.0003037	0.0190296	0.0001275
55	1.05	0.107449	5.37E-05	0.0149095	0.0001118
55	1.1	0.1974969	9.87E-05	0.0140656	0.0001097
55	1.15	0.2726311	0.0001363	0.0133761	0.000107
55	1.2	0.3358469	0.0002015	0.0127647	0.0001047
55	1.25	0.3897673	0.0002339	0.0123256	0.0001023
55	1.3	0.4356503	0.0002614	0.0119111	0.0001001
55	1.35	0.475752	0.0002855	0.0115534	9.94E-05
55	1.4	0.5102986	0.0003062	0.0113135	9.84E-05
60	1.05	0.1080977	5.40E-05	0.0091218	8.76E-05
60	1.1	0.1986371	9.93E-05	0.008569	8.48E-05
60	1.15	0.2741386	0.0001371	0.0081084	8.27E-05
60	1.2	0.3376161	0.0001688	0.0077169	8.10E-05
60	1.25	0.3917544	0.0002351	0.0074368	7.96E-05
60	1.3	0.4377848	0.0002627	0.0071841	7.76E-05
60	1.35	0.4780469	0.0002868	0.0069428	7.64E-05
60	1.4	0.5127295	0.0003076	0.0067553	7.57E-05
65	1.05	0.1084959	5.42E-05	0.0055858	6.87E-05
65	1.1	0.1993245	9.97E-05	0.0052612	6.63E-05
65	1.15	0.2750311	0.0001375	0.0049579	6.45E-05
65	1.2	0.3386627	0.0001693	0.0046854	6.28E-05
65	1.25	0.3929414	0.0002358	0.0044879	6.15E-05
65	1.3	0.4390549	0.0002634	0.0043491	6.05E-05
65	1.35	0.4794481	0.0002877	0.0041435	5.88E-05
65	1.4	0.5141763	0.0003085	0.0040516	5.83E-05
70	1.05	0.1087341	4.35E-05	0.003496	5.42E-05
70	1.1	0.1997348	9.99E-05	0.0032559	5.21E-05
70	1.15	0.2755799	0.0001378	0.0030478	5.06E-05
70	1.2	0.3393125	0.0001697	0.0028591	4.89E-05
70	1.25	0.393664	0.0002362	0.0027186	4.76E-05
70	1.3	0.4398347	0.0002639	0.0026391	4.67E-05
70	1.35	0.4802645	0.0002882	0.0025016	4.55E-05
70	1.4	0.5150264	0.000309	0.0024305	4.47E-05

75	1.05	0.108883	4.36E-05	0.0021656	4.24E-05
75	1.1	0.1999943	0.0001	0.0020152	4.09E-05
75	1.15	0.2759178	0.000138	0.0018771	3.96E-05
75	1.2	0.339717	0.0001699	0.0017485	3.81E-05
75	1.25	0.3940943	0.0002365	0.0016799	3.73E-05
75	1.3	0.4403112	0.0002642	0.0016028	3.64E-05
75	1.35	0.4807484	0.0002884	0.001515	3.53E-05
75	1.4	0.5155351	0.0003093	0.0014618	3.45E-05

## Appendix B

### MCNP Codes

This Appendix records the MCNP input files referenced throughout the thesis. The font of all code has been changed to delineate code and text and to ensure that line wrapping is minimized for future copy and pasting of code.

#### *NPL\_Best\_Validation*

This is the MCNP input file which produced the best results for the NPL validation.

Copied with edits from Roberts, 2001, NPL

```

1 1 -7.93 1 -2 #(-16 14) #(-36 -25)          imp:n=1 $ cavity shell
2 1 -7.93 (3 -4) #(-6 14)                    imp:n=1 $ bath shell
3 0 5                                          imp:n=0 $ neutron termination
4 1 -7.93 (16 -17 -10 2 14):(11 -17 10 -5)   imp:n=1 $ cavity transport rod
7 0 (-1:(-16 -10 1 14):(-11 10 -5)) #11 #12 #(-36 -25 -1) #18 imp:n=1 $ inside cavity
8 2 -1.4046 (2 -3) #(-17 14) #(-24 2 19 -18) #(2 -36 31 -33) #16 #17 imp:n=1 $ MnSO4
9 3 -2.02 22 -23 21 -20                      imp:n=1 $ cavity seal O-ring
10 1 -7.93 (2 -24 19 -18) #9                 imp:n=1 $ cavity seal
11 4 -1.24 -29 27 -26                        imp:n=1 $ source material
12 1 -7.93 (-28 25 -37) #11                 imp:n=1 $ source capsule
13 0 -32 -25 33                              imp:n=1 $ source rod (inside)
14 1 -7.93 (-36 -25 31) #13                 imp:n=1 $ source rod
15 0 (-5 4) #(-17 14)                       imp:n=1 $ outside bath
16 1 -7.93 2 18 -34 -35 17 #17              imp:n=1 $ cavity vacuum cup
17 3 -2.02 2 -9 7 -8 14                     imp:n=1 $ cavity vacuum cup O-ring
18 1 -7.93 (28 -38 -41 40):(36 -28 -25 40)   imp:n=1 $ source cup
20 1 -15.9 (3 -4 -6 14) #(-17 14)           imp:n=1 $ bath lid

1 SO 4.344 $ internal surface of cavity sphere
2 SO 4.4 $ external surface of cavity sphere
3 SO 50 $ internal surface of bath shell
4 SO 50.15 $ external surface of bath shell
5 SO 70 $ boundary sphere surface
6 CZ 15.22 $ edge of bath lid
7 CZ 1.13 $ internal radius of vacuum cup O-ring
8 CZ 1.42 $ external radius of vacuum cup O-ring
9 SO 4.58 $ upper surface of vacuum cup O-ring
10 PZ 7.8 $ upper surface of vacuum cup joint
11 CZ 0.47 $ internal surface of transport rod above joint
14 PZ 4 $ ambiguity surface
16 CZ 0.33 $ internal surface of cavity transport rod
17 CZ 0.65 $ external surface of cavity transport rod
18 PZ 0.35 $ upper surface of cavity seal
19 PZ -0.45 $ lower surface of cavity seal
20 PZ 0 $ upper surface of cavity O-ring
21 PZ -0.22 $ lower surface of cavity O-ring
22 CZ 4.65 $ inside edge of cavity O-ring
23 CZ 4.95 $ outside edge of cavity O-ring
24 CZ 5.28 $ outside edge of cavity seal

```

25 PZ -1.46 \$ bottom of source capsule  
 26 PZ 0.815 \$ top of source material  
 27 PZ -0.815 \$ bottom of source material  
 28 CZ 1.12 \$ outside edge of source capsule  
 29 CZ 0.88 \$ inside edge of source capsule  
 31 PZ -4.6 \$ bottom of source rod  
 32 CZ 0.2 \$ inner surface of source rod  
 33 PZ -3.334 \$ inner bottom surface of source rod  
 34 CZ 1.65 \$ side edge of cavity vacuum cup  
 35 SO 4.75 \$ upper surface of cavity vacuum cup  
 36 CZ 0.303 \$ outer edge of source rod  
 37 PZ 1.39 \$ top of source capsule  
 38 CZ 1.19 \$ outer edge of source cup  
 40 PZ -1.51 \$ outer surface of source cup base  
 41 PZ -0.49 \$ inner surface of source cup base  
 42 SO 1.84011 \$ source emission sphere

SDEF ERG=D1 SUR=42

SI1 H 4.14E-07 0.11 0.33 0.54 0.75 0.97 1.18 1.4 1.61 1.82 2.04  
 2.25 2.47 2.68 2.9 3.11 3.32 3.54 3.75 3.97 4.18 4.39 4.61  
 4.82 5.04 5.25 5.47 5.68 5.89 6.11 6.32 6.54 6.75 6.96 7.18  
 7.39 7.61 7.82 8.03 8.25 8.46 8.68 8.89 9.11 9.32 9.53 9.75  
 9.96 10.18 10.39 10.6 10.82 11.03  
 SP1 D 0 0.0144 0.0334 0.0313 0.0281 0.025 0.0214 0.0198 0.0175  
 0.0192 0.0222 0.0215 0.0225 0.0228 0.0295 0.0356 0.0368  
 0.0346 0.0307 0.03 0.0269 0.0286 0.0318 0.0307 0.0333 0.0304  
 0.0274 0.0233 0.0206 0.0181 0.0177 0.0204 0.0183 0.0163  
 0.0168 0.0168 0.0188 0.0184 0.0169 0.0143 0.0097 0.0065  
 0.0043 0.0037 0.0038 0.0051 0.0062 0.0055 0.0047 0.0037  
 0.0028 0.0015 0.0004

SC1 Am-Be SPECTRUM (ISO 8529)

C

FC1 NEUTRON LEAKAGE FROM BATH

F1:N 5

FC11 THERMAL ENERGY SPECTRUM INSIDE CAVITY

F11:N 1

E11 1.0E-09 1.0E-07 5.0E-07 20

FC21 THERMAL ENERGY SPECTRUM OUTSIDE CAVITY

F21:N 2

E21 1.0E-09 1.0E-07 5.0E-07 20

FC4 NEUTRON CAPTURE IN CAVITY

F4:N 1 4 10 12 14 16 18 T

FM4 8.62157E-02 1 -2

FC14 NEUTRON CAPTURE IN RUBBER SEAL

F14:N 9

FM14 0.225073 3 -2

FC24 NEUTRON CAPTURE IN MnSO4 SOLUTION

F24:N 8

FM24 1.04936E-01 2 -2

FC34 (N,GAMMA) CAPTURE IN MANGANESE

F34:N 8

FM34 1.878E-03 5 -2

FC44 NEUTRON CAPTURE IN SULPHUR: TOTAL, (N,GAMMA), (N,P), (N,ALPHA)

F44:N 8

FM44 1.878E-03 6 (-2) (102) (103) (107)

FC54 NEUTRON CAPTURE IN OXYGEN: TOTAL, (N,GAMMA), (N,ALPHA)

F54:N 8

FM54 3.874E-02 7 (-2) (102) (107)

FC64 (N,GAMMA) CAPTURE IN HYDROGEN

F64:N 8

FM64 6.243E-02 8 -2

FC74 NEUTRON CAPTURE IN SOURCE MATERIAL

F74:N 11

FM74 7.816E-02 4 -2

C

PRINT 110 10 30 40 50 72 102 \$ not original

C

```

M1      26000.55c      -0.65395
        24000.50c      -0.17
        28000.50c      -0.12
        25055.60c      -0.02
        14000.60c      -0.01
        15031.60c      -0.00045
        16032.60c      -0.0003
        6012.50c       -0.0003
        42000.60c      -0.025 $ STEEL
M2      25055.60c      0.0179
        16032.60c      0.0179
        8016.60c       0.3692
        1001.60c      0.5950 $ MnSO4 SOLUTION
M3      6012.50c      0.4
        1001.60c      0.6 $ RUBBER
M4      95241.60c     0.00220
        4009.60c      0.99339
        8016.60c     0.00441 $ SOURCE MATERIAL
M5      25055.60c     1 $ MANGANESE
M6      16032.60c     1 $ SULPHUR
M7      8016.60c     1 $ OXYGEN
M8      1001.60c     1 $ HYDROGEN
MT2 LWTR.01
C
PHYS:N 20 20
C
NPS 1.5e6

```

### *Golestan\_University\_Best\_Validation*

This is the MCNP input file which produced the best results for the Golestan Univeristy validation.

Attempt to Validate Bath Model by Copying Khabaz's Input

C Cell Cards

```

C
1      1      -7.93      1 -2      imp:n=1      $ bath shell
2      2      -1.0934     -1 (9:-10:14)  imp:n=1      $ bath solution
3      5      -1.85      -3 4 -11      imp:n=1      $ Am-Be
4      1      -7.93      -5 6 -12 (3:-4:11) imp:n=1      $ steel source containment
5      9      -0.00129-7     8 -13 (5:-6:12) imp:n=1      $ hollow of the source holder
6      4      -2.2      -9 10 -14 (7:-8:13) imp:n=1      $ PTFE holder
7      0      2      imp:n=0      $ void outside of bath

```

C Surface Cards

```

C
1      SO      50      $ inner sphere for bath shell
2      SO      50.3     $ outer sphere for bath shell
3      PZ      2.84     $ top of Am-Be
4      PZ      -2.84    $ bottom of Am-Be
5      PZ      3      $ top of steel source containment
6      PZ      -3      $ bottom of steel source containment
7      PZ      4.6     $ top inside of PTFE holder
8      PZ      -4.6    $ bottom inside of PTFE holder
9      PZ      5      $ top of PTFE holder
10     PZ      -5      $ bottom of PTFE holder
11     CZ      1.34    $ Am-Be wall
12     CZ      1.5     $ steel containment wall
13     CZ      4.6     $ PTFE holder inside wall

```

14 CZ 5 \$ PTFE holder wall

C Data Cards

C

mode n

SDEF PAR=1 AXS=0 0 1 ERG=d1 SUR=d2 POS=FSUR d3 RAD=FSUR d4 NRM=FSUR d8 EXT=d12

C \$ Am-Be bins from ISO from Roberts 2011

SI1 H 4.14E-07 0.11 0.33 0.54 0.75 0.97 1.18 1.4 1.61 1.82 2.04  
 2.25 2.47 2.68 2.9 3.11 3.32 3.54 3.75 3.97 4.18 4.39 4.61  
 4.82 5.04 5.25 5.47 5.68 5.89 6.11 6.32 6.54 6.75 6.96 7.18  
 7.39 7.61 7.82 8.03 8.25 8.46 8.68 8.89 9.11 9.32 9.53 9.75  
 9.96 10.18 10.39 10.6 10.82 11.03

SP1 D 0 0.0144 0.0334 0.0313 0.0281 0.025 0.0214 0.0198 0.0175  
 0.0192 0.0222 0.0215 0.0225 0.0228 0.0295 0.0356 0.0368  
 0.0346 0.0307 0.03 0.0269 0.0286 0.0318 0.0307 0.0333 0.0304  
 0.0274 0.0233 0.0206 0.0181 0.0177 0.0204 0.0183 0.0163  
 0.0168 0.0168 0.0188 0.0184 0.0169 0.0143 0.0097 0.0065  
 0.0043 0.0037 0.0038 0.0051 0.0062 0.0055 0.0047 0.0037  
 0.0028 0.0015 0.0004

SI2 L 12 5 6

SP2 D 0.666 0.167 0.167

DS3 L 0 0 0 0 0 3 0 0 -3

DS4 S 5 6 7

SI5 L 1.5

SP5 D 1

SI6 0 1.5

SP6 -21 1

SI7 0 1.5

SP7 -21 1

DS8 L 1 1 -1

SI12 -3 3

SP12 -21 0

nps 1E6

C

F12:N 1 \$ inner shell surface avg fkux

FC12 Average neutron flux in inner surface of bath shell [n/cm<sup>2</sup>]

C

F11:N 1 \$ inner shell surface neutron count

FC11 Neutrons passing through inner bath shell surface [n]

C11 0 1 \$ Backscatter and Leakage Bins

C

F14:N 2 \$ volume track length flux for solution volume

FM14 (4.085E-4 3 -2) \$ Mn(n,g), rxn rate multiplier is N\_Mn in [a/b-cm]

FC14 Absorption in Mn per source neutron per volume of bath [n/cm<sup>3</sup>]

C

F24:N 2 \$ volume track length flux for solution volume

FM24 (6.624E-2 6 -2) \$ H(n,t), rxn rate multiplier is N\_H in [a/b-cm]

FC24 Absorption in H per source neutron per volume of bath [n/cm<sup>3</sup>]

C

F34:N 2 \$ volume track length flux for solution volume

FM34 (3.475E-2 7 -2) \$ O(n,t), rxn rate multiplier is N\_O in [a/b-cm]

FC34 Absorption in O per source neutron per volume of bath [n/cm<sup>3</sup>]

C

F44:N 2 \$ volume track length flux for solution volume

FM44 (4.085E-4 8 -2) \$ S(n,t), rxn rate multiplier is N\_S in [a/b-cm]

FC44 Absorption in S per source neutron per volume of bath [n/cm<sup>3</sup>]

C

F54:N 6 \$ volume track length flux for source holder

FM54 (-1 4 -2) \$ PTFE absorption

FC54 Absorption in PTFE source holder [n/cm<sup>3</sup>]

C

F64:N 4 \$ volume track length flux for steel containment

FM64 (-1 1 -2) \$ absorption in steel containment

FC64 Absorption in stainless steel source containment [n/cm<sup>3</sup>]

C

F74:N 3 \$ volume track length flux for Am-Be

FM74 (-1 5 -2) \$ absorption in Am-Be

```

FC74 Self-absorption in Am-Be [n/cm^3]
C
F84:N 2      $ volume track length flux for solution
FM84 (-1 2 -2) $ absorption in all solution
FC84 All absorption in solution [n/cm^3]
C
PRINT 110 10 30 40 50 72 102
C
C Material Cards
C Stainless Steel Shell
M1      26056.60c      -0.65395      $ Fe-56
        24052.60c      -0.17          $ Cr-52
        28058.60c      -0.12          $ Ni-58
        25055.60c      -0.02          $ Mn-55
        14000.60c      -0.01          $ Si-nat
        6000.60c       -0.0003        $ C-nat
        15031.60c      -0.00045       $ P-31
        42000.60c      -0.025         $ Mo-nat
        16032.60c      -0.0003        $ S-32
C MnSO4 Solution
M2      25055.60c      0.0040        $ Mn-55
        1001.60c       0.6506         $ H-1
        8016.60c       0.3414         $ O-16
        16032.60c      0.0040         $ S-32
MT2     LWTR.60t
C Pure Mn for capture tally
M3      25055.60c      1              $ Mn-55
C Teflon
M4      6000.60c       0.33333       $ C-nat
        9019.60c       0.66667       $ F-19
C CfO2
M5      8016.60c       0.66667       $ O-16
        98252.60c      0.33333       $ Cf-252
C Pure H-1 for capture tally
M6      1001.60c       1              $ H-1
C Pure O-16 for capture tally
M7      8016.60c       1              $ O-16
C Pure S-32 for capture tally
M8      16032.60c      1              $ S-32
C Air
M9      7014.60c       0.791         $ N-14
        8016.60c       0.209         $ O-16

```

### ***ENEA-INMRI\_Best\_Validation***

This is the MCNP input file which produced the best results for the ENEA-INMRI validation.

Attempt to Validate Bath Model by Copying Anendola's Input

C Cell Cards

```

C
1      1      -7.93  1 -2          imp:n=1      $ bath shell
2      2      -1.1564 -1 (7:-8:11)  imp:n=1      $ bath solution
3      5      -1.5725 -3 4 -9      imp:n=1      $ Am-Be
4      1      -7.93  -5 6 -10 (3:-4:9)  imp:n=1      $ steel source containment
5      4      -2.2   -7 8 -11 (5:-6:10)  imp:n=1      $ PTFE holder
6      0              2          imp:n=0      $ void outside of bath

```

C Surface Cards

```

C
1      SO      50      $ inner sphere for bath shell
2      SO      50.5    $ outer sphere for bath shell
3      PZ      0.5     $ top of Am-Be
4      PZ      -0.5    $ bottom of Am-Be
5      PZ      1.5     $ top of steel source containment
6      PZ      -1.5    $ bottom of steel source containment
7      PZ      10      $ top of PTFE holder
8      PZ      -10     $ bottom of PTFE holder
9      CZ      1       $ Am-Be wall
10     CZ      1.55    $ steel containment wall
11     CZ      5       $ PTFE holder wall

C Data Cards
C
mode n
SDEF  PAR=1  AXS=0 0 1  ERG=d1  SUR=d2  POS=FSUR d3  RAD=FSUR d4  NRM=FSUR d8  EXT=d12
C Am-Be bins from ISO from Roberts 2011
SI1 H  4.14E-07 0.11 0.33 0.54 0.75 0.97 1.18 1.4 1.61 1.82 2.04
        2.25 2.47 2.68 2.9 3.11 3.32 3.54 3.75 3.97 4.18 4.39 4.61
        4.82 5.04 5.25 5.47 5.68 5.89 6.11 6.32 6.54 6.75 6.96 7.18
        7.39 7.61 7.82 8.03 8.25 8.46 8.68 8.89 9.11 9.32 9.53 9.75
        9.96 10.18 10.39 10.6 10.82 11.03
SP1 D  0 0.0144 0.0334 0.0313 0.0281 0.025 0.0214 0.0198 0.0175
        0.0192 0.0222 0.0215 0.0225 0.0228 0.0295 0.0356 0.0368
        0.0346 0.0307 0.03 0.0269 0.0286 0.0318 0.0307 0.0333 0.0304
        0.0274 0.0233 0.0206 0.0181 0.0177 0.0204 0.0183 0.0163
        0.0168 0.0168 0.0188 0.0184 0.0169 0.0143 0.0097 0.0065
        0.0043 0.0037 0.0038 0.0051 0.0062 0.0055 0.0047 0.0037
        0.0028 0.0015 0.0004
SI2 L 10 5 6
SP2 D 0.6594 0.1703 0.1703
DS3 L 0 0 0 0 1.5 0 0 -1.5
DS4 S 5 6 7
SI5 L 1.55
SP5 D 1
SI6 0 1.55
SP6 -21 1
SI7 0 1.55
SP7 -21 1
DS8 L 1 1 -1
SI12 -1.5 1.5
SP12 -21 0
nps 1E6
C
F12:N 2      $ outer shell surface avg fkux
FC12 Average neutron flux in outer surface of bath shell [n/cm^2]
C
F11:N 1      $ inner shell surface neutron count
FC11 Neutrons passing through inner bath shell surface [n]
C11 0 1      $ Backscatter and Leakage Bins
C
F14:N 2      $ volume track length flux for solution volume
FM14 (6.72E-4 3 -2) $ Mn(n,g), rxn rate multiplier is N_Mn in [a/b-cm]
FC14 Absorption in Mn per source neutron per volume of bath [n/cm^3]
C
F24:N 2      $ volume track length flux for solution volume
FM24 (6.61E-2 6 -2) $ H(n,t), rxn rate multiplier is N_H in [a/b-cm]
FC24 Absorption in H per source neutron per volume of bath [n/cm^3]
C
F34:N 2      $ volume track length flux for solution volume
FM34 (3.57E-2 7 -2) $ O(n,t), rxn rate multiplier is N_O in [a/b-cm]
FC34 Absorption in O per source neutron per volume of bath [n/cm^3]
C
F44:N 2      $ volume track length flux for solution volume
FM44 (6.72E-4 8 -2) $ S(n,t), rxn rate multiplier is N_S in [a/b-cm]
FC44 Absorption in S per source neutron per volume of bath [n/cm^3]

```

```

C
F54:N 5      $ volume track length flux for source holder
FM54 (-1 4 -2) $ PTFE absorption
FC54 Absorption in PTFE source holder [n/cm^3]
C
F64:N 4      $ volume track length flux for steel containment
FM64 (-1 1 -2) $ absorption in steel containment
FC64 Absorption in stainless steel source containment [n/cm^3]
C
F74:N 3      $ volume track length flux for Am-Be
FM74 (-1 5 -2) $ absorption in Am-Be
FC74 Self-absorption in Am-Be [n/cm^3]
C
F84:N 2      $ volume track length flux for solution
FM84 (-1 2 -2) $ absorption in all solution
FC84 All absorption in solution [n/cm^3]
C
PRINT 110 10 30 40 50 72 102
C
C Material Cards
C Stainless Steel Shell
M1      26056.62c      -0.70925      $ Fe-56
        24052.62c      -0.18          $ Cr-52
        28058.62c      -0.08          $ Ni-58
        25055.62c      -0.02          $ Mn-55
        14028.62c      -0.01          $ Si-28
        6000.66c       -0.0003       $ C-nat (12)
        15031.66c      -0.00045     $ P-31
C MnSO4 Solution
M2      25055.62c      0.0065       $ Mn-55
        1001.62c       0.6406       $ H-1
        8016.62c       0.3464       $ O-16
        16032.62c      0.0065       $ S-32
MT2     LWTR.60t
C Pure Mn for capture tally
M3      25055.62c      1            $ Mn-55
C PTFE
M4      6000.66c       0.33333     $ C-nat (12)
        9019.62c       0.66667     $ F-19
C Am-Be
M5      8016.62c       0.0023      $ O-16
        95241.66c      0.0046      $ Am-241
        4009.62c       0.9931     $ Be-9
C Pure H-1 for capture tally
M6      1001.62c       1            $ H-1
C Pure O-16 for capture tally
M7      8016.62c       1            $ O-16
C Pure S-32 for capture tally
M8      16032.62c      1            $ S-32

```

### ***Blank\_Bath***

This is the main simulation input file with input parameters replaced by variables.

```

Blank MCNP Mn bath model to be filled in for each simulation
C CELL CARDS
C
1      1      -SRCDEN -1 -2 3            imp:n=1 $ source material
2      2      -7.93  -4 -5 6 (1:2:-3)  imp:n=1 $ steel container
3      3      -0.0012 -7 -8 9 (4:5:-6)  imp:n=1 $ holder air cavity
4      4      -2.2   -10 -11 12 (7:8:-9)  imp:n=1 $ PTFE/Teflon holder

```

```

5      5      -SOLDEN -13 (10:11:-12)      imp:n=1 $ MnSO4 solution
6      2      -7.93  -14 13                imp:n=1 $ steel bath shell
7      3      -0.0012 -15 14                imp:n=1 $ air around bath
8      0      -16 15                        imp:n=1 $ void around air
9      0      16                            imp:n=0 $ termination of neutrons

```

## C SURFACE CARDS

```

C
1      PZ      h4/2  $ top of source material
2      CZ      r4    $ wall of source material
3      PZ      -h4/2 $ bottom of source material
4      PZ      h3/2  $ top of container
5      CZ      r3    $ wall of container
6      PZ      -h3/2 $ bottom of container
7      PZ      h2/2-t2 $ inside top of holder
8      CZ      r2-t2 $ inside wall of holder
9      PZ      -h2/2-t2 $ inside bottom of holder
10     PZ      h2/2  $ top of holder
11     CZ      r2    $ wall of holder
12     PZ      -h2/2 $ bottom of holder
13     SO      r1    $ inside of bath
14     SO      r1+t1 $ outside of bath
15     SO      1.1*r1 $ outside of air around bath
16     SO      1.2*r1 $ outside of void region around air

```

## C NEUTRON SOURCE

```

C
mode n
SDEF  PAR=1  AXS=0 0 1  ERG=d1  SUR=d2  POS=FSUR d3  RAD=FSUR d4  NRM=FSUR d8  EXT=d9
SPECC
SI2 L 5 4 6
SP2 D fsid ftop fbot
DS3 L 0 0 0 0 0 h3/2 0 0 -h3/2
DS4 S 5 6 7
SI5 L r3
SP5 D 1
SI6 0 r3
SP6 -21 1
SI7 0 r3
SP7 -21 1
DS8 L 1 1 -1
SI9 -h3/2 h3/2
SP9 -21 0
nps 1E6

```

## C TALLIES

```

C
F11:N 13
FC11 Neutrons passing through inner bath shell surface [n]
C11 0 1  $ backscatter and Leakage Bins
C
F21:N 14
FC21 Neutrons passing through outer bath shell surface [n]
C21 0 1  $ backscatter and Leakage Bins
C
F31:N 15
FC31 Neutrons passing through air bubble [n]
C31 0 1  $ backscatter and Leakage Bins
C
F41:N 16
FC41 Neutrons passing through void [n]
C41 0 1  $ backscatter and Leakage Bins
C
F12:N 13
FC12 Average neutron flux on inner surface of bath shell [n/cm^2]
C
F22:N 14

```

FC22 Average neutron flux on outer surface of bath shell [n/cm<sup>2</sup>]  
 C  
 F32:N 15  
 FC32 Average neutron flux on air bubble [n/cm<sup>2</sup>]  
 C  
 F42:N 16  
 FC42 Average neutron flux on void [n/cm<sup>2</sup>]  
 C  
 F14:N 1  
 FM14 (-1 1 -2)  
 FC14 Absorption in source material per source neutron per volume [n/cm<sup>3</sup>]  
 C  
 F24:N 2  
 FM24 (-1 2 -2)  
 FC24 Absorption in containment per source neutron per volume [n/cm<sup>3</sup>]  
 C  
 F34:N 3  
 FM34 (-1 3 -2)  
 FC34 Absorption in cavity per source neutron per volume [n/cm<sup>3</sup>]  
 C  
 F44:N 4  
 FM44 (-1 4 -2)  
 FC44 Absorption in holder per source neutron per volume [n/cm<sup>3</sup>]  
 C  
 F54:N 5  
 FM54 (-1 5 -2)  
 FC54 Absorption in solution per source neutron per volume [n/cm<sup>3</sup>]  
 C  
 F64:N 6  
 FM64 (-1 2 -2)  
 FC64 Absorption in shell per source neutron per volume [n/cm<sup>3</sup>]  
 C  
 F74:N 7  
 FM74 (-1 3 -2)  
 FC74 Absorption in air bubble per source neutron per volume [n/cm<sup>3</sup>]  
 C  
 F84:N 5  
 FM84 (N\_Mn 6 -2)  
 FC84 Absorption in Mn per source neutron per volume [n/cm<sup>3</sup>]  
 C  
 F94:N 5  
 FM94 (N\_H 7 -2)  
 FC94 Absorption in H per source neutron per volume [n/cm<sup>3</sup>]  
 C  
 F104:N 5  
 FM104 (N\_O 8 -2)  
 FC104 Absorption in O per source neutron per volume [n/cm<sup>3</sup>]  
 C  
 F114:N 5  
 FM114 (N\_S 9 -2)  
 FC114 Absorption in S per source neutron per volume [n/cm<sup>3</sup>]  
 C  
 C MATERIALS  
 C  
 C Source Material  
 SRCMATC  
 C Stainless Steel 316L  

M2	26056	-0.65395	\$ Fe-56
	24052	-0.17	\$ Cr-52
	28058	-0.12	\$ Ni-58
	25055	-0.02	\$ Mn-55
	14028	-0.01	\$ Si-28
	06000	-0.0003	\$ C-nat
	15031	-0.00045	\$ P-31
	16032	-0.0003	\$ S-32
	42098	-0.025	\$ Mo-98

  
 C Air

```

M3      07014  0.791      $ N-14
        08016  0.209      $ O-16
C PTFE/Teflon
M4      06000  0.33333  $ C-nat
        09019  0.66667  $ F-19
C MnSO4 Solution
M5      25055  a_Mn      $ Mn-55
        01001  a_H       $ H-1
        08016  a_O       $ O-16
        16032  a_S       $ S-32
MT5     LWTR
C Pure Mn
M6      25055  1          $ Mn-55
C Pure H
M7      01001  1          $ H-1
MT7     LWTR
C Pure O
M8      08016  1          $ O-16
C Pure S
M9      16032  1          $ S-32
C
PRINT 110 10 30 40 50 72 102

```

### *spec\_AmBe*

This file is the Am-Be neutron energy spectrum used to replace the SPEC variable in the blank MCNP input file.

```

SI1     H      7.94E-02
          1.00E-01
          1.26E-01
          1.58E-01
          2.00E-01
          2.51E-01
          3.16E-01
          3.98E-01
          5.01E-01
          6.31E-01
          7.94E-01
          1.00E+00
          1.26E+00
          1.58E+00
          2.00E+00
          2.51E+00
          3.16E+00
          3.98E+00
          5.01E+00
          6.31E+00
          7.94E+00
          1.00E+01
          1.26E+01
          1.58E+01
SP1     D      0.000E+00
          3.346E-03
          4.226E-03
          5.219E-03
          6.890E-03
          8.385E-03
          1.070E-02

```

```

1.262E-02
1.479E-02
1.743E-02
2.046E-02
2.414E-02
2.750E-02
2.939E-02
4.289E-02
5.682E-02
9.621E-02
1.363E-01
1.589E-01
1.463E-01
1.337E-01
4.117E-02
3.101E-03
0.000E+00
$ IAEA source compendium, Griffith et al., 1990

```

### *spec\_Cf*

This file is the Cf neutron energy spectrum used to replace the SPEC variable in the blank MCNP input file.

```
SP1 -3 1.18 1.03419 $ Watt fission spectrum from MCNP 6.2 manual
```

### *spec\_PuBe*

This file is the Pu-Be neutron energy spectrum used to replace the SPEC variable in the blank MCNP input file.

```

SI1      H      5.01E-01
           6.31E-01
           7.94E-01
           1.00E+00
           1.26E+00
           1.58E+00
           2.00E+00
           2.51E+00
           3.16E+00
           3.98E+00
           5.01E+00
           6.31E+00
           7.94E+00
           1.00E+01
           1.26E+01
           1.58E+01
SP1      D      0.000E+00
           9.408E-03
           1.128E-02
           4.268E-02
           1.696E-02
           2.162E-02

```

3.941E-02	
5.800E-02	
1.040E-01	
1.413E-01	
1.589E-01	
1.252E-01	
1.447E-01	
6.642E-02	
6.143E-02	
0.000E+00	\$ IAEA source compendium, Griffith et al., 1990

***mat\_AmBe***

This file is the Am-Be material definition used to replace SRCMAT in the blank input file.

M1	08016	0.0045	\$ O-16
	95241	0.0023	\$ Am-241
	04009	0.9932	\$ Be-9

***mat\_Cf***

This file is the Cf material definition used to replace SRCMAT in the blank input file.

M1	98252	0.4	\$ Cf-252
	08016	0.6	\$ O-16

***mat\_PuBe***

This file is the Pu-Be material definition used to replace SRCMAT in the blank input file.

M1	94239	0.0439	\$ Pu-239
	04009	0.9561	\$ Be-9

## Appendix C

### Python Codes

This Appendix includes the Python codes used to run the blank MCNP file and iterate through the Mn bath parameters. The included runner and looper files are set up for an Am-Be source but may easily be changed by replacing “AmBe” with “Cf” or “PuBe” in the “INPUTS” section. The original (by Nicholas Greci) and modified versions of the tally collection function are also included.

#### *AmBe\_Runner.py*

```
# File to run a single iteration of the blank MCNP bath simulation
# Runs MCNP in the current directory
# Clears the previous outp and runtpe files

# Set up for Am-Be source

import os
import math

# INPUTS -----
dec = 7      # how many decimals to round to
CPUs = 8     # how many processors to runs MCNP on (tasks)
Title1 = 'MCNPrun' # title of MCNP input file to be created
# Dimensions
t1 = 0.5     # [cm] shell thickness
t2 = 0.5     # [cm] holder thickness
t3 = 0.3     # [cm] containment thickness
r1 = !r!    # [cm] bath shell inner radius
r2 = 5       # [cm] holder outer radius
r3 = 1.125   # [cm] containment outer radius
r4 = r3-t3   # [cm] source material radius
h2 = 10      # [cm] holder height
h3 = 3.12    # [cm] containment height
h4 = h3-2*t3# [cm] source material height
# Densities
SRCDEN = 1.96 # [g/cc] source material density
SOLDEN = !den! # [g/cc] solution density
# SDEF
SRC = 'AmBe' # source type - options: AmBe, Cf, or PuBe
EmMe = 'area' # source emission fraction calc method - options: area or angle

# INPUT CALCULATIONS -----
# Energy Spectrum
SRCS = os.path.join('/home/scoutbucks/Desktop/Thesis_Data','spec_' + SRC)
with open(SRCS, 'r') as specfile:
    SPEC = specfile.read()
# Source Material
```

```

SRCM = os.path.join('/home/scoutbucks/Desktop/Thesis_Data','mat_' + SRC)
with open(SRCM, 'r') as matfile:
    SRCMAT = matfile.read()
# Emission Fractions
if EmMe == 'area':      # source emission from side - area method
    fsid = h3/(h3+r3)
if EmMe == 'angle':    # source emission from side - solid angle method
    fsid == h3/math.sqrt(4*r3**2+h3**2)
ftop = (1-fsid)/2      # source emission from top
fbot = ftop            # source emission from bottom
# Solution Composition
NA = 6.022e23          # Avogadro's Number
A_H = 1.008            # [g/mol] atomic masses
A_O = 15.999
A_Mn = 54.938
A_S = 32.06
A_MnSO4 = A_Mn+A_S+4*A_O
A_H2O = 2*A_H + A_O
CSOLDEN = SOLDEN-0.53*10**(-3)*(30-20)      # [g/cc] Temp. correction from Deckwer 1980 p 75
# De Volpi's Curve for Concentration
CM = -1.4088+1.4227*CSOLDEN+0.56713*CSOLDEN**2-0.77726*CSOLDEN**3+0.20073*CSOLDEN**4      # [g/g sol]
CONC = CM*SOLDEN      # [g/cc sol]
# Convert to Number Density [a/b-cm]
N_H = (SOLDEN-CONC)*NA*2/A_H2O*10**(-24)
N_Mn = CONC*NA/A_MnSO4*10**(-24)
N_O = (4*N_Mn+N_H/2)
N_S = N_Mn
x = N_H/N_Mn
# Atom Fractions [a/b-cm]
N_tot = N_H+N_Mn+N_S+N_O
a_Mn = N_Mn/N_tot
a_H = N_H/N_tot
a_O = N_O/N_tot
a_S = N_S/N_tot

# RUNNING MCNP -----
# Clear old runs
path = os.getcwd()
if os.path.isfile(os.path.join(path, 'outp')) == 1:
    os.remove(os.path.join(path, 'outp'))
if os.path.isfile(os.path.join(path, 'runtpe')) == 1:
    os.remove(os.path.join(path, 'runtpe'))
if os.path.isfile(os.path.join(path, 'Results')) == 1:
    os.remove(os.path.join(path, 'Results'))
# Build New MCNP Input File
with open('/home/scoutbucks/Desktop/Thesis1/Blank_Bath', 'r') as Blank_Bath:
    InFi = Blank_Bath.read()
InFi = InFi.replace('SRCDEN', str(round(SRCDEN, dec)))
InFi = InFi.replace('SOLDEN', str(round(SOLDEN, dec)))
InFi = InFi.replace('h4/2', str(round(h4/2, dec)))
InFi = InFi.replace('r4', str(round(r4, dec)))
InFi = InFi.replace('h3/2', str(round(h3/2, dec)))
InFi = InFi.replace('r3', str(round(r3, dec)))
InFi = InFi.replace('h2/2-t2', str(round(h2/2-t2, dec)))
InFi = InFi.replace('r2-t2', str(round(r2-t2, dec)))
InFi = InFi.replace('h2/2', str(round(h2/2, dec)))
InFi = InFi.replace('r2', str(round(r2, dec)))
InFi = InFi.replace('r1+t1', str(round(r1+t1, dec)))
InFi = InFi.replace('1.1*r1', str(round(1.1*r1, dec)))
InFi = InFi.replace('1.2*r1', str(round(1.2*r1, dec)))
InFi = InFi.replace('r1', str(round(r1, dec)))
InFi = InFi.replace('SPEC', SPEC)
InFi = InFi.replace('fsid', str(round(fsid, dec)))
InFi = InFi.replace('ftop', str(round(ftop, dec)))
InFi = InFi.replace('fbot', str(round(fbot, dec)))
InFi = InFi.replace('N_Mn', str(round(N_Mn, dec)))
InFi = InFi.replace('N_H', str(round(N_H, dec)))

```

```

InFi = InFi.replace('N_0',str(round(N_0,dec)))
InFi = InFi.replace('N_S',str(round(N_S,dec)))
InFi = InFi.replace('SRCMAT',SRCMAT)
InFi = InFi.replace('a_Mn',str(round(a_Mn,dec)))
InFi = InFi.replace('a_H',str(round(a_H,dec)))
InFi = InFi.replace('a_O',str(round(a_O,dec)))
InFi = InFi.replace('a_S',str(round(a_S,dec)))
with open(Title1, 'w') as NewInFi:
    NewInFi.write(InFi)
# Run MCNP
command = 'mcnp6 inp=' + Title1 + ' tasks ' + str(CPUs)
os.system(command)

# COLLECTING OUTPUTS -----
# Begin N. Greci
def get_tally(filename, lookup, drop, walk):
    tallyline = -1
    with open(filename, "r") as myFile:
        for num, line in enumerate(myFile,0):
            if line.startswith(lookup):
                tallyline = num + drop
            if tallyline == num:
                data = line.split()
                answer = float(data[walk])
    return answer
# End N. Greci
# Currents
# Inner Shell
tal_out = get_tally(os.path.join(path,'outp'), '1tally', 11, 0)
err_out = get_tally(os.path.join(path,'outp'), '1tally', 11, 1)
var_out = err_out*tal_out
tal_in = get_tally(os.path.join(path,'outp'), '1tally', 11, 7, 0)
err_in = get_tally(os.path.join(path,'outp'), '1tally', 11, 7, 1)
var_in = err_in*tal_in
Cur_InShell = tal_out-tal_in
var_Cur_InShell = math.sqrt(var_out**2+var_in**2)
# Outer Shell
tal_out = get_tally(os.path.join(path,'outp'), '1tally', 21, 0)
err_out = get_tally(os.path.join(path,'outp'), '1tally', 21, 1)
var_out = err_out*tal_out
tal_in = get_tally(os.path.join(path,'outp'), '1tally', 21, 7, 0)
err_in = get_tally(os.path.join(path,'outp'), '1tally', 21, 7, 1)
var_in = err_in*tal_in
Cur_OutShell = tal_out-tal_in
var_Cur_OutShell = math.sqrt(var_out**2+var_in**2)
# Air Boundary
tal_out = get_tally(os.path.join(path,'outp'), '1tally', 31, 0)
err_out = get_tally(os.path.join(path,'outp'), '1tally', 31, 1)
var_out = err_out*tal_out
tal_in = get_tally(os.path.join(path,'outp'), '1tally', 31, 7, 0)
err_in = get_tally(os.path.join(path,'outp'), '1tally', 31, 7, 1)
var_in = err_in*tal_in
Cur_Air = tal_out-tal_in
var_Cur_Air = math.sqrt(var_out**2+var_in**2)
# Void Boundary
tal_out = get_tally(os.path.join(path,'outp'), '1tally', 41, 0)
err_out = get_tally(os.path.join(path,'outp'), '1tally', 41, 1)
var_out = err_out*tal_out
tal_in = get_tally(os.path.join(path,'outp'), '1tally', 41, 7, 0)
err_in = get_tally(os.path.join(path,'outp'), '1tally', 41, 7, 1)
var_in = err_in*tal_in
Cur_Void = tal_out-tal_in
var_Cur_Void = math.sqrt(var_out**2+var_in**2)
# Fluxes
# Inner Shell
tal = get_tally(os.path.join(path,'outp'), '1tally', 12, 10, 0)
err = get_tally(os.path.join(path,'outp'), '1tally', 12, 10, 1)

```

```

area = get_tally(os.path.join(path,'outp'), '1tally'      12      nps', 7, 0)
Flux_InShell = tal*area
var_Flux_InShell = Flux_InShell*err
# Outer Shell
tal = get_tally(os.path.join(path,'outp'), '1tally'      22      nps', 10, 0)
err = get_tally(os.path.join(path,'outp'), '1tally'      22      nps', 10, 1)
area = get_tally(os.path.join(path,'outp'), '1tally'      22      nps', 7, 0)
Flux_OutShell = tal*area
var_Flux_OutShell = Flux_OutShell*err
# Air Boundary
tal = get_tally(os.path.join(path,'outp'), '1tally'      32      nps', 10, 0)
err = get_tally(os.path.join(path,'outp'), '1tally'      32      nps', 10, 1)
area = get_tally(os.path.join(path,'outp'), '1tally'      32      nps', 7, 0)
Flux_Air = tal*area
var_Flux_Air = Flux_Air*err
# Void Boundary
tal = get_tally(os.path.join(path,'outp'), '1tally'      42      nps', 10, 0)
err = get_tally(os.path.join(path,'outp'), '1tally'      42      nps', 10, 1)
area = get_tally(os.path.join(path,'outp'), '1tally'      42      nps', 7, 0)
Flux_Void = tal*area
var_Flux_Void = Flux_Void*err
# Absorptions
# Source Material
tal = get_tally(os.path.join(path,'outp'), '1tally'      14      nps', 11, 0)
err = get_tally(os.path.join(path,'outp'), '1tally'      14      nps', 11, 1)
vol = get_tally(os.path.join(path,'outp'), '1tally'      14      nps', 7, 0)
Abs_Src = tal*vol
var_Abs_Src = Abs_Src*err
# Containment
tal = get_tally(os.path.join(path,'outp'), '1tally'      24      nps', 11, 0)
err = get_tally(os.path.join(path,'outp'), '1tally'      24      nps', 11, 1)
vol = get_tally(os.path.join(path,'outp'), '1tally'      24      nps', 7, 0)
Abs_Cont = tal*vol
var_Abs_Cont = Abs_Cont*err
# Cavity
tal = get_tally(os.path.join(path,'outp'), '1tally'      34      nps', 11, 0)
err = get_tally(os.path.join(path,'outp'), '1tally'      34      nps', 11, 1)
vol = get_tally(os.path.join(path,'outp'), '1tally'      34      nps', 7, 0)
Abs_Cav = tal*vol
var_Abs_Cav = Abs_Cav*err
# Holder
tal = get_tally(os.path.join(path,'outp'), '1tally'      44      nps', 11, 0)
err = get_tally(os.path.join(path,'outp'), '1tally'      44      nps', 11, 1)
vol = get_tally(os.path.join(path,'outp'), '1tally'      44      nps', 7, 0)
Abs_Hold = tal*vol
var_Abs_Hold = Abs_Hold*err
# Solution
tal = get_tally(os.path.join(path,'outp'), '1tally'      54      nps', 11, 0)
err = get_tally(os.path.join(path,'outp'), '1tally'      54      nps', 11, 1)
vol = get_tally(os.path.join(path,'outp'), '1tally'      54      nps', 7, 0)
Abs_Sol = tal*vol
var_Abs_Sol = Abs_Sol*err
# Shell
tal = get_tally(os.path.join(path,'outp'), '1tally'      64      nps', 11, 0)
err = get_tally(os.path.join(path,'outp'), '1tally'      64      nps', 11, 1)
vol = get_tally(os.path.join(path,'outp'), '1tally'      64      nps', 7, 0)
Abs_Shell = tal*vol
var_Abs_Shell = Abs_Shell*err
# Air
tal = get_tally(os.path.join(path,'outp'), '1tally'      74      nps', 11, 0)
err = get_tally(os.path.join(path,'outp'), '1tally'      74      nps', 11, 1)
vol = get_tally(os.path.join(path,'outp'), '1tally'      74      nps', 7, 0)
Abs_Air = tal*vol
var_Abs_Air = Abs_Air*err
# Mn
tal = get_tally(os.path.join(path,'outp'), '1tally'      84      nps', 11, 0)
err = get_tally(os.path.join(path,'outp'), '1tally'      84      nps', 11, 1)

```

```

vol = get_tally(os.path.join(path,'outp'), '1tally      84      nps', 7, 0)
Abs_Mn = tal*vol
var_Abs_Mn = Abs_Mn*err
# H
tal = get_tally(os.path.join(path,'outp'), '1tally      94      nps', 11, 0)
err = get_tally(os.path.join(path,'outp'), '1tally      94      nps', 11, 1)
vol = get_tally(os.path.join(path,'outp'), '1tally      94      nps', 7, 0)
Abs_H = tal*vol
var_Abs_H = Abs_H*err
# O
tal = get_tally(os.path.join(path,'outp'), '1tally     104      nps', 11, 0)
err = get_tally(os.path.join(path,'outp'), '1tally     104      nps', 11, 1)
vol = get_tally(os.path.join(path,'outp'), '1tally     104      nps', 7, 0)
Abs_O = tal*vol
var_Abs_O = Abs_O*err
# s
tal = get_tally(os.path.join(path,'outp'), '1tally     114      nps', 11, 0)
err = get_tally(os.path.join(path,'outp'), '1tally     114      nps', 11, 1)
vol = get_tally(os.path.join(path,'outp'), '1tally     114      nps', 7, 0)
Abs_S = tal*vol
var_Abs_S = Abs_S*err

# OUTPUT CALCULATIONS -----
# Solution Absorption Sum
Sum_Sol = Abs_Mn+Abs_H+Abs_O+Abs_S
var_Sum_Sol = math.sqrt(var_Abs_Mn**2+var_Abs_H**2+var_Abs_O**2+var_Abs_S**2)
# All Absorption Sum
Sum_Abs = Abs_Src+Abs_Cont+Abs_Cav+Abs_Hold+Abs_Sol+Abs_Shell+Abs_Air
AA = var_Abs_Src**2+var_Abs_Cont**2+var_Abs_Cav**2
BB = var_Abs_Hold**2+var_Abs_Sol**2+var_Abs_Shell**2+var_Abs_Air**2
var_Sum_Abs = math.sqrt(AA+BB)

# RESULTS REPORTING
Heading = 'Rxn\tProb\tVar\n'
DL1 = 'C InShell'+'\t'+str(round(Cur_InShell, dec))+'\t'+str(round(var_Cur_InShell, dec))+'\n'
DL2 = 'C OutShell'+'\t'+str(round(Cur_OutShell, dec))+'\t'+str(round(var_Cur_OutShell, dec))+'\n'
DL3 = 'C Air'+'\t'+str(round(Cur_Air, dec))+'\t'+str(round(var_Cur_Air, dec))+'\n'
DL4 = 'C Void'+'\t'+str(round(Cur_Void, dec))+'\t'+str(round(var_Cur_Void, dec))+'\n'
DL5 = 'F InShell'+'\t'+str(round(Flux_InShell, dec))+'\t'+str(round(var_Flux_InShell, dec))+'\n'
DL6 = 'F OutShell'+'\t'+str(round(Flux_OutShell, dec))+'\t'+str(round(var_Flux_OutShell, dec))+'\n'
DL7 = 'F Air'+'\t'+str(round(Flux_Air, dec))+'\t'+str(round(var_Flux_Air, dec))+'\n'
DL8 = 'F Void'+'\t'+str(round(Flux_Void, dec))+'\t'+str(round(var_Flux_Void, dec))+'\n'
DL9 = 'A Src'+'\t'+str(round(Abs_Src, dec))+'\t'+str(round(var_Abs_Src, dec))+'\n'
DL10 = 'A Cont'+'\t'+str(round(Abs_Cont, dec))+'\t'+str(round(var_Abs_Cont, dec))+'\n'
DL11 = 'A Cav'+'\t'+str(round(Abs_Cav, dec))+'\t'+str(round(var_Abs_Cav, dec))+'\n'
DL12 = 'A Hold'+'\t'+str(round(Abs_Hold, dec))+'\t'+str(round(var_Abs_Hold, dec))+'\n'
DL13 = 'A Sol'+'\t'+str(round(Abs_Sol, dec))+'\t'+str(round(var_Abs_Sol, dec))+'\n'
DL14 = 'A Shell'+'\t'+str(round(Abs_Shell, dec))+'\t'+str(round(var_Abs_Shell, dec))+'\n'
DL15 = 'A Air'+'\t'+str(round(Abs_Air, dec))+'\t'+str(round(var_Abs_Air, dec))+'\n'
DL16 = 'A Mn'+'\t'+str(round(Abs_Mn, dec))+'\t'+str(round(var_Abs_Mn, dec))+'\n'
DL17 = 'A H'+'\t'+str(round(Abs_H, dec))+'\t'+str(round(var_Abs_H, dec))+'\n'
DL18 = 'A O'+'\t'+str(round(Abs_O, dec))+'\t'+str(round(var_Abs_O, dec))+'\n'
DL19 = 'A S'+'\t'+str(round(Abs_S, dec))+'\t'+str(round(var_Abs_S, dec))+'\n'
DL20 = 'S SolAbs'+'\t'+str(round(Sum_Sol, dec))+'\t'+str(round(var_Sum_Sol, dec))+'\n'
DL21 = 'S AllAbs'+'\t'+str(round(Sum_Abs, dec))+'\t'+str(round(var_Sum_Abs, dec))+'\n'
with open('Results.txt', 'w') as Results:
    Results.write(Heading)
    Results.write(DL1)
    Results.write(DL2)
    Results.write(DL3)
    Results.write(DL4)
    Results.write(DL5)
    Results.write(DL6)
    Results.write(DL7)
    Results.write(DL8)
    Results.write(DL9)
    Results.write(DL10)

```

```

Results.write(DL11)
Results.write(DL12)
Results.write(DL13)
Results.write(DL14)
Results.write(DL15)
Results.write(DL16)
Results.write(DL17)
Results.write(DL18)
Results.write(DL19)
Results.write(DL20)
Results.write(DL21)

# SHORT RESULTS REPORTING
# For use in larger data file
DL22 = str(round(Abs_Mn, dec))+'\t'+str(round(var_Abs_Mn, dec))+'\t'
DL23 = str(round(Cur_Air, dec))+'\t'+str(round(var_Cur_Air, dec))
DL24 = DL22 + DL23
with open('Short_Results.txt', 'w') as Short_Results:
    Short_Results.write(DL24)

```

### ***AmBE\_Looper.py***

```

# File to run the "Runner" file multiple times
# Iterates over a given range of bath radius and solution density
# Run this file from the Thesis1 folder

import os
import math
import numpy

# INPUTS -----
SourceType = 'AmBe' # n source type, choices are AmBe, Cf, or PuBe
r_min = 10 # [cm] minimum bath radius
r_max = 75 # [cm] maximum bath radius
d_r = 5 # [cm] change in bath radius
den_min = 1.05 # [g/cc] minimum solution density
den_max = 1.40 # [g/cc] maximum solution density
d_den = 0.05 # [g/cc] change in solution density
dec = 3 # number of digits to round to
# -----

# Initialize short results file with Mn abs frac and leakage
Head_Short = 'Radius\tDensity\tAbs Mn\tVar\tLeak\tVar\n'
with open(SourceType+'_Results_Short.txt', 'w') as Results_Short:
    Results_Short.write(Head_Short)
# The long results file with all the tallies will be made later, as there is no singular heading

# Begin iterations
for r in numpy.arange(r_min, round(r_max+d_r/2,dec), d_r):
    for den in numpy.arange(den_min, round(den_max+d_den/2,dec), d_den):
        # Open and edit the runner file contents
        with open('/home/scoutbucks/Desktop/Thesis1/'+SourceType+'_Runner.py', 'r') as Runner:
            RunFi = Runner.read()
            RunFi = RunFi.replace('!r!',str(round(r,dec)))
            RunFi = RunFi.replace('!den!',str(round(den,dec)))

        # Move to case specific folder
        path = os.getcwd()
        os.chdir(os.path.join(path, SourceType+'_data')) # move to source type folder
        Case = str(round(r,dec))+ '_' +str(round(den,dec)) # create folder for specific run
        os.mkdir(Case)
        path = os.getcwd()

```

```

os.chdir(os.path.join(path, Case))                # move folder for specific run

# Write a new runner file for this run
with open('Run_'+Case+'.py', 'w') as NewRunFi:
    NewRunFi.write(RunFi)

# Execute the case runner file
command = 'python3 '+Run_'+Case+'.py'
os.system(command)

# Read the tallies
with open('Results.txt', 'r') as Results:
    Tallies = Results.read()

with open('Short_Results.txt', 'r') as Results:
    Short_Tallies = Results.read()

# Back out to Thesis1 folder
os.chdir('.')
os.chdir('.')

# Append long results
Head_Long = 'Radius '+str(round(r,dec))+ ' '+Density '+str(round(den,dec))+'\n'
with open(SourceType+'_Results_Long.txt', 'a') as Results_Long:
    Results_Long.write(Head_Long)
    Results_Long.write(Tallies)

# Append short results
DataLine = str(round(r,dec))+'\t'+str(round(den,dec))+'\t'+Short_Tallies+'\n'
with open(SourceType+'_Results_Short.txt', 'a') as Results_Short:
    Results_Short.write(DataLine)

print('Done with '+SourceType)

```

### ***Original Tally Collection Function***

Included below is the original Python function written by Nicholas Grecni for collecting tally data from an MCNP output file.

```

def tally_no_bin(filename, lookup1):
    tallyline = -1
    with open(filename, "r") as myFile:
        for num, line in enumerate(myFile,0):
            if line.startswith(lookup1):
                tallyline = num + 1
            if tallyline == num:
                data = line.split()
                tally = data[0]
    return tally

```

### ***Modified Tally Collection Function***

The following is the tally collection Python function written by the author based on the work of Nicholas Greci. It has been updated to give greater flexibility in choosing which tally data to record.

```
def get_tally(filename, lookup, drop, walk):
    tallyline = -1
    with open(filename, "r") as myFile:
        for num, line in enumerate(myFile,0):
            if line.startswith(lookup):
                tallyline = num + drop
            if tallyline == num:
                data = line.split()
                answer = float(data[walk])
    return answer
```

## Appendix D

### MATLAB Codes

This Appendix includes MATLAB codes that were used during the course of this thesis that the author believes may be helpful to others who work on this project. Some codes – those used just to generate graphs for example – are not included. The font of all code has been changed to delineate code and text and to ensure that line wrapping is minimized for future copy and pasting of code.

#### *Mn\_Bath\_MCNP\_Parameters.m*

This code computes number densities and atom fractions for input to MCNP given a range of solution mass density values.

```
% Solution Parameter Calculator for use with Mn Bath MCNP Calculations
% Scout Bucks
% 16 May 2023
% A single density value gives parameters in the command window
% Multiple density values give parameters in a file called "Bath_Sol_Table.txt"
% Choose either Bittencourt or De Volpi curves

clc, clear

rho = 1.0934;
%rho = [1.05:.01:1.35];      % [g/cc] solution density
Correlation = 'De Volpi';
%Correlation = 'Bittencourt';

% Atomic Parameters
NA = 6.022e23;      % Avogadro's

A_H = 1.008;      % Atomic masses [g/mol]
A_O = 15.999;
A_Mn = 54.938;
A_S = 32.06;
A_MnSO4 = A_Mn + A_S + 4*A_O;
A_H2O = 2*A_H + A_O;

switch Correlation
case 'Bittencourt'
    [N, x] = MnSO4_NumDen_B(rho);
case 'De Volpi'
    [N, x] = MnSO4_NumDen_DV2(rho);
otherwise
    warning('No Correlation Chosen')
```

```

        return
end

% Calculations
N_Mn = N(1,:); % [a/cc] Mn number density
N_H = N(2,:); % [a/cc] H ...
N_O = N(3,:); % [a/cc] O ...
N_S = N(4,:); % [a/cc] S ...
N_tot = sum(N); % [a/cc] total number density
a = N./N_tot; % [] all atom fractions
a_Mn = a(1,:); % [] atom fraction of Mn
a_H = a(2,:); % [] atom fraction of H
a_O = a(3,:); % [] atom fraction of O
a_S = a(4,:); % [] atom fraction of S
N_bcm = N*10^(-24); % [a/b-cm] all number densities for MCNP tally F4 inputs

% Outputs to command window for 1 density or .txt file otherwise
if length(rho) == 1
    fprintf('Solution Density [g/cm^3]: %g\n',rho)
    fprintf('H to Mn Ratio: %g\n',x)
    fprintf('Solution Concentration [mol/l]: %g\n',N_Mn/NA*1000)
    fprintf('Solution Concentration [g/l]: %g\n',N_Mn/NA*1000*A_MnSO4)
    fprintf('Atom Fractions of Mn, H, O, S:\n')
    fprintf('%f\n',a_Mn)
    fprintf('%f\n',a_H)
    fprintf('%f\n',a_O)
    fprintf('%f\n',a_S)
    fprintf('Number Densities of Mn, H, O, S [a/b-cm]:\n')
    fprintf('%e\n',N_bcm(1))
    fprintf('%e\n',N_bcm(2))
    fprintf('%e\n',N_bcm(3))
    fprintf('%e\n',N_bcm(4))
else
    Data = vertcat(rho,a,N_bcm);
    file = fopen('Bath_Sol_Table.txt','w');
    fprintf(file, 'rho      a Mn      a H      a O      a S      N Mn      N H      N O      N
S\n');
    fprintf(file, '%.3E %.3E %.3E %.3E %.3E %.3E %.3E %.3E %.3E\n',Data);
    fclose(file);
end

```

### ***MNSO4\_NumDen\_DV2.m***

This function implements Equations (10) through (13) using the empirical correlation given by De Volpi et al. to calculate  $\text{MnSO}_4$  number densities from a given density.<sup>21</sup>

```

function [N, x] = MnSO4_NumDen_DV2(rho_sol)
% Scout Bucks
% 30 May 2023
% Number densities with data from De Volpi et al. 1965 p 599
% Uses the g/kg solution curve to avoid temp dependence
% Solution density input can be a number or row vector in [g/cc]
% Number Density output takes form of:
%       N_Mn
%       N_H
%       N_O
%       N_S      [atoms/cc]

% Atomic Parameters

```

```

NA = 6.022e23;      % Avogadro's
A_H = 1.008;       % Atomic masses [g/mol]
A_O = 15.999;
A_Mn = 54.938;
A_S = 32.06;
A_MnSO4 = A_Mn + A_S + 4*A_O;
A_H2O = 2*A_H + A_O;

% Temp correction from Deckwer 1980 p 75
rho_DeVolpi = rho_sol - .53*10^-3*(30-20); % [g/cc]

% De Volpi's Curve for Concentration
CM = -1.4088 + 1.4227.*rho_DeVolpi + 0.56713.*rho_DeVolpi.^2 + ...
    -0.77726.*rho_DeVolpi.^3 + 0.20073.*rho_DeVolpi.^4; % [g/g sol]
C_MnSO4_DeVolpi = CM.*rho_sol; % [g/cc]
%C_MnSO4_DeVolpi = 1.1152/1000*A_MnSO4; % Use this line to enforce Amendola's numbers
%C_MnSO4_DeVolpi = 93.68/1000*1.0934; % Use this line to enforce Khabaz's numbers

% Convert to Number Density
N_H = (rho_sol-C_MnSO4_DeVolpi)*NA^2/A_H2O; % [a/cc]
N_Mn = C_MnSO4_DeVolpi*NA/A_MnSO4; % [a/cc]
N_O = 4*N_Mn+N_H/2; % [a/cc]
N_S = N_Mn; % [a/cc]

% Final Parameters
x = N_H./N_Mn;
N = vertcat(N_Mn, N_H, N_O, N_S);
end

```

### ***Data\_Processing.m***

This code finds coefficient fit matrices for data given in the form of the short results files seen in Appendix A.

```

% Data Crunching Code for Mn Bath Simualtions
% This method assumes that the Mn abs frac is dependent on density for a
% certain radius according to:
%     epsilon = a(r)*rho^b(r) + c(r)
% The file fits a curve to each "iso-radial" data set. The fitting
% parameters are then plotted as a function of radius and fitted like:
%     a(r) = a1*exp(a2*r) + a3
%     b(r) = b1*exp(b2*r) + b3
%     c(r) = c1*exp(c2*r) + c3
% The final result is a 3x3 matrix for each source type that has the form:
%     [a1 a2 a3;
%      b1 b2 b3;
%      c1 c2 c3]
% For a meshgrid of R and RHO, the empirical correlation can be evaluated
% at each (r,rho) point using the FitMatrixEval function.
% Scout Bucks
% 9/29/23

clc, clear
close all

% INPUTS
Refine = 10; % refines final fit plot domain points by Refine^2 times
DispCoeff = 1; % display coefficient matrix Y/N = 1/0
OrientErrAxes = 1; % make error axes the same size for comparison

```

```

ShowVar = 10;          % 0 = no MCNP errors plotted, # = #*sigma errors included
AmBe_path = % AmBe file location
Cf_path = % Cf file location
PuBe_path = % PuBe file lcoation
% -----

r = linspace(10,75,14);          % [cm] radius range
rho = round(linspace(1.05,1.40,8),5); % [g/cc] density range
[R,RHO] = meshgrid(r,rho);      % r is "x", rho is "y"
blank = zeros(size(R));         % iniitalize a matrix to store f(r,rho)

%% AmBe
AmBe_data = readmatrix(AmBe_path); % read in data
% distribute data to different matrices to match the meshgrid
Abs_Mn_AmBe = blank;
var_Abs_Mn_AmBe = blank;
L_AmBe = blank;
var_L_AmBe = blank;
for ii = 1:size(AmBe_data,1)
    Abs_Mn_AmBe(ii) = AmBe_data(ii,3);
    var_Abs_Mn_AmBe(ii) = AmBe_data(ii,4);
    L_AmBe(ii) = AmBe_data(ii,5);
    var_L_AmBe(ii) = AmBe_data(ii,6);
end
% find and plot a power fit to each radius set over density domain: abs=a*rho^b+c
figure(1)
coeff = zeros(3,length(r)); % power fit coefficient storage for iso-radial lines
for ii = 1:length(r)
    FIT = fit(rho',(Abs_Mn_AmBe(:,ii)),'power2');
    coeff(1,ii) = FIT.a;
    coeff(2,ii) = FIT.b;
    coeff(3,ii) = FIT.c;
    plot(FIT)
    hold on
    plot(rho,Abs_Mn_AmBe(:,ii),'k','MarkerSize',10)
    legend('Fit','Data','Location','best')
end
hold off
annotation('arrow',[0.7 0.4],[0.2 0.7])
str = 'Increasing r';
annotation('textbox',[0.3 0.56 0.2 0.2],'String',str,'FitBoxToText','on','EdgeColor','none');
title('AmBe Density Fit Curve for Each Radius')
xlabel('\rho [g/cm^3]')
ylabel('\epsilon_M_n')
% normalize data for exponential fitting by shifting up or down so that abs(inf) = 0
% this is needed because the exp1 fit does not have a vertical shift term
downshift = coeff(:,end);
a_work = coeff(1,:) - downshift(1); % the working (shiffed) power coefficient curves
b_work = coeff(2,:) - downshift(2);
c_work = coeff(3,:) - downshift(3);
% calcualte exponential fits for each set of power fit paramters as a fuction of radius: a,b,c=a*exp(b*r)
FITa = fit(r',a_work','exp1');
FITb = fit(r',b_work','exp1');
FITc = fit(r',c_work','exp1');
% a more detailed radius domain to check fits for density parameters
r_run = linspace(10,75,14*Refine);
% plot the density parameter fits as a function of radius
figure(2)
plot(r,coeff(1:3,:),'k','MarkerSize',10)
hold on
plot(r,coeff(2,:),'+k')
plot(r,coeff(3,:),'*k')
plot(r_run,FITa(r_run)+downshift(1),'-r')
plot(r_run,FITb(r_run)+downshift(2),'-r')
plot(r_run,FITc(r_run)+downshift(3),'-r')
hold off
legend('a(r)','b(r)','c(r)','Fit','Location','best')

```

```

title('AmBe Density Fit Curve Parameters as a Function of Radius with Fits')
xlabel('r [cm]')
ylabel('Parameter')
% compute a final matrix for the overall absorption fraction fit parameters as a function of r and rho
AmBe_Fit_Coeff = [FITa.a FITa.b; FITb.a FITb.b; FITc.a FITc.b];
AmBe_Fit_Coeff = [AmBe_Fit_Coeff downshift];
if DispCoeff == 1
    AmBe_Fit_Coeff
end

%% Cf
Cf_data = readmatrix(Cf_path); % read in data
% distribute data to different matrices to match the meshgrid
Abs_Mn_Cf = blank;
var_Abs_Mn_Cf = blank;
L_Cf = blank;
var_L_Cf = blank;
for ii = 1:size(Cf_data,1)
    Abs_Mn_Cf(ii) = Cf_data(ii,3);
    var_Abs_Mn_Cf(ii) = Cf_data(ii,4);
    L_Cf(ii) = Cf_data(ii,5);
    var_L_Cf(ii) = Cf_data(ii,6);
end
% find and plot a power fit to each radius set over density domain: abs=a*rho^b+c
figure(3)
coeff = zeros(3,length(r)); % power fit coefficient storage for iso-radial lines
for ii = 1:length(r)
    FIT = fit(rho,(Abs_Mn_Cf(:,ii)),'power2');
    coeff(1,ii) = FIT.a;
    coeff(2,ii) = FIT.b;
    coeff(3,ii) = FIT.c;
    plot(FIT)
    hold on
    plot(rho,Abs_Mn_Cf(:,ii),'.k','MarkerSize',10)
    legend('Fit','Data','Location','best')
end
hold off
annotation('arrow',[0.7 0.4],[0.2 0.7])
str = 'Increasing r';
annotation('textbox',[0.3 0.56 0.2 0.2],'String',str,'FitBoxToText','on','EdgeColor','none');
title('Cf Density Fit Curve for Each Radius')
xlabel('\rho [g/cm^3]')
ylabel('\epsilon_M_n')
% normalize data for exponential fitting by shift up or down so that abs(inf) = 0
% this is needed because the exp1 fit does not have a vertical shift term
downshift = coeff(:,end);
a_work = coeff(1,:) - downshift(1); % the working (shifted) power coefficient curves
b_work = coeff(2,:) - downshift(2);
c_work = coeff(3,:) - downshift(3);
% calculate exponential fits for each set of power fit parameters as a function of radius: a,b,c=a*exp(b*r)
FITa = fit(r,'a_work','exp1');
FITb = fit(r,'b_work','exp1');
FITc = fit(r,'c_work','exp1');
% a more detailed radius domain to check fits for density parameters
r_run = linspace(10,75,14*Refine);
% plot the density parameter fits as a function of radius
figure(4)
plot(r,coeff(1:3,:),'.k','MarkerSize',10)
hold on
plot(r,coeff(2,:),'+k')
plot(r,coeff(3,:),'*k')
plot(r_run,FITa(r_run)+downshift(1),'-r')
plot(r_run,FITb(r_run)+downshift(2),'-r')
plot(r_run,FITc(r_run)+downshift(3),'-r')
hold off
legend('a(r)','b(r)','c(r)','Fit','Location','best')
title('Cf Density Fit Curve Parameters as a Function of Radius with Fits')

```

```

xlabel('r [cm]')
ylabel('Parameter')
% compute a final matrix for the overall absorption fraction fit parameters as a function of r and rho
Cf_Fit_Coeff = [FITa.a FITa.b; FITb.a FITb.b; FITc.a FITc.b];
Cf_Fit_Coeff = [Cf_Fit_Coeff downshift];
if DispCoeff == 1
    Cf_Fit_Coeff
end

%% PuBe
PuBe_data = readmatrix(PuBe_path); % read in data
% distribute data to different matrices to match the meshgrid
Abs_Mn_PuBe = blank;
var_Abs_Mn_PuBe = blank;
L_PuBe = blank;
var_L_PuBe = blank;
for ii = 1:size(PuBe_data,1)
    Abs_Mn_PuBe(ii) = PuBe_data(ii,3);
    var_Abs_Mn_PuBe(ii) = PuBe_data(ii,4);
    L_PuBe(ii) = PuBe_data(ii,5);
    var_L_PuBe(ii) = PuBe_data(ii,6);
end
% find and plot a power fit to each radius set over density domain: abs=a*rho^b+c
figure(5)
coeff = zeros(3,length(r)); % power fit coefficient storage for iso-radial lines
for ii = 1:length(r)
    FIT = fit(rho',(Abs_Mn_PuBe(:,ii)), 'power2');
    coeff(1,ii) = FIT.a;
    coeff(2,ii) = FIT.b;
    coeff(3,ii) = FIT.c;
    plot(FIT)
    hold on
    plot(rho,Abs_Mn_PuBe(:,ii),'.k','MarkerSize',10)
    legend('Fit','Data','Location','best')
end
hold off
annotation('arrow',[0.7 0.4],[0.2 0.7])
str = 'Increasing r';
annotation('textbox',[0.3 0.56 0.2 0.2], 'String',str, 'FitBoxToText', 'on', 'EdgeColor','none');
title('PuBe Density Fit Curve for Each Radius')
xlabel('\rho [g/cm^3]')
ylabel('\epsilon_M_n')
% normalize data for exponential fitting by shift up or down so that abs(inf) = 0
% this is needed because the exp1 fit does not have a vertical shift term
downshift = coeff(:,end);
a_work = coeff(1,:) - downshift(1); % the working (shifted) power coefficient curves
b_work = coeff(2,:) - downshift(2);
c_work = coeff(3,:) - downshift(3);
% calculate exponential fits for each set of power fit parameters as a function of radius: a,b,c=a*exp(b*r)
FITa = fit(r',a_work', 'exp1');
FITb = fit(r',b_work', 'exp1');
FITc = fit(r',c_work', 'exp1');
% a more detailed radius domain to check fits for density parameters
r_run = linspace(10,75,14*Refine);
% plot the density parameter fits as a function of radius
figure(6)
plot(r,coeff(1:3,:),'.k','MarkerSize',10)
hold on
plot(r,coeff(2,:),'+k')
plot(r,coeff(3,:),'*k')
plot(r_run,FITa(r_run)+downshift(1),'-r')
plot(r_run,FITb(r_run)+downshift(2),'-r')
plot(r_run,FITc(r_run)+downshift(3),'-r')
hold off
legend('a(r)', 'b(r)', 'c(r)', 'Fit', 'Location', 'best')
title('PuBe Density Fit Curve Parameters as a Function of Radius with Fits')
xlabel('r [cm]')

```

```

ylabel('Parameter')
% compute a final matrix for the overall absorption fraction fit parameters as a function of r and rho
PuBe_Fit_Coeff = [FITa.a FITa.b; FITb.a FITb.b; FITc.a FITc.b];
PuBe_Fit_Coeff = [PuBe_Fit_Coeff downshift];
if DispCoeff == 1
    PuBe_Fit_Coeff
end

%% Comparison Plots and Errors
% fit domain refinement
[Rfine,RHOfine] = meshgrid(linspace(10,75,14*Refine),round(linspace(1.05,1.40,8*Refine),5));
% plot fits and simulation data
figure(7)
sgtitle('Comparison of Fit and Data for Mn Absorption Fraction')
subplot(1,3,1) % AmBe fit and discrete data
    surf(Rfine,RHOfine,FitMatrixEval(Rfine,RHOfine,AmBe_Fit_Coeff),'EdgeColor','none')
    hold on
    plot3(AmBe_data(:,1),AmBe_data(:,2),AmBe_data(:,3),'.k','MarkerSize',12)
    if ShowVar > 0
        plot3(AmBe_data(:,1),AmBe_data(:,2),AmBe_data(:,3)+ShowVar*AmBe_data(:,4),'.r','MarkerSize',6)
        plot3(AmBe_data(:,1),AmBe_data(:,2),AmBe_data(:,3)-ShowVar*AmBe_data(:,4),'.r','MarkerSize',6)
    end
    hold off
    title('AmBe')
    xlabel('r [cm]')
    ylabel('\rho [g/cm^3]')
    zlabel('\epsilon_M_n')
    legend('Fit','Data','Location','northeast')
subplot(1,3,2) % Cf fit and discrete data
    surf(Rfine,RHOfine,FitMatrixEval(Rfine,RHOfine,Cf_Fit_Coeff),'EdgeColor','none')
    hold on
    plot3(Cf_data(:,1),Cf_data(:,2),Cf_data(:,3),'.k','MarkerSize',12)
    if ShowVar > 0
        plot3(Cf_data(:,1),Cf_data(:,2),Cf_data(:,3)+ShowVar*Cf_data(:,4),'.r','MarkerSize',6)
        plot3(Cf_data(:,1),Cf_data(:,2),Cf_data(:,3)-ShowVar*Cf_data(:,4),'.r','MarkerSize',6)
    end
    hold off
    title('Cf')
    xlabel('r [cm]')
    ylabel('\rho [g/cm^3]')
    zlabel('\epsilon_M_n')
    legend('Fit','Data','Location','northeast')
subplot(1,3,3) % PuBe fit and discrete data
    surf(Rfine,RHOfine,FitMatrixEval(Rfine,RHOfine,PuBe_Fit_Coeff),'EdgeColor','none')
    hold on
    plot3(PuBe_data(:,1),PuBe_data(:,2),PuBe_data(:,3),'.k','MarkerSize',12)
    if ShowVar > 0
        plot3(PuBe_data(:,1),PuBe_data(:,2),PuBe_data(:,3)+ShowVar*PuBe_data(:,4),'.r','MarkerSize',6)
        plot3(PuBe_data(:,1),PuBe_data(:,2),PuBe_data(:,3)-ShowVar*PuBe_data(:,4),'.r','MarkerSize',6)
    end
    hold off
    title('PuBe')
    xlabel('r [cm]')
    ylabel('\rho [g/cm^3]')
    zlabel('\epsilon_M_n')
    legend('Fit','Data','Location','northeast')
% find absolute maximum relative error between fit and simulation data
% first as meshgrid matrices
RelErr_AmBe = (FitMatrixEval(R,RHO,AmBe_Fit_Coeff) - Abs_Mn_AmBe)./Abs_Mn_AmBe*100; % [%]
RelErr_Cf = (FitMatrixEval(R,RHO,Cf_Fit_Coeff) - Abs_Mn_Cf)./Abs_Mn_Cf*100; % [%]
RelErr_PuBe = (FitMatrixEval(R,RHO,PuBe_Fit_Coeff) - Abs_Mn_PuBe)./Abs_Mn_PuBe*100; % [%]
% plot errors
figure(8)
sgtitle('Relative Error Between Fit and Data for Mn Absorption Fraction')
subplot(1,3,1) % AmBe error
    surf(R,RHO,RelErr_AmBe)
    title('AmBe')

```

```

xlabel('r [cm]')
ylabel('\rho [g/cm^3]')
zlabel('Relative Error [%]')
if OrientErrAxes == 1
    set(gca,'xdir','reverse')
    set(gca,'zlim',[-30,10])
end
set(gca,'FontSize',12)
subplot(1,3,2) % Cf error
surf(R,RHO,RelErr_Cf)
title('Cf')
xlabel('r [cm]')
ylabel('\rho [g/cm^3]')
zlabel('Relative Error [%]')
if OrientErrAxes == 1
    set(gca,'xdir','reverse')
    set(gca,'zlim',[-30,10])
end
set(gca,'FontSize',12)
subplot(1,3,3) % PuBe error
surf(R,RHO,RelErr_PuBe)
title('PuBe')
xlabel('r [cm]')
ylabel('\rho [g/cm^3]')
zlabel('Relative Error [%]')
if OrientErrAxes == 1
    set(gca,'xdir','reverse')
    set(gca,'zlim',[-30,10])
end
set(gca,'FontSize',12)
% only report the absolute maximum relative error for each source
MaxRelErr_AmBe = max(max(abs(RelErr_AmBe)));
MaxRelErr_Cf = max(max(abs(RelErr_Cf)));
MaxRelErr_PuBe = max(max(abs(RelErr_PuBe)));
fprintf('The absolute maximum relative error between the fits and the data are:\n')
fprintf('\tAmBe\t%.4f %%\n',MaxRelErr_AmBe)
fprintf('\tCf\t%.4f %%\n',MaxRelErr_Cf)
fprintf('\tPuBe\t%.4f %%\n',MaxRelErr_PuBe)

```

### ***FitMatrixEval.m***

This MATLAB function calculates  $\epsilon_{Mn}$  given a Mn bath radius, solution density, and fit coefficient matrix. The radius and density inputs may be in the form of grids.

```

function [AbsMesh] = FitMatrixEval(R,RHO,coeff)
% Use the fit coefficient matrix defined in Data_Processing.m and
% meshgrid parameters for radius and density to return the appropriate
% output meshgrid
% Scout Bucks
% 9/29/23

% The coefficient matrix has the form:
%     [a1 a2 a3;
%       b1 b2 b3;
%       c1 c2 c3]
% This is the input to the following empirical correlation
%     epsilon = a(r)*rho^b(r) + c(r)
%     a(r) = a1*exp(a2*r) + a3
%     b(r) = b1*exp(b2*r) + b3

```

```
%      c(r) = c1*exp(c2*r) + c3

% check dimensions of R and RHO
if size(R) ~= size(RHO)
    error('Meshgrid inputs for radius and density have different dimensions.')
end

AbsMesh = 0*R; % initialize output variable
% go through each location in AbsMesh and calculate the Mn abs frac using
% the corresponding radius and density
for ii = 1:size(AbsMesh,1)
    for jj = 1:size(AbsMesh,2)
        a = coeff(1,1)*exp(coeff(1,2)*R(ii,jj)) + coeff(1,3);
        b = coeff(2,1)*exp(coeff(2,2)*R(ii,jj)) + coeff(2,3);
        c = coeff(3,1)*exp(coeff(3,2)*R(ii,jj)) + coeff(3,3);
        AbsMesh(ii,jj) = a*RHO(ii,jj)^b + c;
    end
end
end
```

**BIBLIOGRAPHY**

1. N. J. ROBERTS, N. N. MOISEEV, and M. KRÁLIK, “Radionuclide neutron source characterization techniques,” *Metrologia* **48** 6 (2011); <https://doi.org/10.1088/0026-1394/48/6/S02>.
2. A. BORETTI, “Supply of abundant and low-cost total primary energy to a growing world needs nuclear energy and hydrogen energy storage,” *International Journal of Hydrogen Energy* **48** 5, 1649, Elsevier Ltd (2023); <https://doi.org/10.1016/j.ijhydene.2022.06.279>.
3. N. COLONNA et al., “Advanced nuclear energy systems and the need of accurate nuclear data: The n-TOF project at CERN,” *Energy and Environmental Science* **3** 12, 1910 (2010); <https://doi.org/10.1039/c0ee00108b>.
4. J. M. ADAMS, “Present and future trends for neutron source calibrations at the National Institute of Standards and Technology,” *Nuclear Instruments and Methods in Physics Research B* **213**, 218 (2004); [https://doi.org/10.1016/S0168-583X\(03\)01575-1](https://doi.org/10.1016/S0168-583X(03)01575-1).
5. F. OGHEARD, J. L. CHARTIER, and P. CASSETTE, “Monte-Carlo simulations of the new LNHB manganese bath facility,” *Applied Radiation and Isotopes* **70** 4, 794 (2012); <https://doi.org/10.1016/j.apradiso.2012.01.010>.
6. J. R. LAMARSH and A. J. BARATTA, *Introduction to Nuclear Engineering*, 3rd ed., M. Horton et al., Eds., Prentice-Hall, Upper Saddle River, NJ (2001).
7. “Evaluated Nuclear Data File (ENDF) Retrieval & Plotting,” National Nuclear Data Center Brookhaven National Laboratory; 2011; <https://www.nndc.bnl.gov/sigma/index.jsp?as=15&lib=endfb7.1&nsb=10>; (current as of Mar. 13, 2023).

8. “Live Chart of Nuclides,” International Atomic Energy Agency - Nuclear Data Section; 2023; <https://www-nds.iaea.org/relnsd/vcharthtml/VChartHTML.html>; (current as of Mar. 13, 2023).
9. M. AMENDOLA et al., “Experimental and Monte Carlo simulation on new manganese bath facility for absolute neutron source emission rate measurement at ENEA-INMRI,” *Journal of Radioanalytical and Nuclear Chemistry* **301** 1, 109, Kluwer Academic Publishers (2014); <https://doi.org/10.1007/s10967-014-3106-1>.
10. G. F. KNOLL, *Radiation Detection and Measurement*, 3rd ed., B. Zobrist, R. Factor, and S. Malinowski, Eds., John Wiley & Sons, New York, NY (2000).
11. N. J. ROBERTS et al., “International key comparison of measurements of neutron source emission rate,” *Metrologia* **48** (2011); <https://doi.org/10.1088/0026-1394/48/1A/06018>.
12. R. KHABAZ, “Appraisalment of the correction factors for neutron reaction in the manganese bath using Monte Carlo calculation,” *Journal of Radioanalytical and Nuclear Chemistry* **293** 2, 455 (2012); <https://doi.org/10.1007/s10967-012-1792-0>.
13. R. KHABAZ, “An evaluation of a manganese bath system having a new geometry through MCNP modelling,” *Radiation Protection Dosimetry* **152** 4, 400 (2012); <https://doi.org/10.1093/rpd/ncs080>.
14. N. J. ROBERTS and M. J. PARFITT, “MCNPX modelling of the NPL manganese bath facility based on a converted CAD model,” *Radiation Measurements* **45** 10, 1346 (2010); <https://doi.org/10.1016/j.radmeas.2010.06.057>.
15. C. J. WERNER et al., *MCNP User's Manual Code Version 6.2*, C. J. Werner, Ed., Los Alamos National Laboratory, Los Alamos (2017).

16. J. E. SWEEZY et al., *MCNP — A General Monte Carlo N-Particle Transport Code, Version 5*, Los Alamos National Laboratory, Los Alamos (2003).
17. A. VASILIEV et al., “On the performance of ENDF/B-VII.0 data for fast neutron fluence calculations,” *Annals of Nuclear Energy* **35** 12, 2432 (2008);  
<https://doi.org/10.1016/j.anucene.2008.07.009>.
18. N. J. ROBERTS et al., “Subsequent comparison of measurements of neutron source emission rate (2016-17)-CCRI(III)-K9.AmBe.2,” *Metrologia* **58** 1A (2021);  
<https://doi.org/10.1088/0026-1394/58/1A/06025>.
19. D. E. MCGARRY and E. W. BOSWELL, “Neutron source strength calibrations,” in *National Bureau of Standards Special Publication 250* 18, US Department of Commerce National Bureau of Standards, Gaithersburg (1988).
20. G. R. BITTENCOURT et al., “Determination of semi-empirical relationship between the manganese and hydrogen atoms ratio, physical density and concentration in an aqueous solution of manganese sulphate,” *Radiation Measurements* **45** 40, 1505 (2010);  
<https://doi.org/10.1016/j.radmeas.2010.05.038>.
21. A. DE VOLPI, R. J. ARMANI, and K. G. PORGES, “Determination of manganese sulphate content for neutron source measurements,” *Journal of Nuclear Energy Parts A/B* **19**, 597 (1965); [https://doi.org/0368-3230\(65\)90116-3](https://doi.org/0368-3230(65)90116-3).
22. W. D. DECKWER, “Density, viscosity, vapor pressure, and hydrogen solubility of aqueous MnSO<sub>4</sub> solutions,” *Journal of Chemical and Engineering Data* **25** 1, 75 (1980);  
<https://doi.org/10.1021/je60084a022>.

23. R. V. GRIFFITH, J. PALFALVI, and U. MADHVANATH, *Compendium of Neutron Spectra and Detector Responses for Radiation Protection Purposes*, International Atomic Energy Agency, Vienna (1990).
24. P. A. SÖDERSTRÖM et al., “Characterization of a plutonium–beryllium neutron source,” *Applied Radiation and Isotopes* **167**, Elsevier Ltd (2021); <https://doi.org/10.1016/j.apradiso.2020.109441>.
25. N. J. ROBERTS, “Calculations of correction factors for radionuclide neutron source emission rate measurements using the manganese bath,” National Physical Laboratory, Teddington (2001).
26. T. L. BERGMAN and A. S. LAVINE, *Fundamentals of Heat and Mass Transfer*, 8th ed., L. Ratts et al., Eds., John Wiley & Sons, Hoboken, NJ (2017).
27. “Industrial Gauging & Analysis Sealed Radioactive Sources,” QSA Global; 2023; <https://www.qsa-global.com/industrial-gauging-analysis-radioactive-sources>; (current as of Dec. 20, 2023).
28. T. NISHI et al., “Heat capacities and thermal conductivities of AmO<sub>2</sub> and AmO<sub>1.5</sub>,” in *Journal of Nuclear Materials* **414** 2, pp. 109–113 (2011); <https://doi.org/10.1016/j.jnucmat.2011.01.019>.
29. W. R. CORNMAN, W. C. REINIG, and P. H. PERMAR, “Californium-252: a new, promising neutron source,” in Savannah River Laboratory, Savannah River National Laboratory, Aiken (1973); <https://doi.org/DP-MS-73-26>.
30. J. BAGI, T. C. NGUYEN, and L. LAKOSI, “Assessment of the Pu content of Pu-Be neutron sources,” *Nuclear Instruments and Methods in Physics Research B* **222** 1–2, 242 (2004); <https://doi.org/10.1016/j.nimb.2003.12.085>.

ACADEMIC VITA  
**Scout Bucks**

---

<b>Education</b>	The Pennsylvania State University BS Nuclear Engineering, BS Mechanical Engineering, Schreyer Honors Scholar Beginning a PhD in Nuclear Engineering in Fall 2024	Aug 2020 – May 2024
------------------	--	---------------------

---

<b>Work Experience</b>	<p><i>Reactor Operator</i> <span style="float: right;">Nov 2021 – May 2024</span></p> <p>Penn State Breazeale Nuclear Research Reactor, University Park, PA</p> <ul style="list-style-type: none"> <li>• Passed NRC licensing exam and have since operated more than 150 hours</li> <li>• Participated in control rod worth measurements and subcritical physics testing</li> <li>• Operated spent fuel storage alloy neutron transmission testing device</li> <li>• Led liquid nitrogen asphyxiation safety review and pool maintenance projects</li> </ul> <p><i>Machine Shop Teaching Assistant</i> <span style="float: right;">Aug 2021 – Dec 2021</span></p> <p>Penn State Learning Factory, University Park, PA</p> <ul style="list-style-type: none"> <li>• Collaborated with other TAs to arrange shifts and tasks</li> <li>• Supervised shop floor for safety and cleanliness</li> <li>• Taught machine safety and operation courses to new students</li> </ul>
------------------------	--

---

<b>Research</b>	<p><i>Fiber Optic Temperature Sensor for Heat Pipe Applications</i> <span style="float: right;">Aug 2023 – May 2024</span></p> <p>Dr. Saya Lee, Thermal Hydraulics Lab, University Park PA</p> <ul style="list-style-type: none"> <li>• Built an experimental apparatus for testing fiber optic temperature sensors</li> <li>• Investigated and procured equipment for a new lab facility</li> <li>• Submitted <i>Comparison of Fiber Optic Temperature Sensors and Thermocouples at Sodium Heat Pipe Operating Temperatures</i> to the 2024 ANS Student Conference</li> </ul> <p><i>Manganese Sulfate Bath Neutron Detection System</i> <span style="float: right;">Aug 2022 – Mar 2024</span></p> <p>Dr. Marek Flaska, Radiation Detection Lab, University Park PA</p> <ul style="list-style-type: none"> <li>• Designed and validated an MCNP model for a generalized MnSO<sub>4</sub> bath</li> <li>• Developed empirical correlations for bath parameters from 300 simulations</li> <li>• Investigated the feasibility of building a MnSO<sub>4</sub> bath at the university</li> <li>• Submitted <i>Development of an Empirical Correlation for the Manganese Sulfate Bath Neutron Absorption Fraction</i> to the 2024 ANS Student Conference</li> </ul>
-----------------	--

---

<b>Involvement</b>	<p>PSU Navigators</p> <p>ANS PSU Chapter</p> <p>ASME PSU Chapter</p>	<p>Bible Study Leader</p> <p>Member</p> <p>Member</p>	<p>Aug 2020 – May 2024</p> <p>Aug 2020 – May 2024</p> <p>Aug 2020 – May 2024</p>
--------------------	--	---	--

---

<b>Awards</b>	<p>College of Engineering Nuclear Engineering Major Student Marshal</p> <p>DOE University Nuclear Leadership Program Scholarship</p> <p>William R. and Mila Kimel Nuclear Engineering Scholarship</p> <p>John J. Brennan Excellence in Nuclear Engineering Award</p> <p>Francine Battaglia Mechanical Engineering Scholarship</p> <p>Exelon Corporation Endowed Scholarship in Nuclear Engineering</p>	<p>Spring 2024</p> <p>2022 – 2024</p> <p>Fall 2023</p> <p>Spring 2023</p> <p>Fall 2022</p> <p>Spring 2022, 2024</p>
---------------	--	---